

**DEVELOPMENT OF POLY(3-OCTYLTHIOPHENE) THIN FILMS
FOR REGULATING OSTEOBLAST GROWTH**

A Dissertation
Presented to
The Academic Faculty

by

Charlene Rincón-Rosenbaum

In Partial Fulfillment
of the Requirements for the Degree
Doctor of Philosophy in the
School Chemical and Biomolecular Engineering

Georgia Institute of Technology
December 2008

**DEVELOPMENT OF POLY(3-OCTYLTHIOPHENE) THIN FILMS
FOR REGULATING OSTEOLAST GROWTH**

Approved by:

Dr. J. Carson Meredith, Advisor
School of Chemical and Biomolecular
Engineering
Georgia Institute of Technology

Dr. Hang Lu
School of Chemical and Biomolecular
Engineering
Georgia Institute of Technology

Dr. William Koros
School of Chemical and Biomolecular
Engineering
Georgia Institute of Technology

Dr. Joseph Schork
School of Chemical and Biomolecular
Engineering
Georgia Institute of Technology

Dr. Yadong Wang
School of Biomedical Engineering
Georgia Institute of Technology

Date Approved: August 7, 2008

To my parents and sister

ACKNOWLEDGEMENTS

First I would like to thank my parents and sister for their love and support. Mom and dad, I cannot thank you enough for believing in me, for your moral support, and for being there for me always. To Eduardo Vázquez-Figueroa, for being my friend and academic companion for so many years. Thank you for all the support and pep talks you gave me when I needed them the most. Grad school would not have been the same without you. I would like to specially thank my advisor, Carson Meredith, who is one of the most intellectually well-rounded persons I have ever met, for all the guidance, support, and encouragement he always gave me. I would also like to thank all the members of my committee for their interest and support in this work.

I would like to thank all the past and present members of the thin-films and colloidal research group. To Santanu Chattopadhyay—you taught me what I needed to know to get started on my project. To Joe Sormana—thank you for all the helpful discussions and for always bringing joy to the lab. To Jing Su—you are one of the brightest persons I know, for all your help and ideas. I know, it's just one line in Matlab, but not everyone has the gift you have for programming. To Pedro Zapata—you are one of the best LabVIEW programmers and equipment custom-builders I have ever met, for all your helpful discussions. Your breadth of knowledge is impressive. To Keith Reed—thank you for all your good insights and for the great talks about food, wine, running, and life in general. To Jung-Hyun Lee—thank you for always being willing to help me with AFM. To Gracy Wingkono, Reginald Thio, and Chien-Chiang Chen for your help and support.

I would like to thank Professors Andreas Bommarius and Mark Prausnitz for giving me the opportunity to organize the Drug Design Development, and Delivery plant tour. It was a challenging, yet enjoyable experience. I will be glad to help you with future trips.

My Numerical Methods class would have been unbearable without the help of Nikolaos Pratikakis and Christos Fountoukis, the only two people I know that do well in a math test without doing practice problems. You became very good friends and I am grateful for it. I would like to thank Mariefel Olarte, Chris Russell, Genggeng Qi, Ingu Song, Benita Comeau, Yeny Hudiono, Ryan Kincer, Kane Barker, Jae Kyu Cho, and Yueming Hua for their help with different laboratory equipments.

I would like to thank the ES&T personnel that have helped me in one way or another. To Juanita Lewis, Janice Whatley, Josie Giles, Brenda Mattox, Pat Wade, Donna Bondy, Rochelle Moses, and Claudia Clarkson, for reserving a room, lending me an envelope, a post-it, or a pen, ordering lab supplies, clarifying my finances, or any other favor I ever asked from you. To Kevin, Jason, Jeff Andrews, Brad Parker, Todd Clarkson, Tommie Taylor, Kirk Guger, and Kevin Guger for receiving packages, for moving my job requests to the top of the machine shop queue, for taking care of our building and lab maintenance, or for taking care of my IT issues. Your help was always appreciated.

I would like to thank numerous friends that have supported me in many ways. To Ernesto Angueira and José Ricardo Méndez, for your friendship and for being my “big brothers” in the Ph.D. program. To José “Kinsi” Rodríguez, for offering your friendship since my very first week in Atlanta. To Jun Sato and Enrique Michel, for all the good

times we had together in and outside the school. To Tito, Kiki, Ramón, Robby, Virginia, Adriana, and Tania, for being my friends and family in Atlanta and for making my free weekends very enjoyable.

I would like to thank the different sources of funding I received throughout my five years as a graduate student. To the Goizueta Foundation, Jorge Bretón, and Millie Trotter, for not only providing me with economic assistance for four years, but for allowing me to meet and interact with people from different disciplines and backgrounds. To Professor Carlos Santamarina, the Goizueta Foundation faculty chair, for being an excellent mentor and for his words of wisdom and encouraging talks. To the Hispanic Scholarship Fund, for giving me the opportunity to be part of the Peer Counselor Pilot Program. I really appreciated the opportunity to mentor six Hispanic students from the Georgia Perimeter College on the importance of education. To the GAANN Polymer Fellowship, for the financial assistance. To the National Institutes of Health – NRSA Pre-doctoral Fellowship, for the economic assistance and for the opportunity to travel the world to present my research.

Finally, but most importantly, I would like to thank God because without Him none of this would have been possible. Thank you for guiding my life and for always setting the path you believe is right for me.

TABLE OF CONTENTS

	Page
ACKNOWLEDGEMENTS	iv
LIST OF TABLES	xi
LIST OF FIGURES	xii
LIST OF SYMBOLS AND ABBREVIATIONS	xvi
SUMMARY	xviii
 <u>CHAPTER</u>	
1 INTRODUCTION	1
1.1 Specific Aims	1
1.2 Thesis Outline	3
2 BACKGROUND AND SIGNIFICANCE	4
2.1 Conducting polymers	4
2.1.1 Substituted polythiophenes	6
2.1.2 Poly(3-octylthiophene)	7
2.2 P3OT as substrate for cell attachment and proliferation	8
2.3 Modified P3OT as substrate for cell attachment and proliferation	10
3 MC3T3-E1 ATTACHMENT AND PROLIFERATION ON P3OT THIN FILMS	12
3.1 Abstract	12
3.2 Introduction	12
3.3 Materials and Methods	14
3.3.1 Characterization of P3OT in solution	14
3.3.2 Preparation of P3OT films	15

3.3.3	Characterization of P3OT films	16
3.3.4	Cell culture	16
3.3.5	Cell attachment and spreading	17
3.3.6	Cell proliferation	17
3.3.7	Leaching experiments	18
3.3.8	Image acquisition and analysis	18
3.4	Results and Discussion	21
3.4.1	P3OT characterization	21
3.4.2	Surface characterization	23
3.4.3	Cell attachment and spreading	24
3.4.4	Cell proliferation	27
3.5	Conclusions	33
4	EFFECT OF P3OT DOPING ON THE ATTACHMENT AND PROLIFERATION OF OSTEOBLASTS	34
4.1	Abstract	34
4.2	Introduction	34
4.3	Materials and Methods	36
4.3.1	Preparation of P3OT films	36
4.3.2	Doping of P3OT films	37
4.3.3	Characterization of P3OT films	37
4.3.4	Cell culture	37
4.3.5	Cell attachment and spreading	38
4.3.6	Cell proliferation	38
4.3.7	Image acquisition and analysis	39
4.4	Results and Discussion	41
4.4.1	Surface characterization	41

4.4.2	Cell attachment and spreading – global analysis	46
4.4.3	Cell attachment and spreading – local analysis	47
4.4.4	Cell proliferation – global analysis	49
4.4.5	Cell proliferation – local analysis	50
4.5	Conclusions	56
5	EFFECT OF P3OT THICKNESS AND FILM PREPARATION CONDITIONS ON OSTEOBLAST ATTACHMENT AND PROLIFERATION	57
5.1	Abstract	57
5.2	Introduction	58
5.3	Materials and Methods	60
5.3.1	Preparation of P3OT films	60
5.3.2	Characterization of P3OT films	61
5.3.3	Cell culture	61
5.3.4	Cell attachment and spreading	62
5.3.5	Cell proliferation	62
5.3.6	Image acquisition and analysis	62
5.4	Results and Discussion	63
5.4.1	Surface characterization	63
5.4.2	Cell attachment – high thickness range	68
5.4.3	Cell proliferation – high thickness range	69
5.4.4	Cell attachment – film thickness and preparation conditions	70
5.5	Conclusions	75
6	CONCLUSIONS AND FUTURE DIRECTIONS	77
6.1	Conclusions	77
6.2	Future directions	77
6.2.1	Protein expression and mineralization	78

6.2.2 Regulating P3OT-cell interactions by adsorbed proteins	78
6.2.3 Combinatorial methods to generate doping gradients	79
6.2.4 Combination of electrical and topographical characteristics	79
6.2.5 Electrical stimulation	82
APPENDIX A: Additional figures	84
REFERENCES	91
VITA	102

LIST OF TABLES

	Page
Table 4.1: Comparison of FTIR peak areas of undoped and FeCl ₃ -doped P3OT.	45

LIST OF FIGURES

	Page
Figure 2.1: Chemical structures of common conducting polymers: a) polyacetylene and b) most commonly explored conducting polymers for biomedical applications.	4
Figure 2.2: Schematic of a biosensor. A biological sensing element detects a specific analyte (e.g., enzyme, antibody) producing a biochemical signal that is transferred to the transducer (e.g., conducting polymer), which ultimately produces a digital electronic signal that is proportional to the amount of analyte present.	5
Figure 2.3: Schematic of an artificial muscle device.	6
Figure 2.4: Different coupling of pairs of 3-alkylthiophene monomers.	7
Figure 2.5: Chemical structure of poly(3-octylthiophene).	7
Figure 3.1: Image and schematic representation of the knife-edge coating apparatus used to prepare P3OT films.	15
Figure 3.2: Schematic of two operating modes for the knife-edge coating apparatus.	16
Figure 3.3: Demonstration of the image capture and analysis for the attachment experiments: a) blue channel image, b) green channel image, c-d) masks of the blue and green channel images, and e) output of results for area and circularity.	19
Figure 3.4: Representative Minitab graphical summary output for cell area on P3OT films.	20
Figure 3.5: Representative Minitab graphical summary output for cell proliferation on P3OT films.	21
Figure 3.6: ^1H NMR spectra of regioregular P3OT in CDCl_3 .	22
Figure 3.7: UV-Vis absorption spectra of P3OT in solution.	22
Figure 3.8: Emission spectra of P3OT in solution.	23
Figure 3.9: Representative film thickness as a function of P3OT film position. Typical thickness was $30 \text{ nm} \pm 2 \text{ nm}$. Values are presented as mean \pm SEM.	24
Figure 3.10: Representative water contact angle for P3OT ($106.6^\circ \pm 0.3^\circ$). Angles were measured using the instrument's software.	24
Figure 3.11: MC3T3-E1 cell attachment density on P3OT, Si, and TCPS 4 hours after seeding. Values are presented as median \pm 95% confidence intervals.	25



Figure 3.12: F-actin visualization of Alexa Fluor 488 phalloidin-stained MC3T3-E1 osteoblasts adhered on P3OT, Si, and TCPS. Image width is 1280 μm .	25
Figure 3.13: Area and circularity of MC3T3-E1 cells after 4 hours of culture on P3OT, Si, and TCPS. Values are presented as median \pm 95% confidence intervals.	26
Figure 3.14: Relationship between water contact angle and cell area for P3OT, Si, and TCPS.	27
Figure 3.15: Representative fluorescent images of cells cultured on P3OT films: a) cell nuclei, b) cells positive for BrdU incorporation, and c) overlap of cell nuclei and proliferating cells.	28
Figure 3.16: Proliferation ratio of MC3T3-E1 cells after 24, 48, and 72 hours of culture on P3OT, Si, and TCPS. Values are presented as mean \pm 95% confidence intervals.	29
Figure 3.17: Proliferation ratio of MC3T3-E1 cells on P3OT pre-soaked with a) cell culture media and b) DPBS, after 24 and 48 hours of culture. Values are presented as mean \pm 95% confidence intervals.	31
Figure 3.18: Proliferation ratio of MC3T3-E1 cells on TCPS with a) pre-soaked cell culture media and b) freshly prepared cell culture media, after 24 and 48 hours of culture. Values are presented as mean \pm 95% confidence intervals.	32
Figure 4.1: Global and local metrics to analyze proliferation.  proliferated cells  cells at rest.	39
Figure 4.2: Water contact angle as a function of doping concentration.	42
Figure 4.3: UV-Vis absorption spectra for uP3OT, D001, and D125 films.	42
Figure 4.4: AFM 3-D topography images of (a) uP3OT, (b) D001, and (c) D125 thin films (30 nm).	43
Figure 4.5: FTIR spectra of uP3OT and dP3OT films.	44
Figure 4.6: Schematic representation of cationic P3OT chains–anionic dopant (FeCl_4^-) adducts comprising the doped region of polymer matrix.	45
Figure 4.7: MC3T3-E1 cell attachment density on uP3OT, D001, and D125 4 hours after seeding. Values are presented as median \pm 95% confidence intervals.	46
Figure 4.8: Area and circularity of MC3T3-E1 cells after 4 hours of culture on uP3OT, D001, and D125. Values are presented as median \pm 95% confidence intervals.	47

Figure 4.9: Normalized distribution, \tilde{f}_{AA} , for cells cultured for a period of 4 hours on uP3OT and D125.	48
Figure 4.10: Proliferation ratio of MC3T3-E1 cells after 24, 48, and 72 hours of culture on uP3OT, D001, and D125. Values are presented as mean \pm 95% confidence intervals.	50
Figure 4.11: Effect of cell density on cell proliferation for MC3T3-E1 cultured on (a) uP3OT and (b) D125 for a period of 24 hours.	51
Figure 4.12: Normalized distributions: a) \tilde{f}_{AA} , b) \tilde{f}_{PP} , and c) f_{PR}/f_{RR} for cells cultured for a period of 24 hours on uP3OT and D125.	53
Figure 4.13: Normalized distribution, \tilde{f}_{RR} , for cells cultured for a period of 24 hours on uP3OT and D125.	55
Figure 5.1: Adhesive pull of force profile of P3OT thickness gradient film.	59
Figure 5.2: SEM micrographs of pristine P3OT films annealed at 373 K for different interval of time (a) unannealed—303 K (b) 1 h, (c) 5 h, (d) 12 h, (e) 24 h, (f) 48 h, and (g) 72 h.	59
Figure 5.3: Representative three-dimensional thickness map of the thickness gradient P3OT films.	64
Figure 5.4: Representative plots of constant thickness films: a) 20 nm, b) 30 nm, and c) 50 nm. Values are presented as mean \pm SEM.	64
Figure 5.5: Water contact angle for thickness gradient films.	65
Figure 5.6: UV-Vis absorption spectra for aP3OT and uaP3OT films made from CHCl_3 and THF.	66
Figure 5.7: AFM topography images of (a) uaP3OT/ CHCl_3 , (b) aP3OT/ CHCl_3 , (c) uaP3OT/THF, and (d) aP3OT/THF.	67
Figure 5.8: MC3T3-E1 cell attachment density on thickness gradient films. Values are presented as median \pm 95% confidence intervals.	68
Figure 5.9: Area and circularity of MC3T3-E1 cells after 4 hours of culture on thickness gradient films. Values are presented as median \pm 95% confidence intervals.	69
Figure 5.10: Proliferation ratio as a function of P3OT thickness of cells cultured for a period of 24, 48, and 72 hours. Values are presented as mean \pm 95% confidence intervals.	70

Figure 5.11: MC3T3-E1 cell attachment density on P3OT films (20, 30, and 50 nm) made from CHCl_3 and THF 4 hours after seeding. Values are presented as median \pm 95% confidence intervals.	71
Figure 5.12: Area of MC3T3-E1 cells after 4 hours of culture on P3OT films (20, 30, and 50 nm) made from CHCl_3 and THF. Values are presented as median \pm 95% confidence intervals.	72
Figure 5.13: Circularity of MC3T3-E1 cells after 4 hours of culture on P3OT films (20, 30, and 50 nm) made from CHCl_3 and THF. Values are presented as median \pm 95% confidence intervals.	73
Figure 5.14: MC3T3-E1 cell attachment density on aP3OT and uaP3OT films made from CHCl_3 and THF 4 hours after seeding. Values are presented as median \pm 95% confidence intervals.	74
Figure 5.15: Area and circularity of MC3T3-E1 cells after 4 hours of culture on aP3OT and uaP3OT films made from CHCl_3 and THF. Values are presented as median \pm 95% confidence intervals.	75
Figure 6.1: Schematic of the conductor/insulator bilayer system.	80
Figure 6.2: Optical micrograph and corresponding AFM topograph of dewetting pattern for various PS thicknesses in 10 min at 100°C on P3OT coated silicon substrate of 170 nm P3OT thickness.	81
Figure 6.3: Proliferation ratio of MC3T3-E1 cells after 24, 48, and 72 hours of culture on P3OT, PS, and TCPS. Values are presented as mean \pm 95% confidence intervals.	81
Figure A.1: XPS spectra of P3OT thin films (30 nm).	84
Figure A.2: Effect of cell density on cell proliferation for MC3T3-E1 cultured on (a) undoped P3OT and (b) 0.125M FeCl_3 -doped P3OT for a period of 48 hours.	85
Figure A.3: Effect of cell density on cell proliferation for MC3T3-E1 cultured on (a) undoped P3OT and (b) 0.125M FeCl_3 -doped P3OT for a period of 72 hours.	86
Figure A.4: Normalized distributions: a) \tilde{f}_{AA} , b) \tilde{f}_{PP} , c) f_{PR}/f_{RR} , and d) \tilde{f}_{RR} for cells cultured for a period of 48 hours on undoped and 0.125M FeCl_3 -doped P3OT.	87
Figure A.5: Normalized distributions: a) \tilde{f}_{AA} , b) \tilde{f}_{PP} , c) f_{PR}/f_{RR} , and d) \tilde{f}_{RR} for cells cultured for a period of 72 hours on undoped and 0.125M FeCl_3 -doped P3OT.	89

LIST OF SYMBOLS AND ABBREVIATIONS

α -MEM	Eagle's minimum essential medium
A	Cell type: Any cell
AFM	Atomic force microscopy
ANOVA	Analysis of variance
BrdU	5-Bromo-2'-deoxyuridine
CHCl ₃	Chloroform
CDCl ₃	Deuterated chloroform
CPs	Conducting polymers
DPBS	Dulbecco's Phosphate Buffered Saline
ECM	Extracellular matrix
f_{AA}	The frequency function for cell-to-cell distances AA
FBS	Fetal bovine serum
FeCl ₃	Ferric chloride
f_{PP}	The frequency function for cell-to-cell distances PP
f_{std}	The standard frequency distribution
FTIR	Fourier Transform Infrared Spectroscopy
GPC	Gel permeation chromatography
HF	Hydrofluoric acid
HT	Head-to-tail
LCFA	Local cell-feature analysis
M_w	Molecular weight

NaOH	Sodium hydroxide
NMR	Nuclear magnetic resonance
P	Cell type: Proliferating cell
PBS	Phosphate Buffered Saline
P3ATs	Poly(3-alkylthiophenes)
P3HT	Poly(3-hexylthiophene)
P3OT	Poly(3-octylthiophene)
<i>PO</i>	Posterior odds
PPy	Polypyrrole
PS	Polystyrene
PTs	Polythiophenes
R	Cell type: Cells at rest
RMS	Root-mean-square
SEM	Standard error of the mean
Si	Silicon
TCPS	Tissue culture polystyrene
THF	Tetrahydrofuran
VDW	van der Waals
XPS	X-ray photoelectron spectroscopy

SUMMARY

The investigation of electrically conducting polymers (CPs) for use in biomedical applications has expanded greatly since the discovery in the 1980s that these materials are compatible with many biological molecules. CPs are able, via electrical stimulation, to modulate the behavior of certain electrically responsive cells (i.e., nerve, muscle, bone, and cardiac cells). CPs such as polypyrrole, polyaniline, and polythiophene have a conjugated structure that upon doping allows interchain hopping of electrons. In addition, most CPs have numerous attractive properties for biomedical applications, including the ability to transfer charges, to entrap and release biological molecules, and the potential to vary their chemical, electrical, and physical properties. Even though there has been significant progress, many biomedical issues remain unexplored, especially the interaction between different cell types (e.g., neurons, fibroblasts, and osteoblasts) and substituted polythiophenes (PTs) in both the undoped and doped states. PTs are one of the most widely studied CPs, therefore ample knowledge exists on their chemical, electrical, and physical properties. They also have great potential for biomedical applications as they have been used as biosensors, molecular actuators, and cell support substrates.

The *overall objective* of this work is to assess the suitability of poly(3-octylthiophene) (P3OT) to sustain MC3T3-E1 osteoblast attachment and growth. The *central hypothesis* is that specific P3OT film properties (e.g., thickness, film preparation conditions, and level of doping) are able to regulate osteoblast functions (e.g., attachment and proliferation). Discrete and combinatorial techniques were utilized in this work to prepare and characterize thin films of P3OT, a semiconductor in its undoped state, and to

study its interaction with MC3T3-E1 osteoblasts. The MC3T3-E1 cell line was chosen because it is well understood, is known to exhibit a developmental sequence analogous to osteoblasts in bone tissue, and because of previous success in regulating proliferation and attachment using conducting substrates.

In this work we demonstrate that P3OT is a suitable surface to sustain MC3T3-E1 attachment and proliferation with no observed cytotoxicity. We show that P3OT has an effect on MC3T3-E1 attachment and proliferation as area, circularity, and proliferation ratio are significantly different for P3OT compared to control surfaces. We also demonstrate that P3OT doping and film preparation conditions have an effect on osteoblast attachment and proliferation but that thickness over a low and high range does not affect osteoblast functions.

This work is *significant* because it contributes to the growing area of conducting polymers in biomedical applications and establishes P3OT as a potential cell substrate that sustains MC3T3-E1 attachment and promotes high levels of cell proliferation.

CHAPTER 1

INTRODUCTION

1.1 Specific Aims

CPs are attractive because they combine the electrical and optical properties of metals with properties associated with conventional polymers (i.e., ease of synthesis and processability). There are many advantages of using CPs for biomedical applications; most CPs are biocompatible, able to transfer charge from a biochemical reaction, able to entrap and release biological molecules, and their physical, chemical, and electrical properties can be modified to suit specific applications. Substituted polythiophenes (PTs) are a class of CPs that have been used as neural electrodes, biosensors, molecular actuators, and cell support substrates. Although there has been significant progress on the use of substituted PTs for biomedical applications, more information is needed in order to engineer optimal biomedical devices. For example, it is necessary to understand the interaction between different cell types (e.g., neurons, fibroblasts, and osteoblasts) and substituted PTs in both their undoped and doped states.

The *objective* of this research was to assess the suitability of P3OT to sustain MC3T3-E1 osteoblasts attachment and growth. The *central hypothesis* is that specific P3OT film properties (e.g., thickness, film preparation conditions, and level of doping) are able to regulate osteoblast functions (e.g., attachment and proliferation). Using conventional and combinatorial methods to prepare, modify, and characterize P3OT thin films, immunofluorescent labeling assays for cell attachment and proliferation, and high-throughput fluorescent microscopy and image analysis the following aims have been addressed:

1. Assess the suitability of P3OT to sustain osteoblast attachment and proliferation

Constant thickness P3OT films (30 nm) were prepared using a knife-edge coating apparatus and characterized by thickness, contact angle, topography, FTIR, and UV-Vis absorption measurements. MC3T3-E1 cell attachment and proliferation were assessed on P3OT and control surfaces by fluorescent labeling of F-actin fibers and 5-Bromo-2'-deoxyuridine (BrdU) incorporation, respectively. Potential toxicological factors were investigated by pre-soaking P3OT films in media to remove leachants.

Hypothesis: Conducting polymers can be used to regulate cell functions.

2. Investigate the effect of P3OT doping on the attachment and proliferation of osteoblasts

P3OT constant thickness films (30 nm) were modified by doping with two concentrations of ferric chloride (FeCl_3) to assess the effect of doping on the attachment and proliferation of osteoblasts. Undoped and doped films were characterized by contact angle, topography, FTIR, and UV-Vis absorption measurements. MC3T3-E1 cell attachment and proliferation were assessed on undoped and doped P3OT by fluorescent labeling of F-actin fibers and BrdU incorporation, respectively. Global and local metrics were used to measure cell density, area, circularity, and proliferation and to investigate cell contact effects on proliferation, respectively.

Hypothesis: Doping of P3OT can regulate osteoblast attachment and proliferation.

3. Investigate the effect of P3OT thickness and film preparation conditions on osteoblast attachment and proliferation

P3OT thin films were prepared using a knife-edge coating apparatus in two operation modes: constant thickness and thickness gradient. Attachment and proliferation were

assessed over two thickness ranges. Thickness gradient films were prepared for the high thickness range (130 – 200 nm) and discrete films were prepared for the low thicknesses (20, 30, and 50 nm). The effect of thermal annealing (annealed at 80°C vs. unannealed) and solvent used for film preparation (CHCl₃ vs. THF) on cell attachment was also assessed. MC3T3-E1 cell attachment and proliferation were assessed by fluorescent labeling of F-actin fibers and BrdU incorporation, respectively

Hypothesis: Thickness and film preparation conditions through their effects on surface forces and surface morphology can regulate osteoblast attachment and proliferation.

1.2 Thesis Outline

Chapter 2 provides detailed background information and describes the significance of studying the initial events (i.e., attachment and proliferation) that occur when cells interact with a conducting polymer. Chapter 3 addresses the suitability of P3OT to sustain attachment and proliferation of MC3T3-E1 osteoblasts. Chapter 4 addresses the effect of P3OT doping and doping concentration on the attachment and proliferation of MC3T3-E1 osteoblasts. Chapter 5 addresses the effect of P3OT thickness and film preparation conditions on the attachment and proliferation of MC3T3-E1 osteoblasts. Chapter 6 concludes with a summary of the important findings and provides future recommendations based on this work.

CHAPTER 2

BACKGROUND AND SIGNIFICANCE

2.1 Conducting polymers

The discovery of stable organic materials that could conduct electricity dates back to the 1960s,[1] but it was not until 1977 when three professors, Alan Heeger, Alan MacDiarmid and Hideki Shirakawa, reported on the high conductivities achieved by exposing polyacetylene to iodine vapors, that the first inherently conducting polymer was recognized.[2] In 2000 the three professors were awarded the Nobel prize in Chemistry for the discovery and development of electrically conductive polymers.[3] By doping polyacetylene with iodine they were able to achieve conductivities of 10^3 S/cm. For comparison, Teflon has a conductivity of 10^{-18} S/cm and silver and copper have a conductivity of 10^6 S/cm. A key property of conducting polymers (CPs) is the presence of conjugated double bonds along the backbone of the polymer (Figure 2.1).

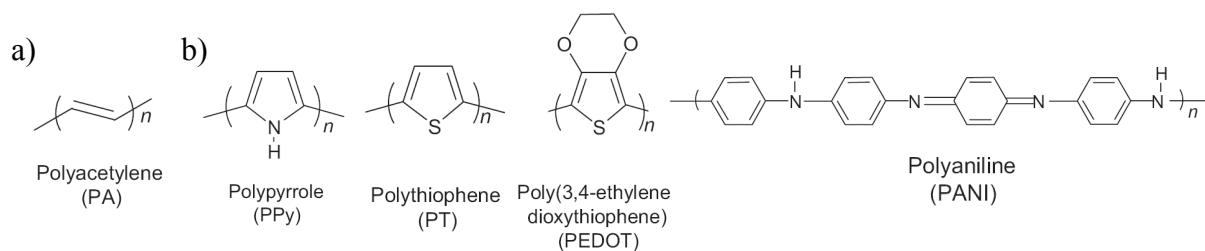


Figure 2.1. Chemical structures of common conducting polymers: a) polyacetylene and b) most commonly explored conducting polymers for biomedical applications.[4]

However, conjugation is not enough to render polymers conductive. In addition, charge carriers in the form of “holes” (a position where an electron is missing), allow charge to migrate rendering the polymer conductive.[3] Doping is the process of oxidizing (p-doping) or reducing (n-doping) the neutral polymer to form positively

charged or negatively charged defects, respectively.[5] Charge neutrality is maintained by a charged counter ion, which is usually derived from the doping agent.

CPs have electrical and optical properties similar to those of metals, but also exhibit properties associated with conventional polymers, such as the ease of synthesis and processing.[5, 6] This has given CPs a wide range of technological applications (e.g., light emitting diodes, electrochromic displays, transistors, solar cells, and photovoltaic devices),[7] and more recently in biological systems. CPs, such as the ones shown in Figure 2.1, have been used in many biomedical applications including tissue engineering,[8, 9] neural probes,[10, 11] biosensors,[12, 13] bio-actuators,[14, 15] and drug delivery devices.[16, 17]

For example, in the case of biosensors (Figure 2.2), conducting polymers act as the transducer converting a biochemical signal into an electronic signal. Biosensors can be classified into several categories depending on the transduction principle (e.g., amperometric, potentiometric, conductometric, optical, calorimetric, and piezoelectric). The most common types of biosensors are amperometric (measure current) and potentiometric (measure potential).

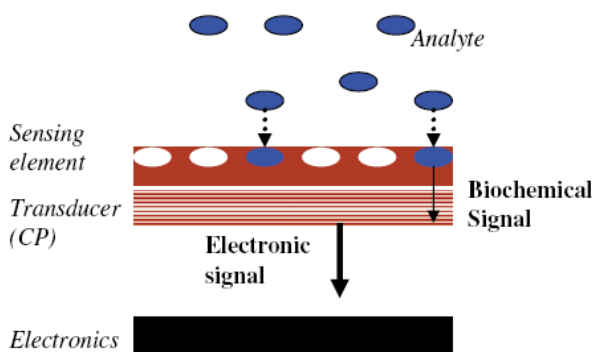


Figure 2.2. Schematic of a biosensor. A biological sensing element detects a specific analyte (e.g., enzyme, antibody) producing a biochemical signal that is transferred to the transducer (e.g., conducting polymer), which ultimately produces a digital electronic signal that is proportional to the amount of analyte present.[4]

In the case of bio-actuators (“artificial muscles”), conducting polymers act as “soft” materials by undergoing a change in volume upon electrical stimulation. Figure 2.3 shows an artificial muscle device developed by Otero et al.[14, 18] In this device two layers of polypyrrole (PPy) are placed in a triple layer arrangement separated by a non-conductive material. When a flow of current, in the presence of an aqueous electrolyte, is applied across the two PPy films a PPy film oxidizes and swells while the other PPy film reduces (expels ions) and shinks.

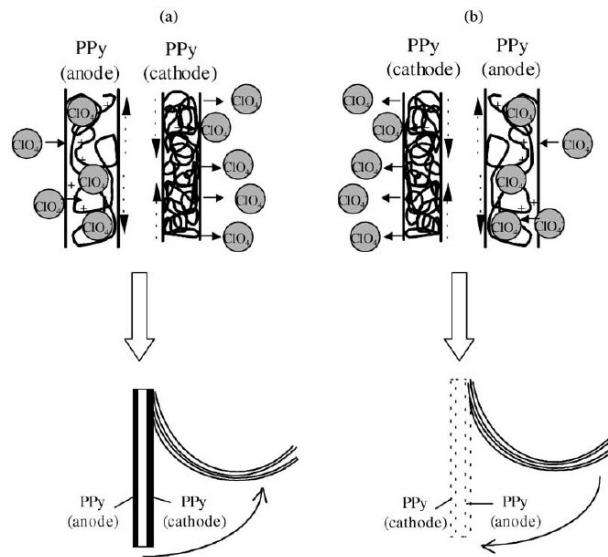


Figure 2.3. Schematic of an artificial muscle device.[14]

2.1.1 Substituted polythiophenes (PTs)

Substituted PTs are a class of CPs that have received significant attention due to the wide range of relevant electronic, electrochemical and optical applications.[19] Substituted PTs are of interest in biomedical applications because they can achieve high conductivities and they can be customized with a variety of functional groups that can be incorporated into their polymer backbones. For example, Widge et al.[20] used self-assembled monolayers of end-thiolated poly(3-(2-ethylhexyl)thiophene) as neural electrodes and Bera-Aberem et al.[21] developed biosensors from substituted PTs to

detect alkali metal ions and nucleic acids. Other substituted PTs have been used as cell support substrates for epithelial cells[22] and human ovarian cancer cells (HeLa cells).[23]

Poly(3-alkylthiophenes) (P3ATs) are a class of substituted PTs that have been synthesized and developed as environmentally stable, organic solvent-soluble semiconducting polymers.[5, 24, 25] The thiophene ring in 3-alkylthiophenes can be coupled with three different regioregularities: head-to-tail (HT) head-to-head (HH), and tail-to-tail (TT) (Figure 2.4). Regioregular, head-to-tail poly(3-substituted)thiophene can access a low energy planar conformation, leading to a highly conjugated polymer.[5]

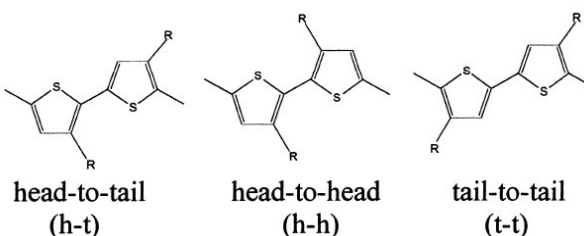


Figure 2.4. Different coupling of pairs of 3-alkylthiophene monomers.[26]

2.1.2 Poly(3-octylthiophene)

The poly(3-octylthiophene) (P3OT) (Figure 2.5) used in this work is an alkyl-substituted HT regioregular polythiophene that is of particular interest because of its reasonably good environmental stability, structural versatility, and electronic and optical applications.[27, 28] P3OT is a well characterized conducting polymer that has been used extensively in the fabrication of organic electronic devices.[29]

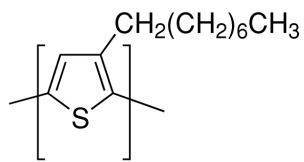


Figure 2.5. Chemical structure of poly(3-octylthiophene).

In addition, P3OT properties can be regulated by the extent of doping and dopant chemistry,[30-33] changes in thickness,[28, 34] solvent used for film preparation,[35, 36] and thermal annealing.[37, 38] For example, Chattopadhyay et al.[28, 34] recently showed that thickness strongly affects the surface energy of P3OT and others have explained the photo-physical, structural, and morphological changes that occur upon P3OT doping.[30, 33, 39-42] It has also been shown that different solvents have different effect on the structure (e.g., crystallinity) of P3OT films made from solution[35] and that thermal annealing has an effect on the surface morphology and physical properties of P3OT films.[37]

Despite the wealth of knowledge available for P3OT and P3ATs in general (e.g., charge transport mechanisms,[32] stability,[43] and structural and optical properties[27, 44-46]), their potential use in biomedical applications has not been exploited. To the best of our knowledge, P3OT has not been previously studied as a potential cell support substrate.

2.2 P3OT as substrate for cell attachment and proliferation

Most studies of CPs in biological fields involve nerve, muscle, bone, and cardiac cells, as these cell types are known to respond to electrical stimulation. In 1957 Fukada and Yasuda reported on the piezoelectric properties of bone[47] and since then, electrical stimulation has been explored as a treatment to stimulate in vivo bone regeneration and healing. Other studies in vitro have shown that osteoblasts (bone-forming cells) are stimulated when metals and conducting polymers are used as substrates.[48-50]

The immature mouse osteoblast-like (MC3T3-E1) cell line is typically used to study events such as attachment, proliferation, matrix synthesis, and matrix calcification

that occur in the interaction with a material surface.[51] This cell line is known to exhibit a developmental sequence analogous to osteoblasts in bone tissue, namely proliferation of undifferentiated osteoblast precursors followed by expression of differentiated osteoblast phenotype, and subsequent mineralization of extracellular matrix (ECM) when mature.[52] MC3T3-E1 cells are anchorage-dependent and therefore adhesion is a critical prerequisite for subsequent cell functions such as proliferation and protein expression. Once cells attach to a surface it is assumed they are well adapted to the culture if they are well-spread.[51] Three types of protein filaments called intermediate filaments, microtubules, and microfilaments form the cytoskeleton within mammalian cells.[53] Microfilaments are made of a structural protein called actin which polymerizes to form actin filaments (F-actin). F-actin can be labeled and identified using fluorescence-labeled phalloidin, which is a toxin that binds at the interface between subunits in F-actin.[53]

If cells attach, proliferation should be studied next, as it is a subsequent event that occurs in the interaction with the material surface. Studies to distinguish DNA synthesizing cells were traditionally based on the determination of incorporated radioactive DNA precursors such as tritiated thymidine. Currently, most cell proliferation studies are based on the incorporation of 5-bromo-2-deoxyuridine (BrdU), a thymidine analog, into newly replicated DNA. The application of monoclonal antibodies which react specifically with BrdU is well documented in the literature[54] as well as procedures for immunofluorescence staining.[55]

2.3 Modified P3OT as substrate for cell attachment and proliferation

CP modification tends to be specific for the desired biomedical application. In general, manipulation of CP properties (e.g., conductivity, roughness/topography, hydrophobicity, mechanical strength, degradability, redox stability) can be achieved through various methods (e.g., doping, incorporation of bioactive molecules by physical adsorption, entrapment, or covalent attachment). The process of doping can be exploited to modify CPs with desired properties (e.g., conductivity) to modulate cellular response. For example, Wong et al.[56] studied the effect of doped PPy on the attachment and spreading of endothelial cells. They showed that oxidized PPy resulted in cell spreading, whereas reduction of PPy to its neutral state led to cell rounding. Stauffer et al.[57] showed that PPy surfaces doped with two laminin peptide sequences improved neuronal growth and neurite extension compared to undoped PPy.

Variation in thickness,[28, 34] thermal annealing,[37] and solvent used for film preparation[35] can be used to modify CPs properties such as surface energy, morphology, and crystallinity. These modifications in turn can be used to alter cellular response. For example, Castano et al.[49] used admicellar polymerization to control PPy film thickness and modulate surface topography, thereby influencing mesenchymal stem cell adhesion and differentiation.

In this work we assessed the suitability of P3OT to sustain attachment and proliferation of osteoblasts by fluorescent labeling of F-actin fibers and BrdU incorporation, respectively. We also investigated the effect of P3OT doping, thickness, and film preparation conditions (i.e., thermal annealing and solvent used for film

preparation) on osteoblast attachment and proliferation. Details on the experimental procedures are given in each chapter.

CHAPTER 3

MC3T3-E1 ATTACHMENT AND PROLIFERATION ON

P3OT THIN FILMS

3.1 Abstract

A rapidly growing area in biomaterials is the use of conducting polymers (CPs) as biosensors, molecular actuators, and as cell support substrates. Although these materials have been extensively studied for the use in devices such as solar cells, organic light emitting diodes, and field-effect transistors, many biomedical applications remain unexplored. In this study we assessed the suitability of poly(3-octylthiophene) (P3OT) thin films (30 nm) to sustain attachment, spreading, and proliferation of MC3T3-E1 osteoblasts. Cell area correlated to surface wettability; it was larger in the more hydrophilic surface (TCPS) and lower in the more hydrophobic surface (P3OT). Cells on TCPS and Si—characterized via circularity—were rounder relative to P3OT. An interesting trend was observed for proliferation on P3OT: proliferation was suppressed two-fold after 48 hours but recovered at 72 hours to a value significantly higher than that on TCPS. Pre-soaking P3OT films with serum containing media or DPBS enhanced proliferation after 24 and 48 hours, and did not result in any cytotoxic effects of potential P3OT leachants. Overall, we conclude that P3OT is a viable substrate for osteoblast attachment and proliferation.

3.2 Introduction

The investigation of electrically conducting polymers (CPs) for use in biomedical applications is an expanding area of research.[4] A central goal is to utilize CPs to

incorporate chemical and physical cues capable of stimulating electrical and biological pathways that modulate cellular behavior. Most studies of CPs in biological fields involve nerve, muscle, bone, and cardiac cells, as these models are known to respond to electrical stimulation. CPs such as polypyrrole, polyaniline, and polythiophene are unique in that they have a conjugated structure that allows interchain hopping of electrons upon doping. Substituted polythiophenes have been studied as neural electrodes,[20] biosensors,[21, 58, 59] molecular actuators,[60] and as cell support substrates.[22, 23] Even though there has been significant progress, many biomedical issues remain unexplored, especially the interaction between different cell types and substituted polythiophenes in their undoped and doped states.

Poly(3-alkylthiophenes) (P3ATs) are a class of substituted polythiophenes that have been synthesized and developed as environmentally stable, organic solvent-soluble semiconducting polymers.[5, 24, 25] Despite the wealth of knowledge available for P3ATs (e.g., charge transport mechanisms,[32] stability,[43] and structural and optical properties[27, 44-46]) their potential use in biomedical applications has not been exploited. Regioregular, head-to-tail P3ATs can access a low energy planar conformation, leading to a highly conjugated structure.[5] Poly(3-octylthiophene) (P3OT) is an alkyl-substituted polythiophene that is of interest due to its good environmental stability, structural versatility, and electronic and optical applications.[27, 28] In this work we assessed the suitability of undoped P3OT to sustain osteoblasts (bone-forming cells) attachment and growth.

Osteoblasts were chosen for this study because they respond to electrical stimuli,[61] and this gives a rationale for expecting to be able to influence their function

when cultured on CPs. For example, electrical stimulation has been explored as a treatment to stimulate *in vivo* bone regeneration and healing[62-65] ever since the discovery of the piezoelectric properties of bone.[47] Other studies have shown that cell proliferation *in vitro* can be regulated by electrical stimulation[66] and that bone cells are influenced when conducting polymers are used as substrates.[48, 49, 61] The immature mouse osteoblast-like MC3T3-E1 cell line is typically used to study events such as attachment, proliferation, matrix synthesis, and matrix calcification that occur upon interaction with a material surface.[51] MC3T3-E1 cells are anchorage-dependent and thus adhesion is a critical prerequisite for subsequent cell functions such as proliferation and protein expression. In this work we study the initial events that occur when MC3T3-E1 cells are cultured on P3OT thin films (30 nm) by fluorescent labeling of F-actin fibers and 5-Bromo-2'-deoxyuridine (BrdU) incorporation to study cell attachment and proliferation, respectively. To the best of our knowledge, P3OT has not been previously studied as a potential cell support substrate.

3.3 Materials and Methods

3.3.1 Characterization of P3OT in solution

P3OT (>98.5% head-to-tail regioregular, Aldrich) physical and chemical properties were verified by several methods. Molecular weight (M_w) was measured by gel permeation chromatography (GPC) using a Waters 2690 separations module system with THF as solvent. The instrument was calibrated with polystyrene standards. ^1H nuclear magnetic resonance (NMR) spectroscopy was performed on a Bruker AMX400 spectrometer. The UV-Vis absorption spectra was obtained with a Beckman Coulter

DU® 800 spectrophotometer and the emission spectra was obtained with a fluorometer luminescent spectrometer (Photon Technology International).

3.3.2 Preparation of P3OT films

P3OT films were prepared from 0.7 wt% chloroform solution on 24 mm x 24 mm silicon chips (Silicon Inc.) that were previously cleaned in a Piranha solution (70% sulfuric acid – 30% hydrogen peroxide) followed by 48% hydrofluoric acid (HF) etching. HF etching was required to render the surface hydrophobic and prevent film delamination during the cell culture period. P3OT films were prepared using a knife-edge coating apparatus[67, 68] (Figure 3.1).

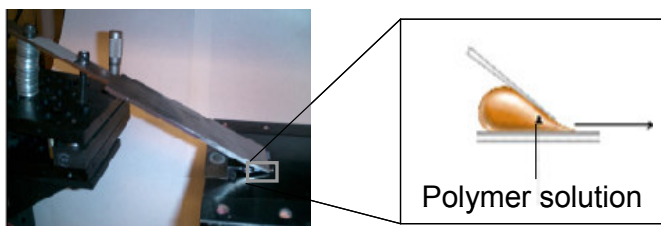


Figure 3.1. Image and schematic representation of the knife-edge coating apparatus used to prepare P3OT films.

Figure 3.2 shows two operating modes for the knife-edge coating apparatus.[69] Mode I consists of a maximum acceleration and deceleration with a plateaued velocity profile which results in a uniform thickness film. Mode II consists of a ramped velocity profile with a constant acceleration and a maximum deceleration. The result of this mode is a thickness gradient film in which the steepness of the gradient is controlled by the acceleration of the stage. Here we prepared discrete (30 nm) P3OT films using the constant thickness mode. After coating, films were kept under vacuum at room temperature for several days to remove residual solvent.

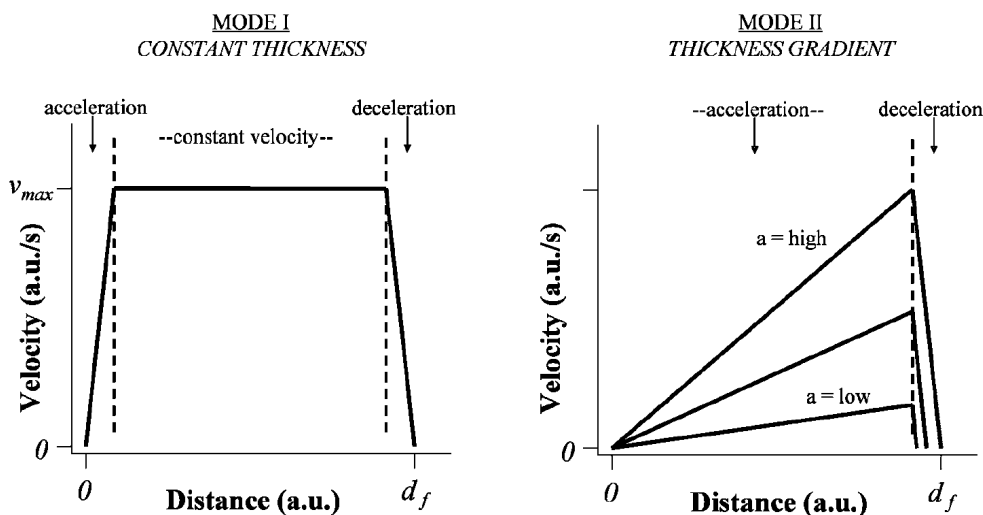


Figure 3.2. Schematic of two operating modes for the knife-edge coating apparatus.[69]

3.3.3 Characterization of P3OT films

Film thickness was measured using a high-throughput UV-Vis-NIR reflectance interferometer (Stellar Net EPP 2000). Surface topography characterization was performed by non-contact mode atomic force microscopy (AFM) with an Explorer scanning probe microscope (Veeco Instruments). Root-mean-square (RMS) roughness for a 10 x 10 μm scan size was calculated using the instrument's software. The elemental composition of P3OT films was determined by X-ray photoelectron spectroscopy (XPS) using a Physical Electronics PHI 1600 XPS system and water contact angle was measured using a VCA 2500 XE contact angle system (AST Products, Inc.).

3.3.4 Cell culture

MC3T3-E1 osteoblast-like cells (Riken Cell Bank, Japan) were cultured in alpha modification of Eagle's minimum essential medium (α -MEM) (Mediatech, Inc.) supplemented with 10% fetal bovine serum (FBS) (ATCC) and 1% penicillin-streptomycin (Mediatech, Inc.) at 37°C in a fully humidified atmosphere at 5% CO_2 . Prior to seeding, cells were washed with Dulbecco's Phosphate Buffered Saline (DPBS)

without Ca^{2+} and Mg^{2+} (Mediatech, Inc.) and trypsinized with 0.05% Trypsin/0.53mM EDTA in HBSS (Mediatech, Inc.). P3OT films were placed in Costar six-well microplates (Corning, Inc.) and sterilized by immersion in a 70% ethanol solution for 30 min followed by 3 washes of DPBS with Ca^{2+} and Mg^{2+} (5 min each). Cells, at passage 6, were seeded at a density of 5000 cells/cm². Cells were cultured at identical conditions on silicon wafers (Si) and tissue culture polystyrene (TCPS) wells as controls.

3.3.5 Cell attachment and spreading

Cell attachment and spreading were observed by fluorescent labeling of F-actin fibers with Alexa Fluor 488 phalloidin (Invitrogen) 4 hours after seeding. Cells were fixed in 3.6% paraformaldehyde (w/v) for 10 min and then permeabilized with 0.1% Triton X-100 in 1% BSA/PBS for 5 min. F-actin fibers were stained with Alexa Fluor 488 phalloidin (Invitrogen) in 1% BSA/PBS at a proportion of 1:20 for 30 min at room temperature. Cells were washed with PBS and cell nuclei were counterstained with Hoechst (Invitrogen) at a proportion of 1:10,000 in water for 15 min at room temperature.

3.3.6 Cell proliferation

Cell proliferation was assayed at 24, 48, and 72 hours using 5-Bromo-2'-deoxyuridine (BrdU) (Sigma), a thymidine analog that incorporates into newly replicated DNA. BrdU (10 μM) was added to the cell culture media 1 hour prior to cell fixation. Cells were fixed with 70% ethanol for 30 min and then treated with 0.07N NaOH for 2 minutes followed by immersion in PBS (pH 8.5). Cells were then incubated for 30 min in a humidified chamber with monoclonal anti-BrdU (Becton Dickinson) mixed with 0.5% Tween 20/PBS at proportion of 20:50. Following washing with PBS, cells were incubated in Alexa Fluor 488 conjugated goat anti-mouse IgG antibody (Invitrogen) at a

proportion of 1:200 in PBS. After washing with PBS cell nuclei were counterstained with Hoechst (Invitrogen) at a proportion of 1:10,000 in water for 15 min.

3.3.7 Leaching experiments

To determine the effect of pre-soaking the surface on cell proliferation, P3OT films were sterilized as previously described and submerged in either complete media (α -MEM supplemented with 10%FBS and 1% penicillin-streptomycin) or DPBS with Ca^{2+} and Mg^{2+} for 48 hours prior to cell seeding. After pre-soaking, films were washed with DPBS with Ca^{2+} and Mg^{2+} and cells were seeded as previously described. Cell proliferation was assayed at 24 and 48 hours after culture. Cell culture media used to pre-soak P3OT films was used to culture cells on TCPS to determine the effect of possible soluble components leached from P3OT on cell proliferation. After pre-soaking P3OT films for 48 hours, the cell culture media was withdrawn and added to TCPS wells. Cells were seeded, cultured for 24 and 48 hours, and tested for proliferation.

3.3.8 Image acquisition and analysis

Cell attachment, spreading, and proliferation were assayed by fluorescence microscopy with an Olympus BX51 upright microscope equipped with a translation stage. The samples were imaged in a (13 x 4) grid at a magnification of 10X. Two fluorescent images were captured at each grid position: (1) a green channel image for Alexa Fluor 488 phalloidin (F-actin, attachment experiments) or Alexa Fluor 488 conjugated antibody (BrdU, proliferation experiments); and (2) a blue channel image of Hoechst-stained cell nuclei. For the attachment experiments, green images were used to determine cell area and circularity and blue images were used to determine cell number. Values of cell area and circularity represent ~2000 cells analyzed for each surface. Cells

were scored for proliferation as the ratio of cells positive for BrdU incorporation (green channel images) relative to cell nuclei (blue channel images).

Image processing was carried out with ImageJ. A demonstration of image capture and analysis for the attachment experiments is shown in Figure 3.3. ImageJ was used to open and create masks of green channel images (cell cytoskeleton) and blue channel images (cell nuclei). Area (pixels²) and circularity values were displayed in the output screen.

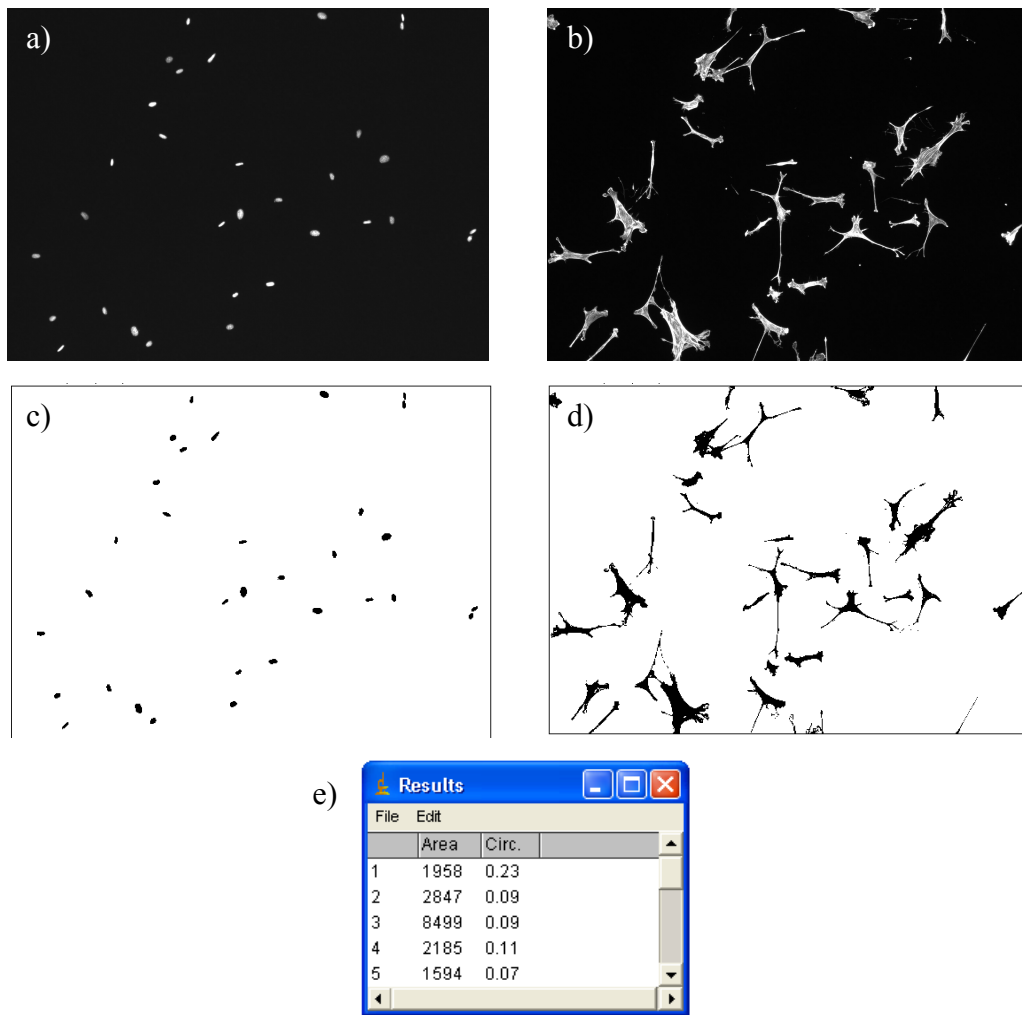


Figure 3.3. Demonstration of the image capture and analysis for the attachment experiments: a) blue channel image, b) green channel image, c-d) masks of the blue and green channel images, and e) output of results for area and circularity.

Statistical analysis was carried out with Minitab software. Figures 3.4 and 3.5 show representative Minitab graphical summary outputs of cell area and proliferation, respectively. The graphical summary of Minitab includes four graphs: histogram of data with an overlaid normal curve, boxplot, 95% confidence intervals for the mean, and 95% confidence intervals for the median. It also includes the Anderson-Darling normality test, a table of descriptive statistics, and the 95% confidence intervals for the mean, median, and standard deviation. Cell density, area, and circularity medians were compared using the Mann-Whitney nonparametric test because variances were not equal and values were not normally distributed; $p < 0.05$ was considered significant. Proliferation ratio means were compared by performing 2-sample t-tests; $p < 0.05$ was considered significant. All results are expressed as medians or means \pm 95% confidence intervals.

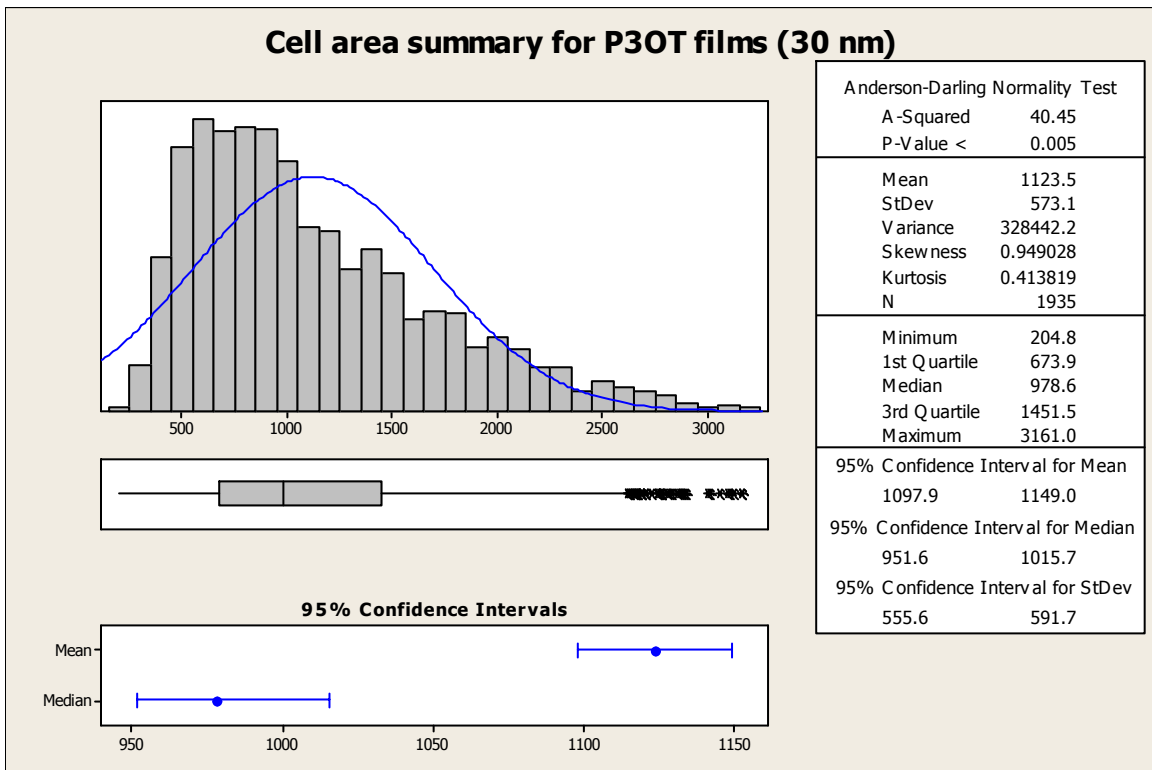


Figure 3.4. Representative Minitab graphical summary output for cell area on P3OT films.

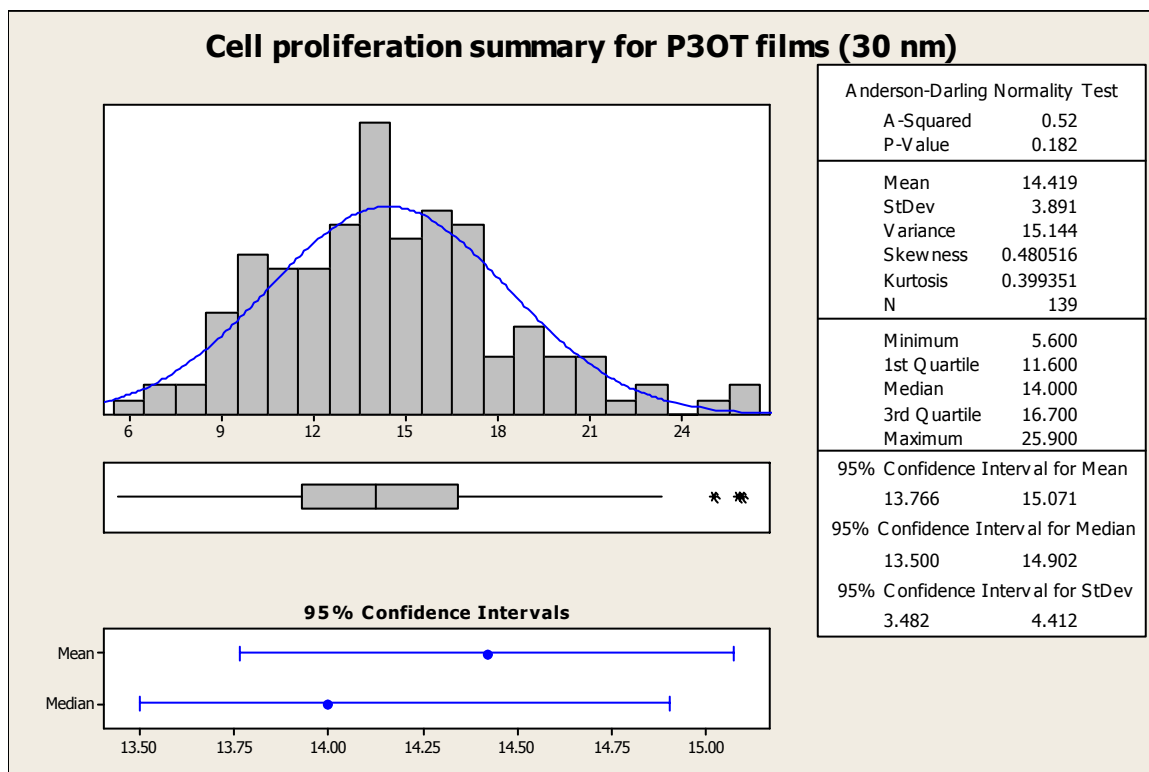


Figure 3.5. Representative Minitab graphical summary output for cell proliferation on P3OT films.

3.4 Results and Discussion

3.4.1 P3OT characterization

The P3OT M_w obtained from GPC was 76,770. The chemical structure and regioregularity was verified with NMR spectroscopy. The thiophene ring in 3-alkylthiophenes can be coupled with three different regioregularities: head-to-tail (HT) head-to-head (HH), and tail-to-tail (TT) which results in 4 possible triad regioisomers: HT-HT, TT-HT, HT-HH, and TT-HH.[5] Therefore, the proton in the 4-position of the thiophene ring bears 4 different chemical environments depending on the regioregularity of the polymer. Figure 3.6 shows the ^1H NMR spectra for P3OT in solution. A single peak is observed at 6.96 ppm which corresponds to the HT-HT structure of the polymer.[70]

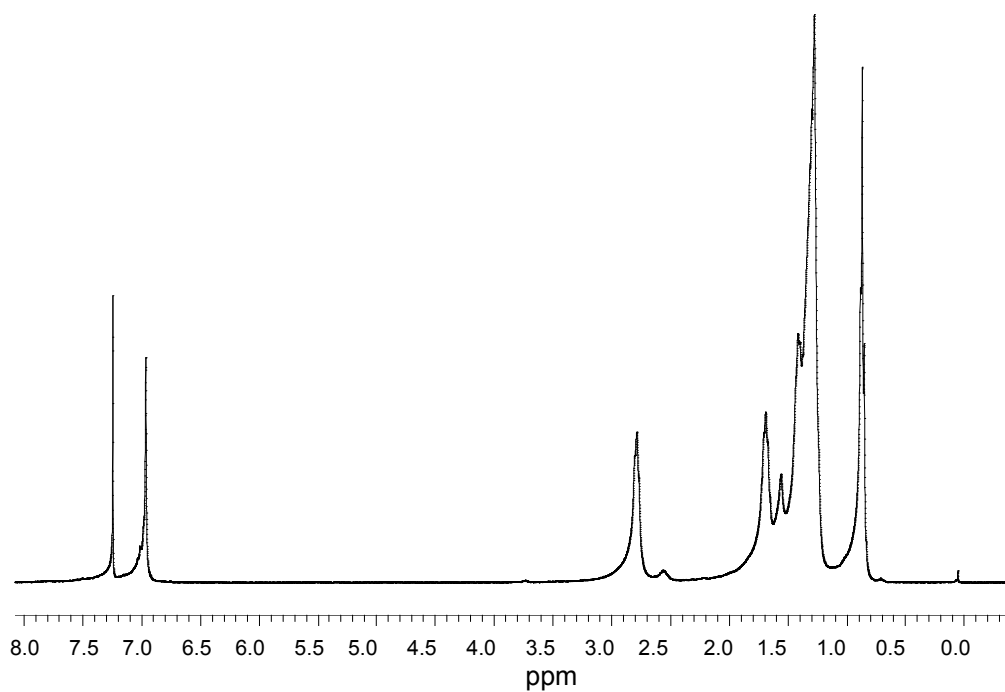


Figure 3.6. ^1H NMR spectra of regioregular P3OT in CDCl_3 .

Figure 3.7 shows the UV-Vis absorbance spectra for P3OT in CHCl_3 . A maximum absorption is observed at 449 nm, which correlates to what is expected for regioregular HT P3ATs in solution.[70]

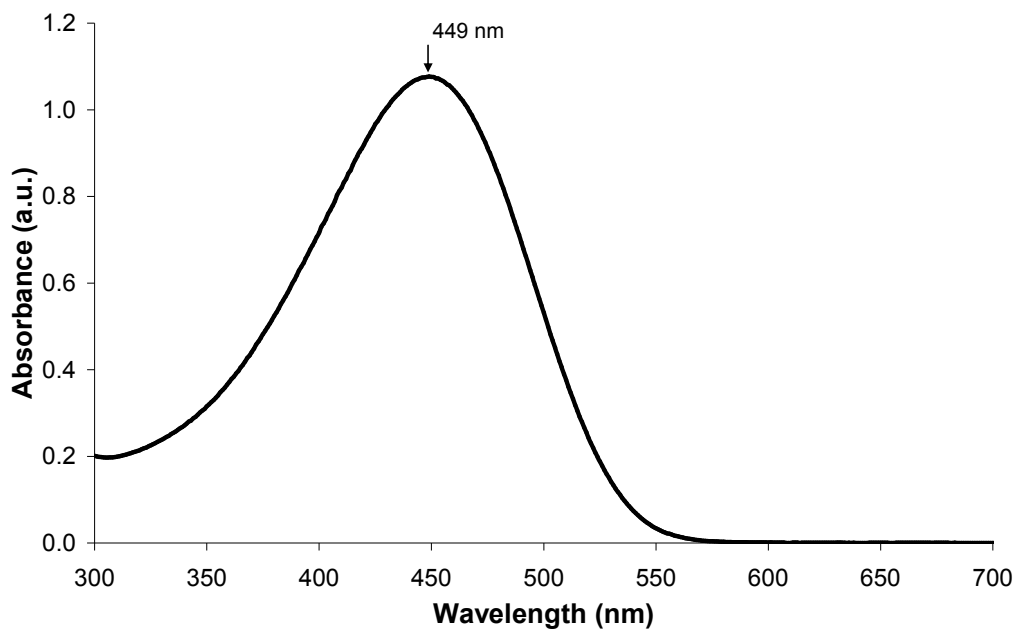


Figure 3.7. UV-Vis absorption spectra of P3OT in solution.

The emission spectra for P3OT in CHCl_3 is shown in Figure 3.8. Chloroform solutions of regioregular P3ATs give a bright yellow fluorescence with a maximum emission wavelength of 570 nm, which we observe at 578 nm and corresponds to the onset of the π - π^* transition of the electronic absorption spectra.[70]

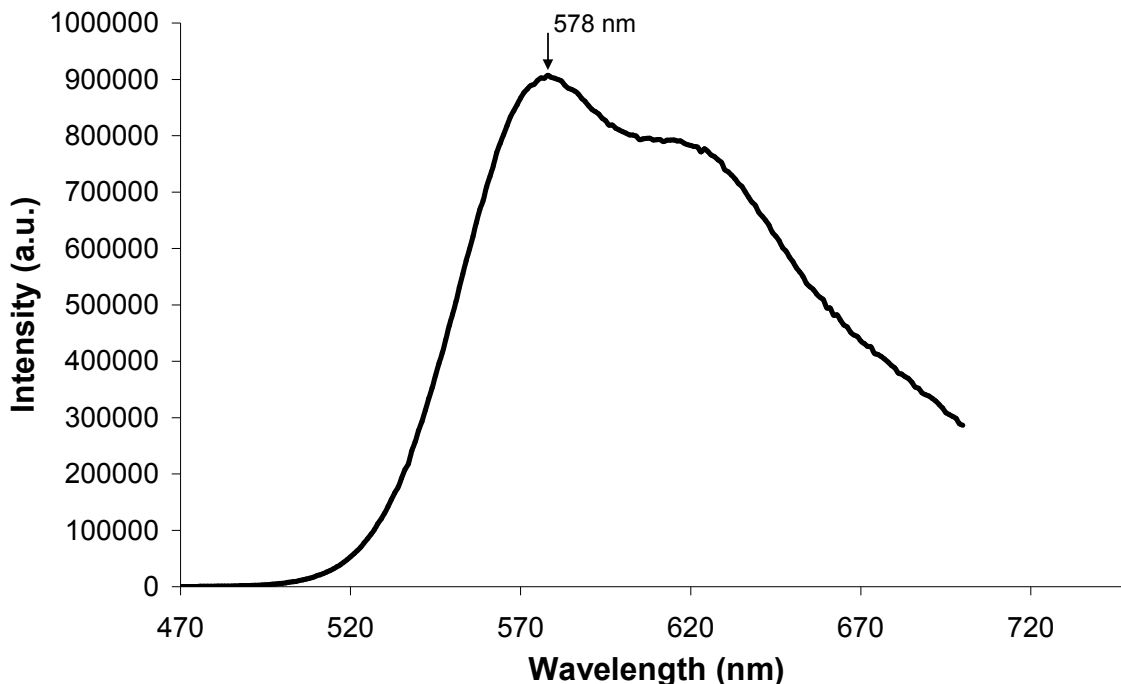


Figure 3.8. Emission spectra of P3OT in solution.

3.4.2 Surface characterization

Figure 3.9 shows a representative thickness plot for P3OT films. Film thickness was $30 \text{ nm} \pm 2 \text{ nm}$ for all films, which shows the precise control and repeatability achieved in the preparation of P3OT films. The RMS value for P3OT films was 0.759 nm. The XPS spectra obtained for P3OT films corroborates the purity of the polymer as only carbon and sulfur peaks were observed (Figure A.1). Water contact angles were

$106.6^\circ \pm 0.3^\circ$, $64.8^\circ \pm 1.5^\circ$, and $45.3^\circ \pm 0.3^\circ$ for P3OT, Si, and TCPS, respectively. Figure 3.10 shows a representative image of the water contact angle obtained for P3OT.

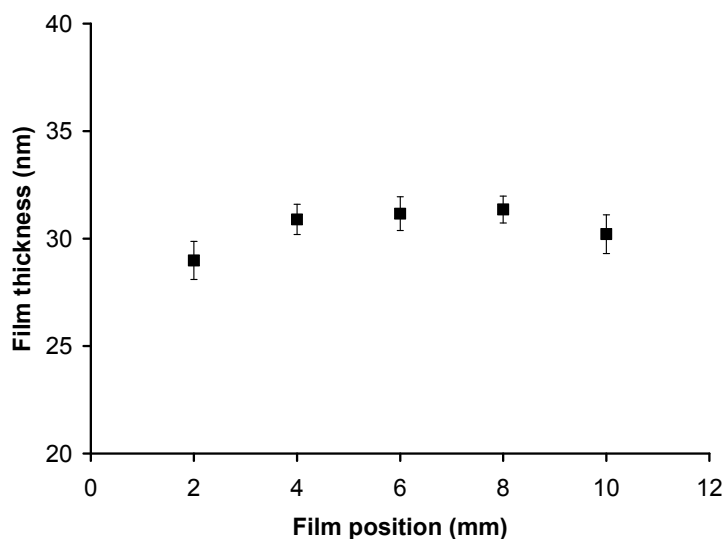


Figure 3.9. Representative film thickness as a function of P3OT film position. Typical thickness was $30 \text{ nm} \pm 2 \text{ nm}$. Values are presented as mean \pm SEM.

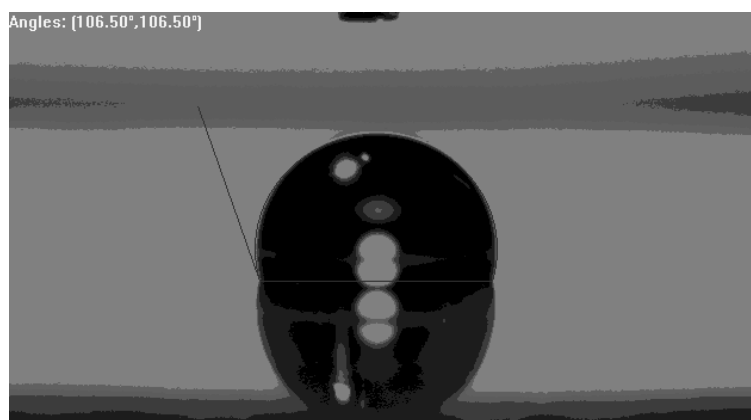


Figure 3.10. Representative water contact angle for P3OT ($106.6^\circ \pm 0.3^\circ$). Angles were measured using the instrument's software.

3.4.3 Cell attachment and spreading

Cell attachment density 4 hours after seeding is shown in Figure 3.11. The number of adherent cells was significantly greater ($p < 0.05$) on Si and TCPS (~ 4100 cells/cm²) compared to P3OT (~ 3000 cells/cm²).

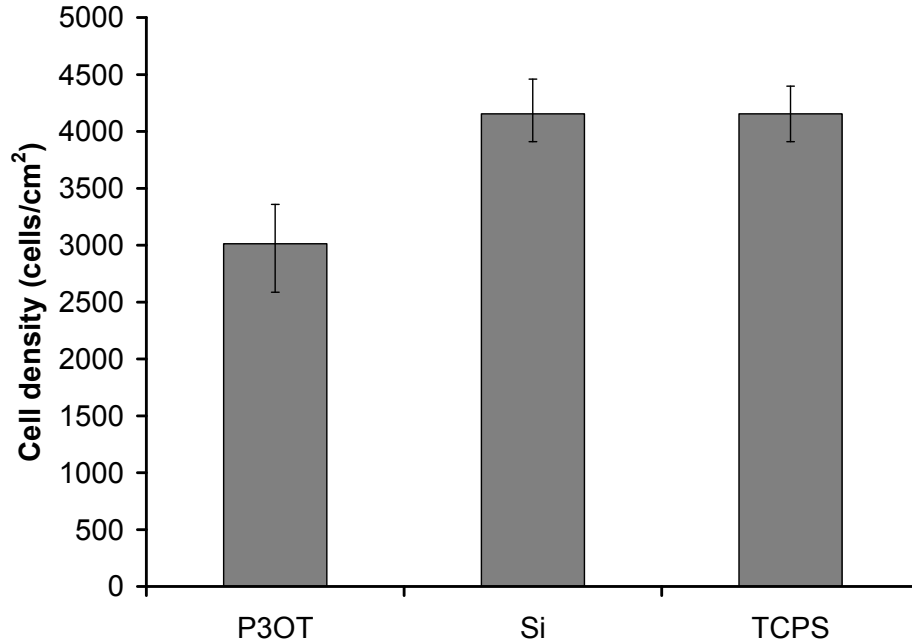


Figure 3.11. MC3T3-E1 cell attachment density on P3OT, Si, and TCPS 4 hours after seeding. Values are presented as median \pm 95% confidence intervals.

Since cell shape is tightly coupled with cell growth,[71, 72] cell area and circularity were also determined. Figure 3.12 shows representative images of F-actin labeled cells on P3OT, Si, and TCPS. Cells presented a high level of cytoskeletal organization characterized by a complex network of actin stress fibers. Although cells exhibited various shapes on all the surfaces, cell area showed significant dependence on surface type. Cell area and circularity was only determined for isolated cells (i.e., cells not touching any other cells).

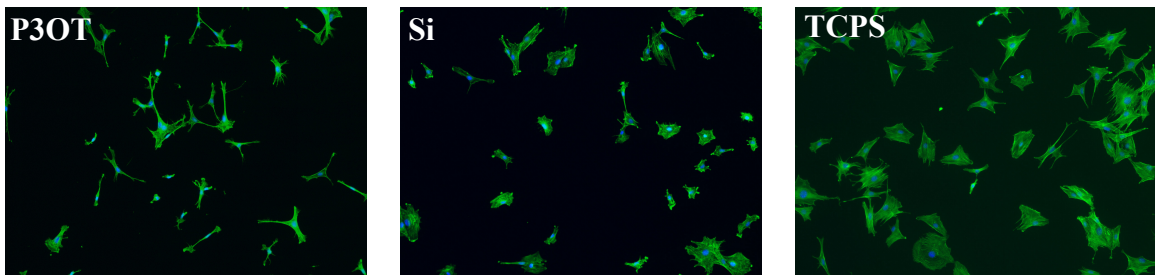


Figure 3.12. F-actin visualization of Alexa Fluor 488 phalloidin-stained MC3T3-E1 osteoblasts adhered on P3OT, Si, and TCPS. Image width is 1280 μ m.

Cell area was highest on TCPS ($\sim 2500 \mu\text{m}^2$) followed by Si ($\sim 1500 \mu\text{m}^2$) and P3OT ($\sim 1000 \mu\text{m}^2$) (Figure 3.13). This result correlates with surface wettability measurements as greater cell area was observed on the more hydrophilic surface (TCPS) and lower cell area was observed on the more hydrophobic surface (P3OT) (Figure 3.14).

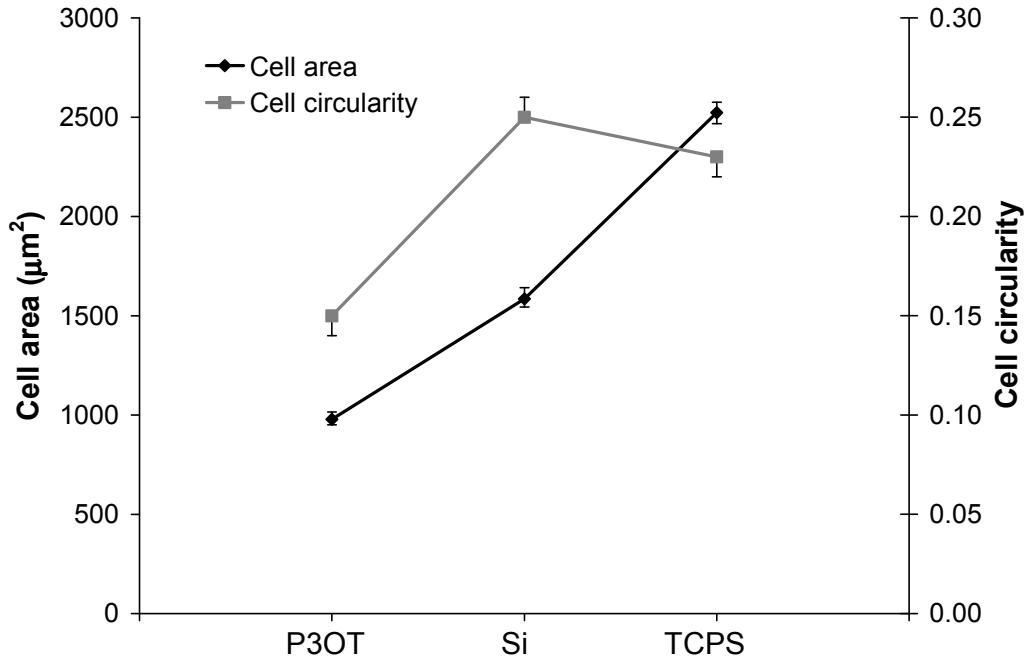


Figure 3.13. Area and circularity of MC3T3-E1 cells after 4 hours of culture on P3OT, Si, and TCPS. Values are presented as median \pm 95% confidence intervals.

This finding is consistent with what other studies have shown regarding surface wettability and cell area.[73, 74] Cell circularity (equation 3.1), a metric that compares cell aspect to that of a circle of the same area, was used to quantify cell spreading. A circularity value of 1 indicates a perfect circle and a value approaching 0 indicates an increasingly elongated polygon.

$$Circularity = 4\pi \left[\frac{area}{perimeter^2} \right] \quad (3.1)$$

Cells on Si and TCPS showed increased spreading and rounder morphologies than on P3OT where cells were more elongated. Circularity median values were 0.15, 0.25, and 0.23 for P3OT, Si, and TCPS, respectively (Figure 3.13). Although in the present study cell area was correlated to surface wettability, no correlation was observed for cell circularity. It has been proposed that MC3T3-E1 cell morphology (aspect ratio) varies with surface chemistry rather than general surface properties such as wettability.[75] This could provide an explanation for the results observed, as P3OT, Si, and TCPS present three distinct surface chemistries.

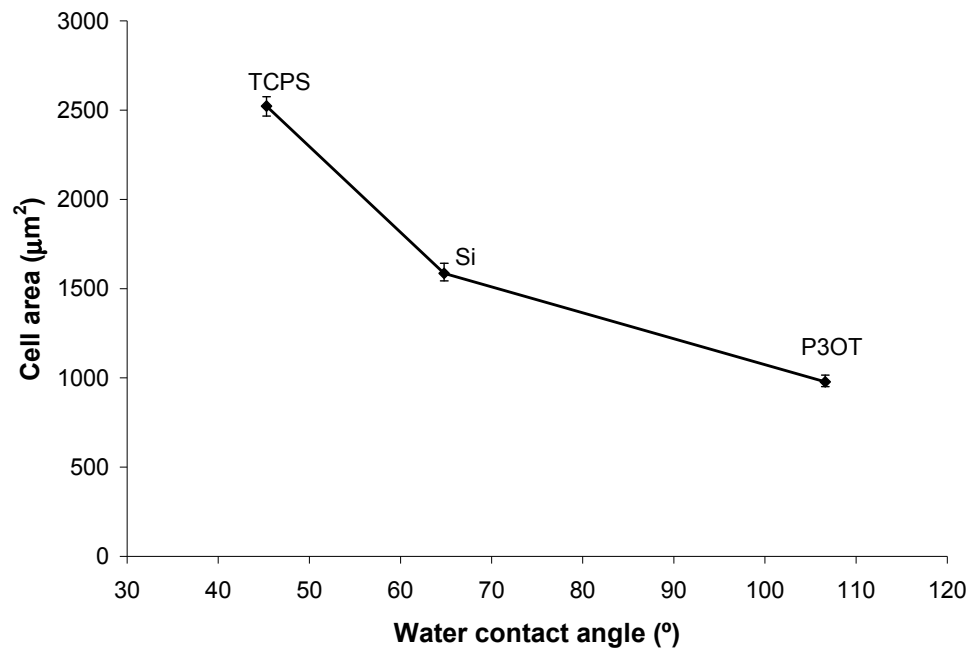


Figure 3.14. Relationship between water contact angle and cell area for P3OT, Si, and TCPS.

3.4.4 Cell proliferation

Figure 3.15 shows representative images of: a) blue channel image (cell nuclei), b) green channel image (cells positive for BrdU incorporation), and c) overlap green and blue channel images.

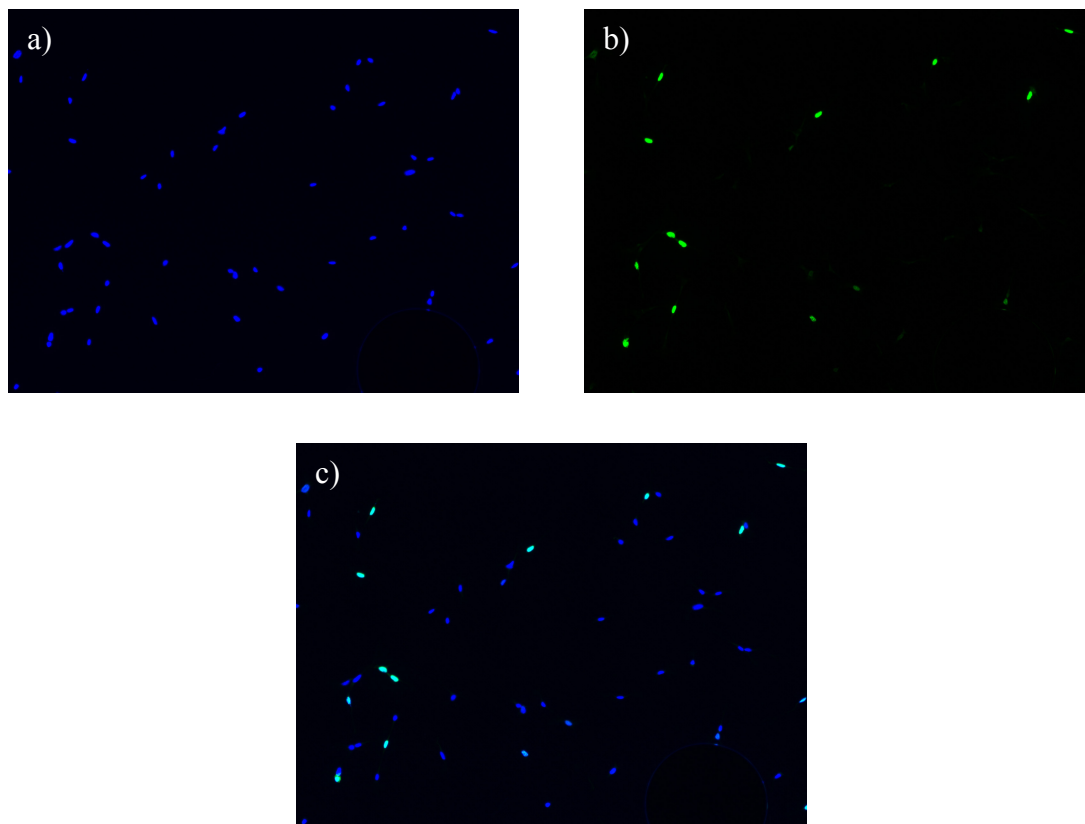


Figure 3.15. Representative fluorescent images of cells cultured on P3OT films: a) cell nuclei, b) cells positive for BrdU incorporation, and c) overlap of cell nuclei and proliferating cells.

Figure 3.16 shows the proliferation ratio (equation 3.2) of MC3T3-E1 cells after 24, 48, and 72 hours of culture on P3OT, Si, and TCPS.

$$\text{Proliferation ratio} = \frac{\text{Proliferating cells}}{\text{Total \# cells}} \times 100 \quad (3.2)$$

The proliferation ratio on P3OT after 24 hours of culture (28%) was comparable to the proliferation ratio on TCPS (26%), but lower than that on Si (31%, $p < 0.05$). Results at 48 hours showed higher proliferation on Si (30%) and TCPS (20%) compared to P3OT (13%, $p < 0.05$). Then, at 72 hours P3OT showed significantly lower proliferation (24%) compared to Si (30%, $p < 0.05$) but significantly higher proliferation compared to TCPS (19%, $p < 0.05$). Hence, the trend in proliferation observed for P3OT

was a decrease by a factor of 2 after 48 hours followed by a 45% recovery at 72 hours. This trend was repeated using a different batch of P3OT conducted several months later as well. On the other hand, for Si and TCPS there was a decrease in proliferation at 48 hours, but the proliferation ratio did not change further at 72 hours.

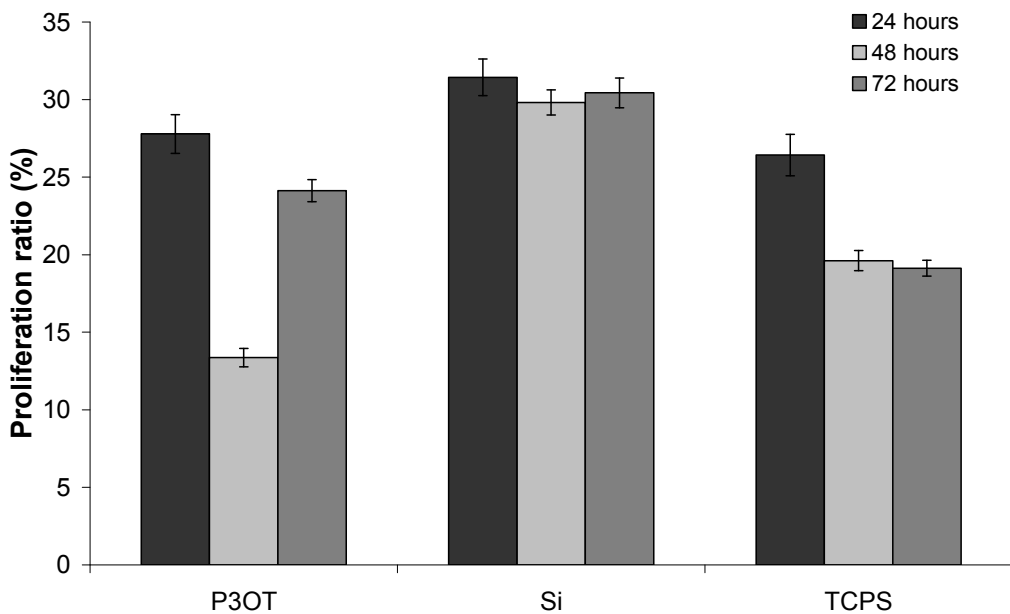


Figure 3.16. Proliferation ratio of MC3T3-E1 cells after 24, 48, and 72 hours of culture on P3OT, Si, and TCPS. Values are presented as mean \pm 95% confidence intervals.

In order to rule out the possibility that the 2-fold decrease in proliferation on P3OT after 48 hours was the result of leached contaminants, we ran the following tests: 1) pre-soaking P3OT films with serum containing media, 2) pre-soaking P3OT films with DPBS, and 3) culturing cells with pre-soaked media on TCPS. By pre-soaking P3OT films with cell culture media we expected to remove any possible soluble P3OT leachants.

Figure 3.17a shows the proliferation ratio of MC3T3-E1 cells cultured for 24 and 48 hours on untreated P3OT films and P3OT films that were previously soaked with serum containing media. The proliferation ratio was significantly higher in pre-soaked

P3OT compared to untreated P3OT at 24 and 48 hours after culture ($p < 0.05$). Pre-soaking P3OT films with media enhanced proliferation ratio by 13% and 45% at 24 and 48 hours, respectively. Pre-adsorbed serum proteins are known to play an important role in modifying surface characteristics which in turn modulate cell attachment and growth.[74, 76, 77] Therefore, as a non-serum-containing control, we pre-soaked P3OT films with DPBS. Figure 3.17b shows the proliferation ratio of MC3T3-E1 cells cultured for 24 and 48 hours on untreated P3OT films and P3OT films that were previously soaked with DPBS. Proliferation ratio was significantly higher in pre-soaked P3OT compared to untreated P3OT at 24 and 48 hours after culture ($p < 0.05$). Pre-soaking P3OT films with DPBS enhanced proliferation ratio by 19% and 30% at 24 and 48 hours, respectively. Since pre-soaking in both serum-containing media and non-serum DPBS resulted in roughly equivalent enhancements in proliferation, we conclude that the serum proteins did not interfere with the pre-soaking experiments. However, the mechanism by which pre-soaking P3OT films with DPBS enhances MC3T3-E1 proliferation remains unknown. One possibility is that soluble contaminants that act to suppress proliferation are removed (leached) from the P3OT during pre-soaking, and therefore not exposed to the cells when cultured. In addition, the pre-soaking solution may have a synergistic effect on the properties of the P3OT that improves its function as a cell growth substrate. For example, both α -MEM and DPBS contain inorganic salts such as CaCl_2 , KCl , NaCl , and NaH_2PO_4 that could potentially influence the properties of P3OT.

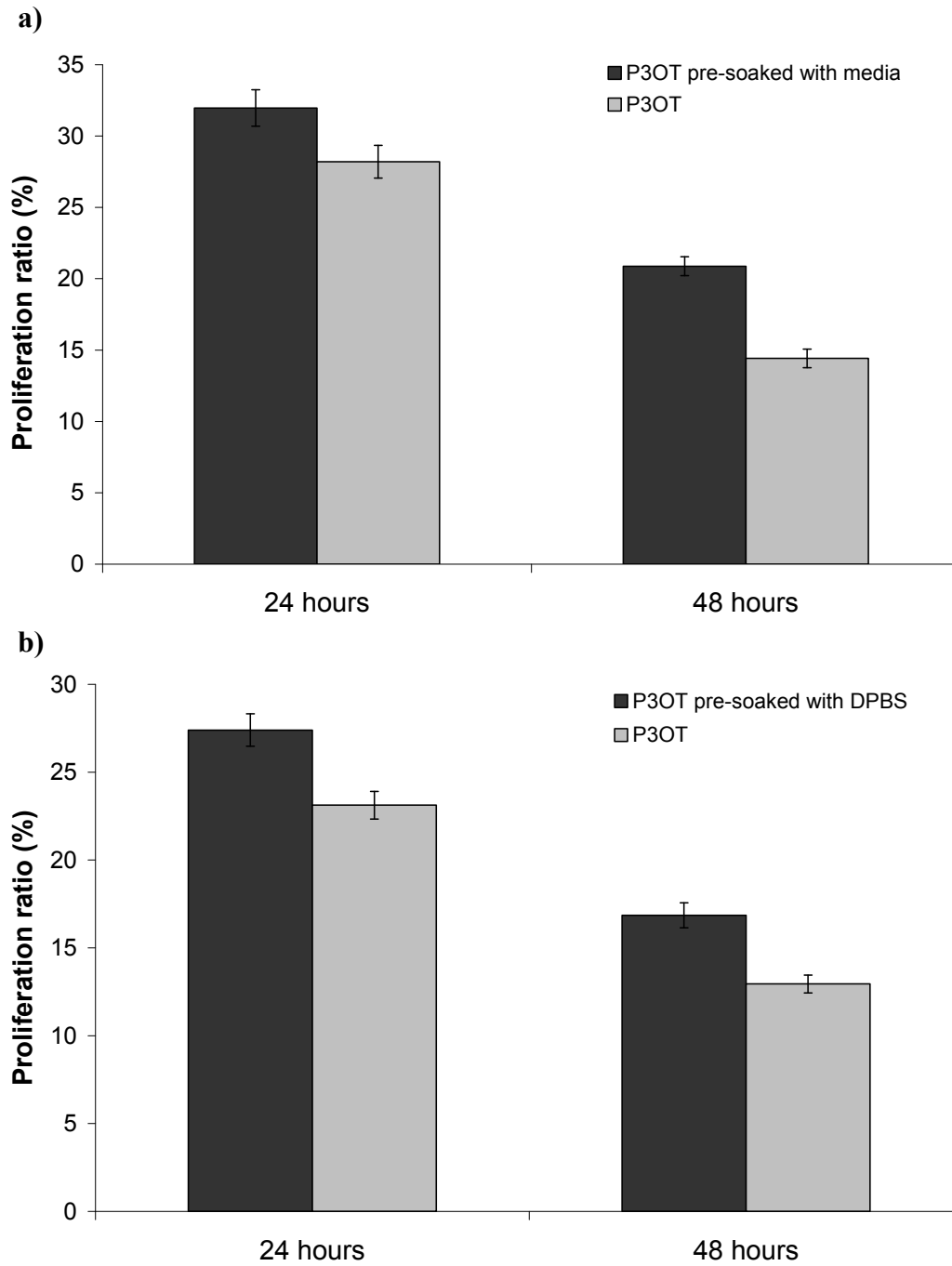


Figure 3.17. Proliferation ratio of MC3T3-E1 cells on P3OT pre-soaked with a) cell culture media and b) DPBS, after 24 and 48 hours of culture. Values are presented as mean \pm 95% confidence intervals.

To further investigate potential leaching of toxic substances from P3OT into the media, we pre-soaked P3OT films in cell culture media and used the pre-soaked media to culture cells on TCPS substrates. We used fresh media on TCPS as positive controls for this set of experiments. Figure 3.18 shows the proliferation ratio of MC3T3-E1 cells cultured for 24 and 48 hours on TCPS with P3OT-soaked and fresh media. There was no significant difference between the pre-soaked and fresh media suggesting the absence of a proliferation-suppressing soluble P3OT leachant. Or, if present, the leachant concentration is not high enough to suppress cell proliferation. While we cannot reach a definitive conclusion based on these results, they suggest that enhanced proliferation on pre-soaked P3OT was the result of a synergistic effect of the presoaking on the P3OT, rather than removal of possible cytotoxic components from P3OT.

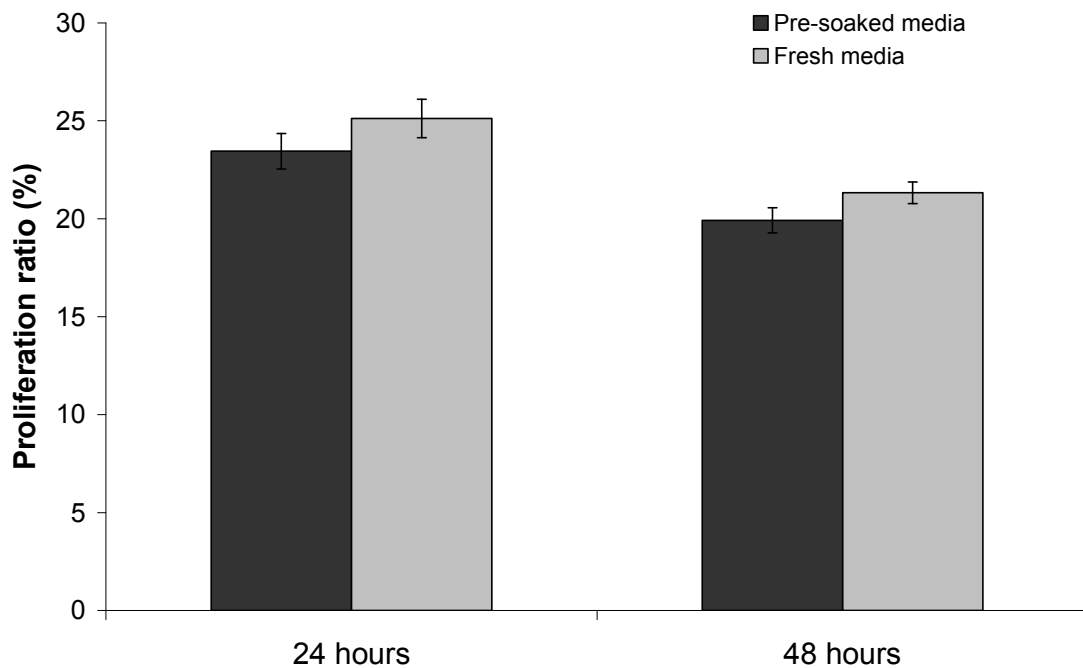


Figure 3.18. Proliferation ratio of MC3T3-E1 cells on TCPS with a) pre-soaked cell culture media and b) freshly prepared cell culture media, after 24 and 48 hours of culture. Values are presented as mean \pm 95% confidence intervals.

3.5 Conclusions

In summary, we demonstrated that P3OT is a suitable surface to sustain MC3T3-E1 attachment and proliferation with no cytotoxicity observed relative to TCPS. We showed that chemistry and wettability have an effect on MC3T3-E1 attachment and proliferation as cell area, circularity, and proliferation ratio varied for P3OT, Si, and TCPS. Cell proliferation on P3OT showed an interesting trend in which the proliferation ratio was reduced two-fold after 48 hours of culture but recovered after 72 hours to a value higher than that on TCPS. Pre-soaking P3OT films with either cell culture media or DPBS enhanced the proliferation ratio of MC3T3-E1 cells. This investigation contributes to the growing area of conducting polymers in biomedical applications and establishes P3OT as a potential cell substrate that sustains MC3T3-E1 attachment and promotes high levels of cell proliferation.

CHAPTER 4

EFFECT OF P3OT DOPING ON THE ATTACHMENT AND PROLIFERATION OF OSTEOBLASTS

4.1 Abstract

Conducting polymers (CPs) are of increasing interest as biomaterials. It is proposed that one may utilize the unique electrical properties and large surface forces of CPs to regulate cell functions, to stimulate cell activity, or to develop a sensor of cell activity. Since dopants are generally utilized to adjust conductivity in CPs, an interesting question is whether the extent of doping might be used to fine-tune desired functions of cultured cells. In the present work we studied the effect of doping poly(3-octylthiophene) (P3OT) with FeCl_3 on the attachment and proliferation of MC3T3-E1 osteoblasts. Analysis was performed using both global and local metrics of cell function. The global values of cell density and area correlated strongly with doping concentration. In addition, an unusual trend in proliferation (decrease in proliferation after 48 hours followed by a recovery after 72 hours) on undoped P3OT was diminished significantly upon doping. Local analysis showed that cells were sensitive to the presence of other cells on both undoped and doped P3OT and that contact inhibition of proliferation was observed for both surfaces.

4.2 Introduction

Conducting polymers (CPs) have been extensively studied for the use in devices such as solar cells,[78, 79] light emitting diodes,[27, 80] and field-effect transistors.[81,

82] Because of their ability to transfer charges and to stimulate electrical and biological pathways that trigger desired cellular responses, their use has recently expanded to biomedical devices such as biosensors,[83-85] molecular actuators,[60] and cell support substrates.[22, 23, 49] CPs are unique in that they have a conjugated electronic structure, rendering the undoped material to be semiconducting. One consequence of conjugation is unusually large van der Waals forces at the interface, the effects of which have been explored in previous work.[28, 34, 86] The addition of a suitable dopant increases conductivity significantly, by allowing interchain hopping of electrons. Doping is the process of oxidizing (p-doping) or reducing (n-doping) the neutral polymer to form a positively charged or a negatively charged defect, respectively.[5] Charge neutrality is maintained by a charged counter ion, which is usually derived from the doping agent.

Along with the unique surface properties exhibited by CPs, the extent of doping and dopant chemistry are additional features that might be exploited for biomedical applications. For example, Wong et al.[56] studied the effect of doped polypyrrole (PPy) on the attachment and spreading of endothelial cells. They showed that oxidized PPy resulted in cell spreading, whereas reduction of PPy to its neutral state led to cell rounding. Stauffer et al.[57] showed that PPy surfaces doped with two laminin peptide sequences improved neuronal growth and neurite extension compared to undoped PPy. These findings provide evidence that CPs can be tailored to elicit desired functions in cell types that are known to respond to electrical stimulation such as nerve, muscle, bone, and cardiac cells.

Substituted polythiophenes are a class of CPs with increasing potential for use in biomedical applications such as neural electrodes,[20] biosensors,[21, 58, 59] molecular

actuators,[60] and cell support substrates.[22, 23] In order to expand these applications the use of doped substituted polythiophenes to regulate cell functions should be explored. Numerous studies of poly(3-alkylthiophenes) such as poly(3-hexylthiophene) (P3HT) and poly(3-octylthiophene) (P3OT) have explained the photo-physical, structural, and morphological changes that occur upon doping.[30, 33, 39-42] In our previous work[86] we assessed the suitability of undoped P3OT to sustain attachment and proliferation of MC3T3-E1 osteoblasts. In this work we study the effect of doped P3OT on the attachment and proliferation of MC3T3-E1 cells. We doped P3OT thin films (30nm) with ferric chloride (FeCl_3), which has a relatively low cytotoxicity towards MC3T3-E1 cells[87, 88] and is one of the most stable P3OT dopants.[89] We studied the response of cell attachment and proliferation by fluorescent labeling of F-actin fibers and 5-Bromo-2'-deoxyuridine (BrdU) incorporation, respectively.

4.3 Materials and Methods

4.3.1 Preparation of P3OT films

P3OT (>98.5% head-to-tail regioregular, Aldrich) films were prepared from 0.7 wt% chloroform solution on 24 mm x 24 mm silicon chips (Silicon Inc.) that were previously cleaned in a Piranha solution (70% sulfuric acid – 30% hydrogen peroxide) followed by 48% hydrofluoric acid (HF) etching. HF etching was required to render the surface hydrophobic and prevent film delamination during the cell culture period. Films of discrete thickness (30 nm) were prepared using a knife-edge coating apparatus[67] and kept under vacuum at room temperature for several days to remove residual solvent.

4.3.2 Doping of P3OT films

Doping of P3OT films was performed by dipping the films in freshly prepared 0.001M and 0.125M solutions of anhydrous ferric chloride (FeCl_3) (Fisher) in nitromethane (CH_3NO_2) (Aldrich) for one hour at room temperature. The doped P3OT films were thoroughly washed with methanol and then dried with compressed nitrogen. This procedure has been shown to induce significant conductivity (4.9×10^{-4} S/cm and 2.9×10^{-2} S/cm for 0.001M FeCl_3 -doped P3OT and 0.125M FeCl_3 -doped P3OT, respectively) in P3OT films at room temperature.[33]

4.3.3 Characterization of P3OT films

Film thickness was measured using a high-throughput UV-Vis-NIR reflectance interferometer (Stellar Net EPP 2000). The UV-Vis spectra of undoped and doped films were obtained using a Cary 5000 Spectrophotometer (Varian Inc.). Surface topography characterization was performed by tapping mode atomic force microscopy (AFM) with an MFP-3D AFM system (Asylum Research). Root-mean-square (RMS) roughness for a $4 \times 4 \mu\text{m}$ scan size was calculated using the instrument's software. Structural characterization of the films was carried out using a Nicolet Nexus Fourier transform infrared (FTIR) spectrometer equipped with a GATR accessory. Water contact angle was measured with a VCA 2500 XE contact angle system (AST Products, Inc.).

4.3.4 Cell culture

MC3T3-E1 osteoblast-like cells (Riken Cell Bank, Japan) were cultured in alpha modification of Eagle's minimum essential medium (α -MEM) (Mediatech, Inc.) supplemented with 10% fetal bovine serum (FBS) (ATCC) and 1% penicillin-

streptomycin (Mediatech, Inc.) at 37°C in a fully humidified atmosphere at 5% CO₂. Prior to seeding, cells were washed with Dulbecco's Phosphate Buffered Saline (DPBS) without Ca²⁺ and Mg²⁺ (Mediatech, Inc.) and trypsinized with 0.05% Trypsin/0.53mM EDTA in HBSS (Mediatech, Inc.). Undoped and doped P3OT films were placed in Costar six-well microplates (Corning, Inc.) and sterilized by immersion in a 70% ethanol solution for 30 min followed by 3 washes of DPBS with Ca²⁺ and Mg²⁺ (5 min each). Cells, at passage 6, were seeded at a density of 5000 cells/cm².

4.3.5 Cell attachment and spreading

Cell attachment and spreading were observed by fluorescent labeling of F-actin fibers with Alexa Fluor 488 phalloidin (Invitrogen) 4 hours after seeding. Cells were fixed in 3.6% paraformaldehyde (w/v) for 10 min and then permeabilized with 0.1% Triton X-100 in 1% BSA/PBS for 5 min. F-actin fibers were stained with Alexa Fluor 488 phalloidin (Invitrogen) in 1% BSA/PBS at a proportion of 1:20 for 30 min at room temperature. Cells were washed with PBS and cell nuclei were counterstained with Hoechst (Invitrogen) at a proportion of 1:10,000 in water for 15 min at room temperature.

4.3.6 Cell proliferation

Cell proliferation was assayed at 24, 48, and 72 hours using 5-Bromo-2'-deoxyuridine (BrdU) (Sigma), a thymidine analog that incorporates into newly replicated DNA. BrdU (10 μM) was added to the cell culture media 1 hour prior to cell fixation. Cells were fixed with 70% ethanol for 30 min and then treated with 0.07N NaOH for 2 minutes followed by immersion in PBS (pH 8.5). Cells were then incubated for 30 min in a humidified chamber with monoclonal anti-BrdU (Becton Dickinson) mixed with 0.5% Tween 20/PBS at proportion of 20:50. Following washing with PBS, cells were

incubated in Alexa Fluor 488 conjugated goat anti-mouse IgG antibody (Invitrogen) at a proportion of 1:200 in PBS for 30 min at room temperature. After washing with PBS cell nuclei were counterstained with Hoechst (Invitrogen) at a proportion of 1:10,000 in water for 15 min.

4.3.7 Image acquisition and analysis

Cell attachment, spreading, and proliferation were assayed by fluorescence microscopy with an Olympus BX51 upright microscope equipped with a translation stage. The samples were imaged in a (13 x 4) grid at a magnification of 10X. Two fluorescent images were captured at each grid position: (1) a green channel image for Alexa Fluor 488 phalloidin (F-actin, attachment experiments) or Alexa Fluor 488 conjugated antibody (BrdU, proliferation experiments); and (2) a blue channel image of Hoechst-stained cell nuclei.

Attachment and proliferation images were analyzed using global and local metrics. Figure 4.1 illustrates the concept of global and local metrics for proliferation analysis. From a global approach a single value of cell density and proliferation is obtained for each image while in the local approach cell-to-cell distances (i.e., **proliferated-proliferated**, **proliferated-non-proliferated**) are used to describe the proliferative status of cells.

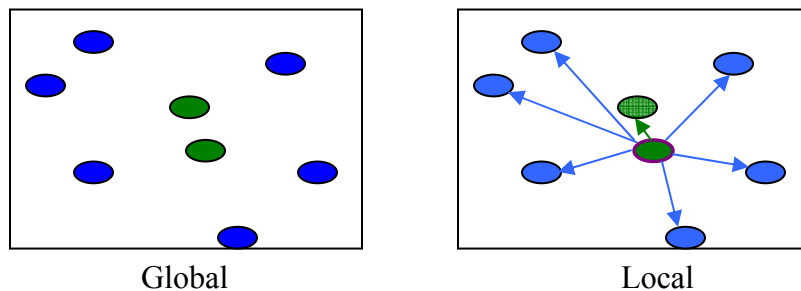


Figure 4.1. Global and local metrics to analyze proliferation. ● proliferated cells
● cells at rest.

In the attachment experiments, a global approach was used to measure cell density, area, and circularity. Green images were used to determine cell area and circularity and blue images were used to determine cell number. Values of cell area and circularity represent ~2000 cells analyzed for each surface. Cell density, area, and circularity medians were compared using the Mann-Whitney nonparametric test because variances were not equal and values were not normally distributed; $p < 0.05$ was considered significant. Global attachment results are expressed as medians \pm 95% confidence intervals. In the global approach for proliferation, a proliferation ratio was obtained for each image—cells were scored for proliferation as the ratio of cells positive for BrdU incorporation (green channel images) relative to all cells (blue channel images). Proliferation ratio means were compared by 2-sample t-tests; $p < 0.05$ was considered significant. Global proliferation results are expressed as means \pm 95% confidence. Image processing was carried out with ImageJ and statistical analysis was carried out with Minitab software. A demonstration of the image capture and analysis and a representative Minitab graphical summary output can be seen in Section 3.3.8.

A local cell-feature analysis (LCFA), [90, 91] based on histograms of distances between different types of cell-to-cell distances, was used to compare cell-to-cell interactions 4 hours after seeding and to study cell-to-cell contact effects on proliferation for the undoped and the 0.125M FeCl₃-doped P3OT films.

Images were processed with self-adaptive algorithms using the Image Processing Toolbox of Matlab™ R14 (MathWorks). Briefly, binary images of cell nuclei (blue channel) and BrdU (green channel) were obtained from raw grayscale microscopic images. Adjacent cell nuclei were segmented using the marker-controlled watershed

method[92] and the number and location were determined by statistical analysis of regional properties. Cells positive for BrdU incorporation were determined by using a variation-adjusted iterative selection method to choose the optimal threshold for BrdU intensity.

In LCFA, cell-to-cell distance is defined as the distance between the centroids of two cell nuclei. Cell-to-cell distances are sorted into frequency histograms and classified to represent distances between: proliferated cells (P), cells at rest (R), and any cell (A, not distinguishing proliferation state). The frequency functions (e.g., f_{AA} , f_{PP} , f_{RR} , and f_{PR}) are then normalized against a standard frequency distribution (f_{std}) for a completely random occurrence of cell-cell distances that is calculated using a *Monte Carlo* simulation. Normalizing against f_{std} allows us to determine the deviation (a value greater than or less than unity) from the randomized probability distribution and to directly compare different types of cells distances on different surfaces.

4.4 Results and Discussion

For simplicity, undoped P3OT will be referred to as uP3OT, doped P3OT as dP3OT, 0.001M FeCl₃-doped P3OT as D001, and 0.125M FeCl₃-doped P3OT as D125, throughout the rest of this chapter.

4.4.1 Surface characterization

Film thickness, measured by a UV-Vis-NIR reflectance interferometer, was 30 nm \pm 2 nm for all films. Water contact angles indicated that while all films were hydrophobic, wettability slightly increased with doping (Figure 4.2), with values of 107.0° \pm 0.1°, 105.7° \pm 0.1°, and 100.8° \pm 0.8° for uP3OT, D001, and D125, respectively. Although there were small differences in contact angles (2° and 7° for D001 and D125,

respectively, when compared to uP3OT), the trend observed was similar to what others have shown for doped/oxidized poly(3-alkylthiophenes).[93, 94]

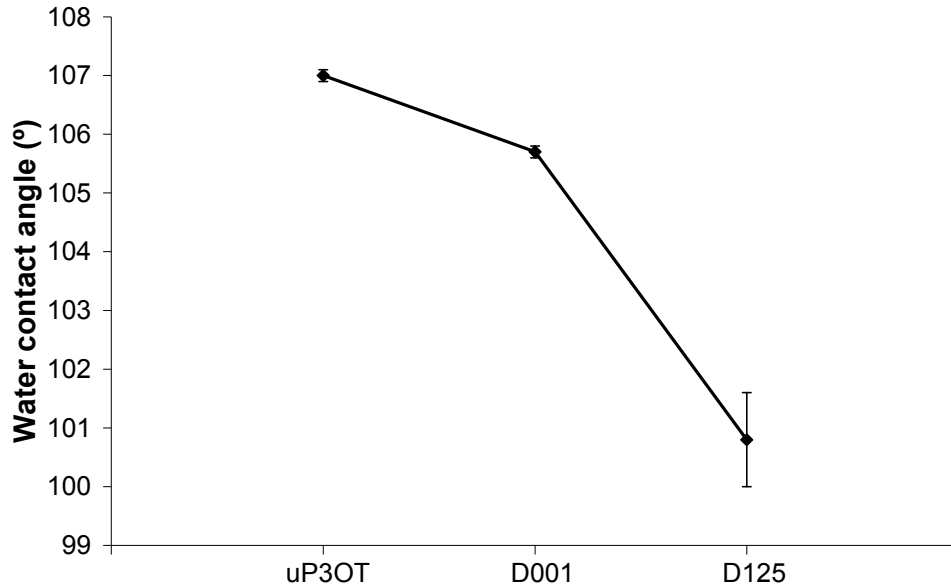


Figure 4.2. Water contact angle as a function of doping concentration.

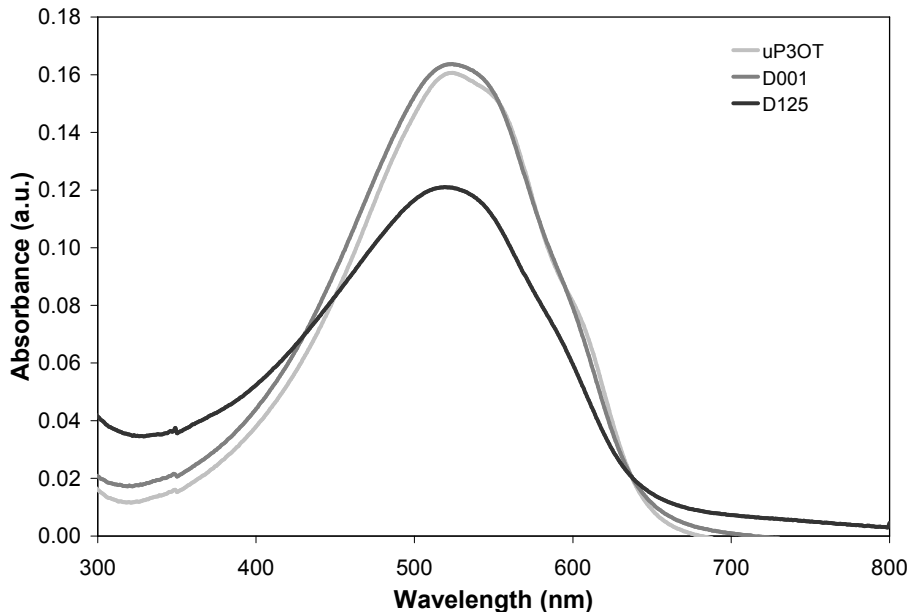


Figure 4.3. UV-Vis absorption spectra for uP3OT, D001, and D125 films.

Figure 4.3 shows the UV-Vis spectra of uP3OT, D001, and D125 P3OT films. The uP3OT and dP3OT films show a maximum absorption peak at ~520 nm, which

corresponds to the characteristic π - π^* transition between the highest occupied π electron band and the lowest unoccupied one of the polymer film.[95] As expected, a transition from sharp to broader peaks with a decrease in peak height, due to a reduction in electron density along the π -conjugated backbone, was observed with doping. A similar trend was shown for P3HT films doped with increasing FeCl_3 concentrations.[42]

Figure 4.4 shows AFM topography images of uP3OT and dP3OT films. It can be seen that doped films have a surface characterized by pits in the P3OT films. The RMS values determined by the instrument's software were 0.645 nm, 0.912 nm, and 1.29 nm for the uP3OT, D001, and D125 P3OT films, respectively. An increase in the number of pits and in surface roughness caused by an increase in dopant concentration has been observed previously for P3HT[42, 96] and P3OT.[33, 97]

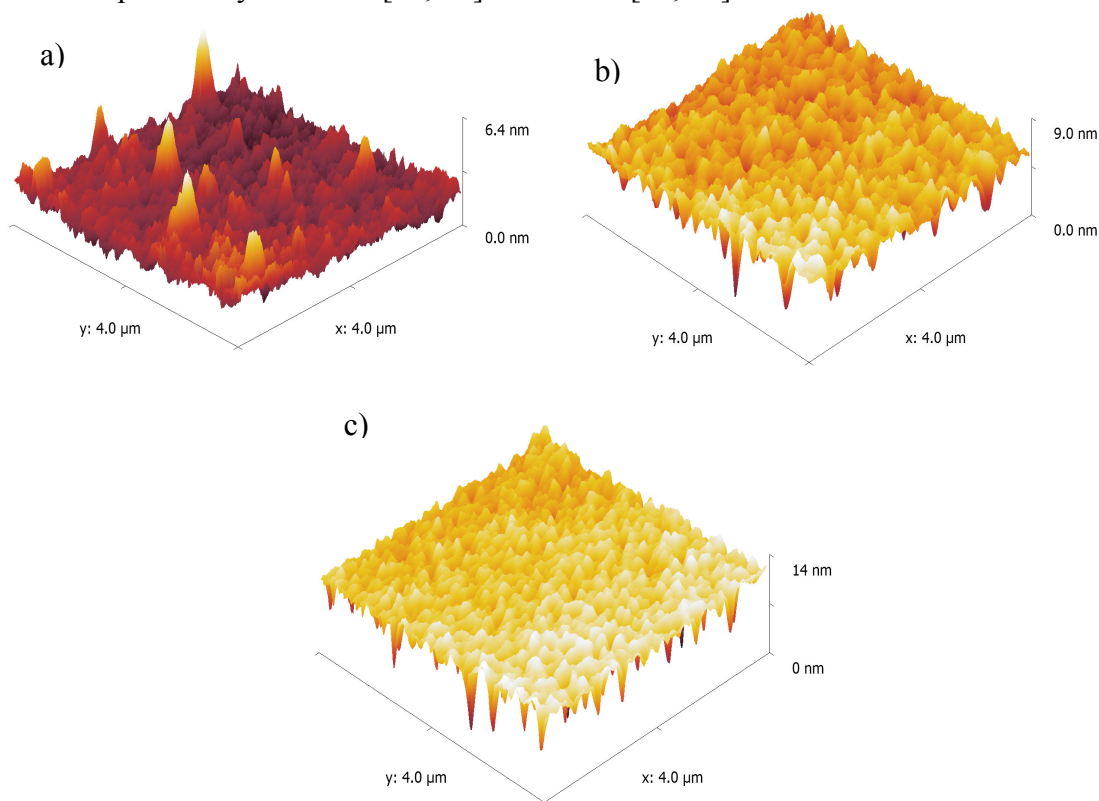


Figure 4.4. AFM 3-D topography images of (a) uP3OT, (b) D001, and (c) D125 P3OT thin films (30 nm).

Figure 4.5 shows the FTIR spectra of uP3OT and dP3OT films in transmission mode in the range of 4000 – 650 cm^{-1} . The band positions are similar to those observed for uP3OT films.[32, 70, 98] The methyl rock is observed at 725 cm^{-1} ; the aromatic C–H out-of-plane is around 825 cm^{-1} ; the methyl deformation is at 1377 cm^{-1} ; the ring stretching bands are observed at 1510 and 1465 cm^{-1} ; the aliphatic C–H stretching bands are observed at 2958, 2923, and 2854 cm^{-1} . An unexpected band observed at 1745 cm^{-1} is tentatively assigned to carbonyl (C=O). Kumar et al.[33] observed a band at 1789 cm^{-1} for FeCl_3 -dP3OT and assigned it to a carbonyl group that is inserted on the π -conjugated backbone of P3OT during doping and is responsible for the disruption of conjugation by the formation of sp^3 defects. However, we observe this band in the undoped samples as well.

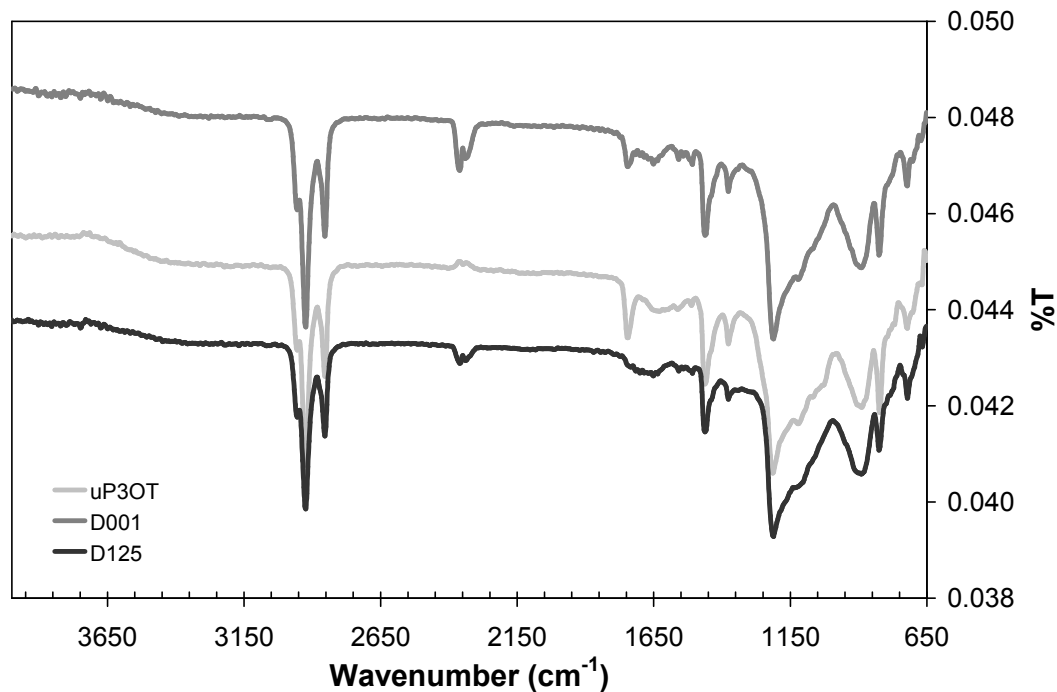


Figure 4.5. FTIR spectra of uP3OT and dP3OT films.

In order to quantitatively describe the effect of doping on P3OT films, spectra were corrected for thickness and peak areas for the uP3OT and dP3OT were compared. A summary of the changes in peak areas for the characteristic bands is shown in Table 4.1.

Table 4.1. Comparison of FTIR peak areas of uP3OT and dP3OT.

Wavenumber (cm ⁻¹)	Band Assignment	uP3OT	D001	D125	%Reduction uP3OT vs. D001	%Reduction uP3OT vs. D125
2958, 2923, 2854	Aliphatic C—H stretching	4.87	4.90	4.25	—	13
1745	Carbonyl	0.48	0.19	0.04	61	92
1510, 1465	Ring stretching	1.23	1.08	0.85	12	30
1377	Methyl deformation	0.24	0.17	0.08	32	66
825	Aromatic C—H out-of-plane	0.50	0.45	0.32	10	35
725	Methyl rock	0.07	0.12	0.11	—	—

When P3OT is doped with FeCl₃ an acid-base pair (cationic P3OT chain-anionic FeCl₄⁻) is formed (Figure 4.6),[39] which is known to cause losses in vibrational intensity in numerous characteristic peaks of P3OT.[33, 41]

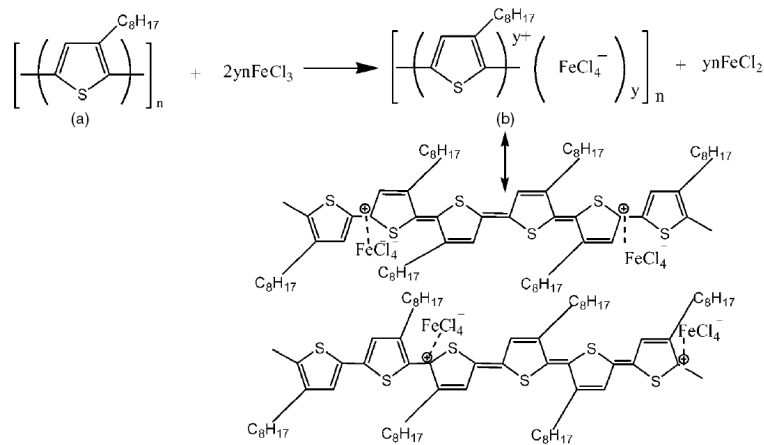


Figure 4.6. Schematic representation of cationic P3OT chains–anionic dopant (FeCl₄⁻) adducts comprising the doped region of polymer matrix.[39]

We observed a reduction in peak area that increases with dopant composition for all the FTIR bands except for the aliphatic C—H stretching bands, which remained unchanged in D001, and the methyl rock band, which increased for D001 and D125 by 67% and 49%, respectively, when compared to uP3OT.

4.4.2 Cell attachment and spreading – global analysis

Cell attachment density 4 hours after seeding is shown in Figure 4.7. The number of adherent cells was significantly greater ($p < 0.05$) on D001 and D125 (~3800 cells/cm² and ~4300 cells/cm², respectively) compared to uP3OT (~3000 cells/cm²). There was no significant difference in cell density between the doped samples.

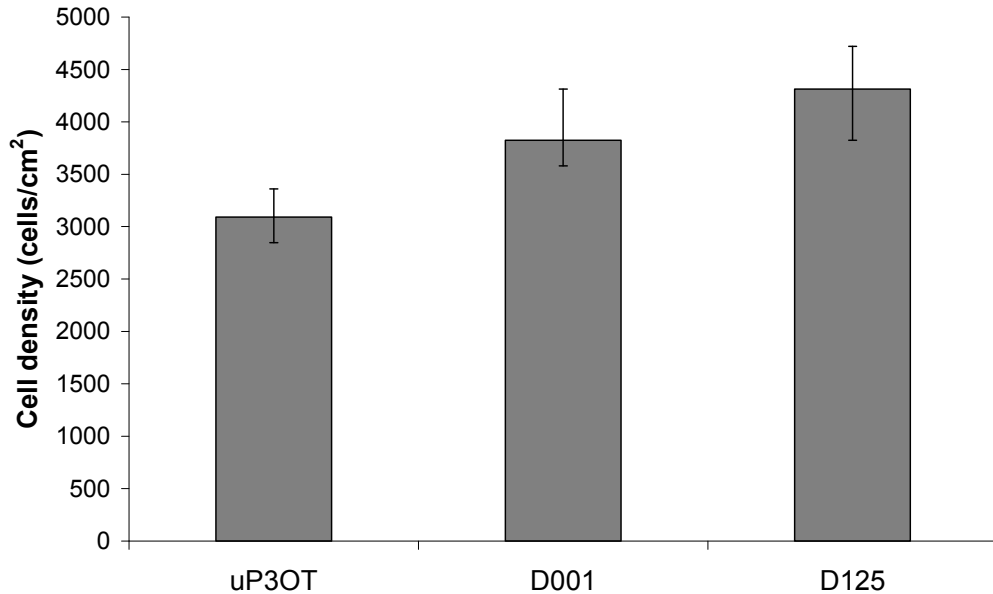


Figure 4.7. MC3T3-E1 cell attachment density on uP3OT, D001, and D125 4 hours after seeding. Values are presented as median \pm 95% confidence intervals.

Since cell shape is tightly coupled with cell growth,[71, 72] cell area and circularity were also determined. Cell area and circularity were only determined for isolated cells (i.e., cells not touching any other cells). Cell area correlated strongly with the level of doping; it was lowest on uP3OT (~1200 μm^2) followed by D001 (~1650 μm^2) and D125 (~1750 μm^2) (Figure 4.8). All values were significantly different ($p < 0.05$). Cell area on D001 increased by 35% compared to uP3OT but it only increased by 7% on D125 compared to D001. Cell circularity (equation 3.1), a metric that compares cell

aspect to that of a circle of the same area, was used to quantify cell spreading. A circularity value of 1 indicates a perfect circle and a value approaching 0 indicates an increasingly elongated polygon. Cell circularity for D125 (0.13) was significantly lower than uP3OT and D001 ($p < 0.05$) (Figure 4.8). In general, cells showed elongated structures in both undoped and doped surfaces

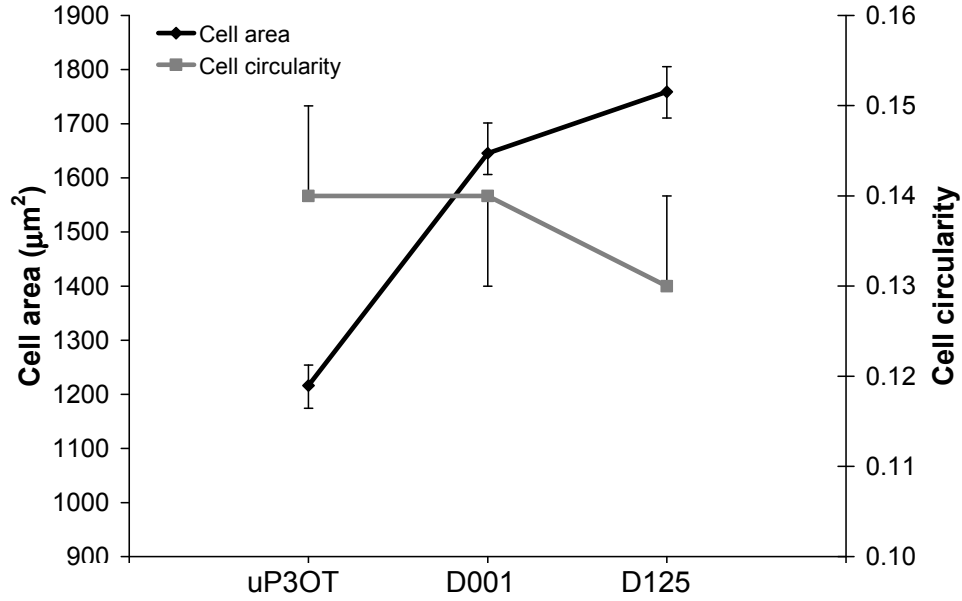


Figure 4.8. Area and circularity of MC3T3-E1 cells after 4 hours of culture on uP3OT, D001, and D125. Values are presented as median \pm 95% confidence intervals.

4.4.3 Cell attachment and spreading – local analysis

A local cell-feature analysis (LCFA) was recently developed by Su et al. in order to detect cell-cell and cell-microstructure interactions of cultured cells.[91] Here we use the same approach to study the interactions between cells 4 hours after seeding. Briefly, LCFA generates a standard frequency distribution (f_{std}) for a completely random occurrence of cell-cell distances using a *Monte Carlo* simulation. The experimental frequency distribution, f_{AA} in this case, is then normalized against f_{std} to determine the

deviation (a value greater than or less than unity) from the randomized probability distribution.

Figure 4.9 shows the normalized distribution $\tilde{f}_{AA} = f_{AA} / f_{std}$ for the attachment results. It can be seen that deviations from f_{std} are always less than 1 when the distance becomes less than $\sim 20 \mu\text{m}$ and $\sim 50 \mu\text{m}$ for uP3OT and dP3OT, respectively. This indicates that cells tend to avoid each other at close distances on dP3OT when compared to uP3OT. Interestingly, cell density was lower for uP3OT (3000 cells/cm^2) compared to D125 (4300 cells/cm^2), suggesting that initial (4 hours) cell attachment and cell-to-cell contact might be influenced by cell density. In previous studies Marx et al.[99] provided evidence for cell density dependence, or cell-cell cooperativity, in the initial (2 hours) adhesion and steady-state (24 hours) behavior of endothelial cells. From our observations we hypothesize that there is a cell density threshold for the onset of cell self-avoidance effects on initial cell attachment.

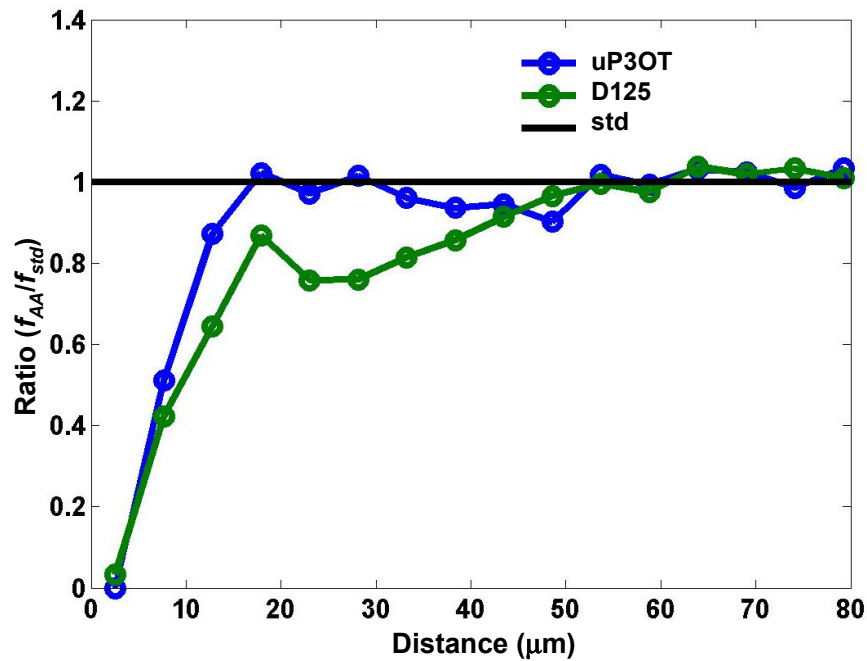


Figure 4.9. Normalized distribution, \tilde{f}_{AA} , for cells cultured for a period of 4 hours on uP3OT and D125.

4.4.4 Cell proliferation – global analysis

Figure 4.10 shows the proliferation ratio of MC3T3-E1 cells after 24, 48, and 72 hours of culture on uP3OT and dP3OT films. The proliferation ratio on uP3OT after 24 hours of culture (32%) was significantly higher than that on D001 (27%) and D125 (20%) ($p < 0.05$). Results at 48 hours showed higher proliferation on the doped surfaces (21% and 20% for D001 and D125, respectively) compared to uP3OT (17%). At 72 hours, uP3OT (23%) and D001 (22%) showed significantly higher proliferation compared to D125 (20%) ($p < 0.05$). In general, when comparing surfaces at each time point (i.e., 24 hours, 48 hours, and 72 hours) the proliferation values were significantly different ($p < 0.05$), except for uP3OT vs. D001 at 72 hours. Undoped P3OT showed a 45% decrease in proliferation after 48 hours followed by a 34% recovery at 72 hours. A similar trend in proliferation was observed previously for uP3OT.[86] This trend changes significantly with doping: the percent decrease in proliferation after 48 hours for the D001 is only about half the undoped case (22% decrease for D001). The recovery is only 7% for D001 compared to 34% for uP3OT. The proliferation-time trend disappears for the D125, with a 48 hour decrease of 3% and 72 hour recovery of 2%, both which yield $p > 0.05$.

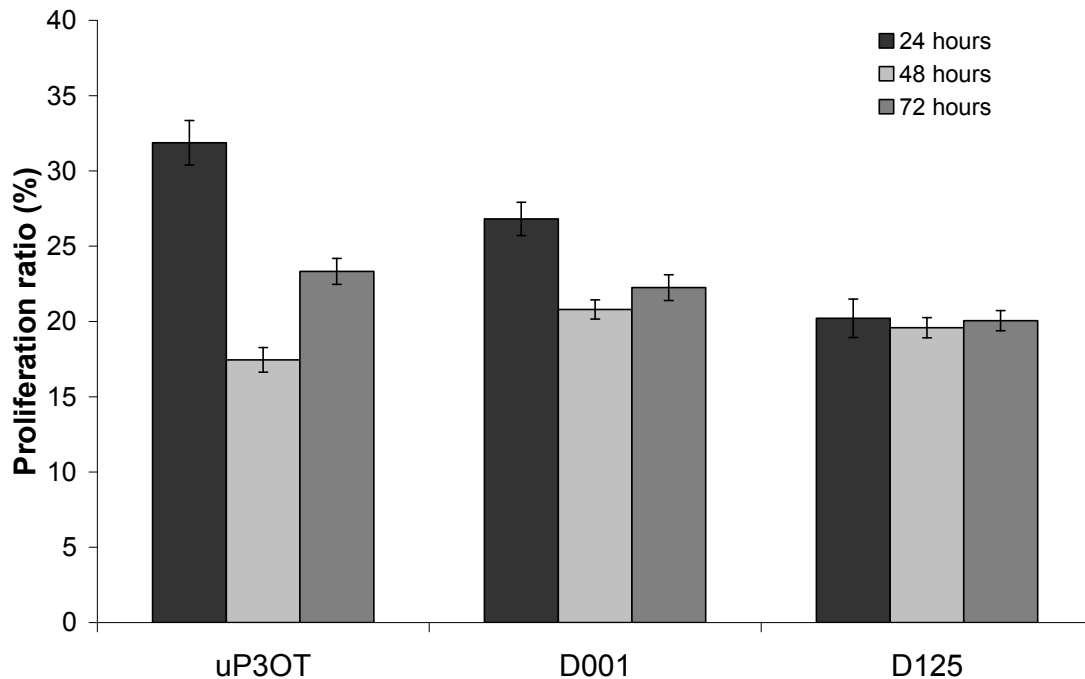


Figure 4.10. Proliferation ratio of MC3T3-E1 cells after 24, 48, and 72 hours of culture on uP3OT, D001, and D125. Values are presented as mean \pm 95% confidence intervals.

4.4.5 Cell proliferation – local analysis

In order to investigate cell contact effects on proliferation of uP3OT and D125 we used LCFA to study the interactions between proliferated cells (P), cells at rest (R), and any cell (A, not distinguishing proliferation state). Specifically, AA, PP, PR, and RR distances were used to detect local contact inhibition or cell self-avoidance effects on proliferation not observed using the global analysis (Figure 4.11). Global effects of cell density on cell proliferation after 48 and 72 hours of culture are shown in Figures A.2 and A.3, respectively.

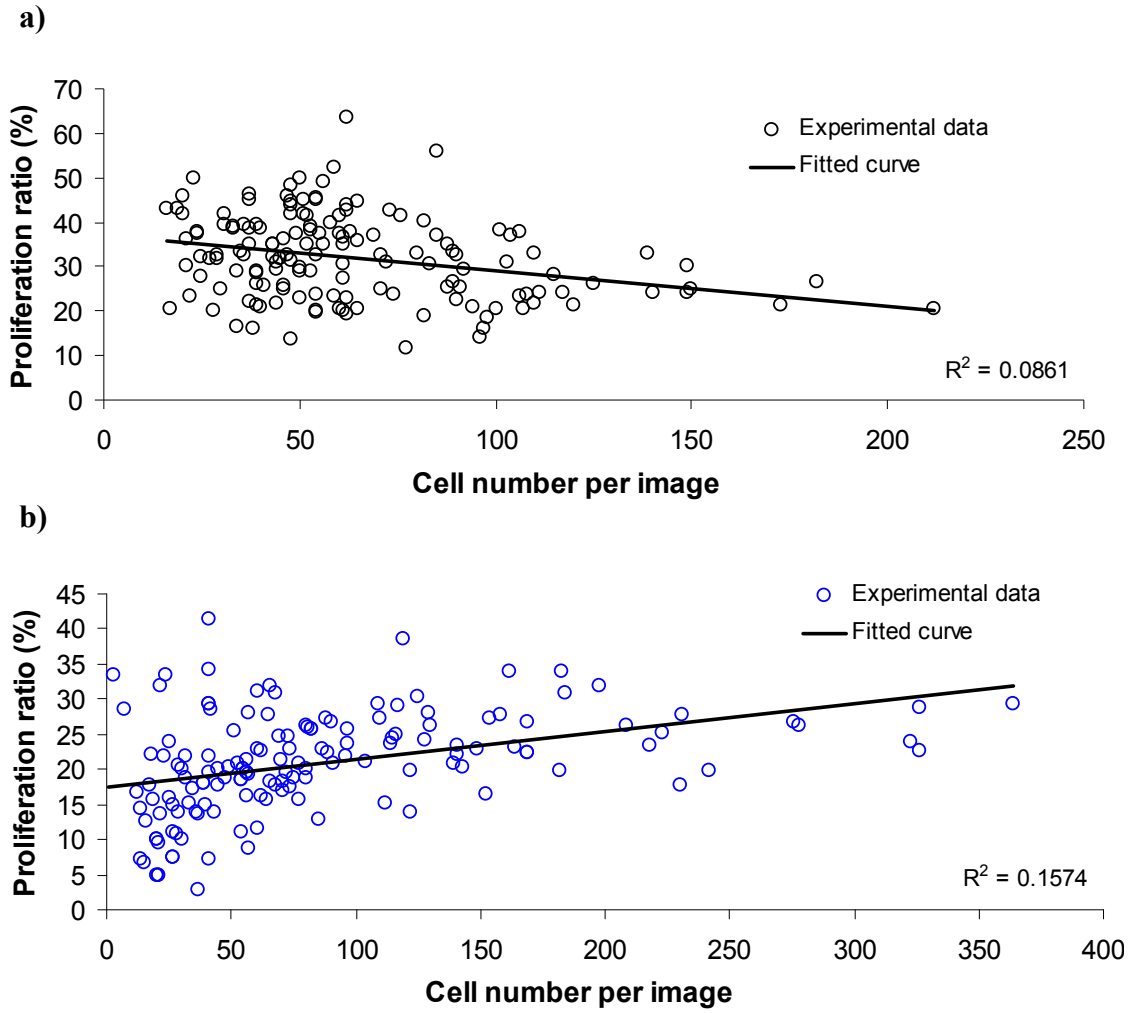


Figure 4.11. Effect of cell density on cell proliferation for MC3T3-E1 cultured on (a) uP3OT and (b) D125 for a period of 24 hours.

We used the experimental frequency distributions, f_{AA} , f_{PP} , f_{PR} , and f_{RR} and normalized them against f_{std} to determine the deviation from the randomized probability distribution. Figure 4.12a shows the normalized distribution $\tilde{f}_{AA} = f_{AA} / f_{std}$ for uP3OT and D125 after 24 hours of culture. Deviations from f_{std} are greater than one (higher likelihood of finding a neighbor) when the distance between cell nuclei becomes less than $\sim 50 \mu\text{m}$ for both surfaces. It can also be seen that \tilde{f}_{AA} for uP3OT is always greater than

\tilde{f}_{AA} for D125 at distances less than $\sim 50 \mu\text{m}$, indicating that there is higher frequency of AA pairs on uP3OT when compared to D125. In other words, cells are more likely to be close to each other on uP3OT than on D125.

A similar behavior was observed for the normalized distribution $\tilde{f}_{PP} = f_{PP} / f_{std}$ (Figure 4.12b) indicating that there is a higher occurrence of PP pairs on uP3OT vs. D125 at distances below $\sim 30 \mu\text{m}$. uP3OT shows a higher intensity peak at $13 \mu\text{m}$ when compared to D125 which may result from higher proliferation ratio on uP3OT compared to D125 after 24 hours of culture. The local analysis gives insight of the cell-to-cell distance at which proliferation is enhanced and allows a quantitative comparison of the likelihood of finding a PP pair at a certain distance on doped vs. undoped P3OT. From RR curves we observed global enhancement peaks similar to those observed in the AA and PP curves (Figure 4.13). Hence, we suggest that the peaks observed are due to a combination of factors: two daughter cells that have just proliferated are always very close to each other and the fact that on these surfaces (uP3OT and dP3OT) cells prefer to be in close proximity.

With the LCFA approach an experimental frequency distribution can also be normalized against another experimental frequency distribution to highlight specific effects among different pairs of distances. We looked at the PR/RR ratio, r_{PRIRR} , which can be used to determine the posterior odds (PO) of proliferation at different separation distances. Figure 4.12c shows the r_{PRIRR} profiles for uP3OT and D125 after 24 hours of culture. In order to explain this plot, consider two cells that are separated at a distance of $18 \mu\text{m}$ and another two cells that are separated at a distance of $13 \mu\text{m}$. The posterior odds that one of the two cells has proliferated is $PO_{PRIRR} = r_{PRIRR}(18) / r_{PRIRR}(13) = 1.3$

(uP3OT) or = 2 (D125) fold lower at 13 μm than at a distance of 18 μm for uP3OT and D125, respectively. Similarly, we can choose any other two distances and compare the PO on uP3OT vs. dP3OT. The profile for uP3OT varies somewhat, therefore no definite conclusion can be made on whether the PO on uP3OT are always higher or lower compared to dP3OT at any given distance combinations, but we can conclude that contact inhibition is observed for both surfaces and that the effect of contact inhibition on proliferation increases as the cell-cell distance decreases.

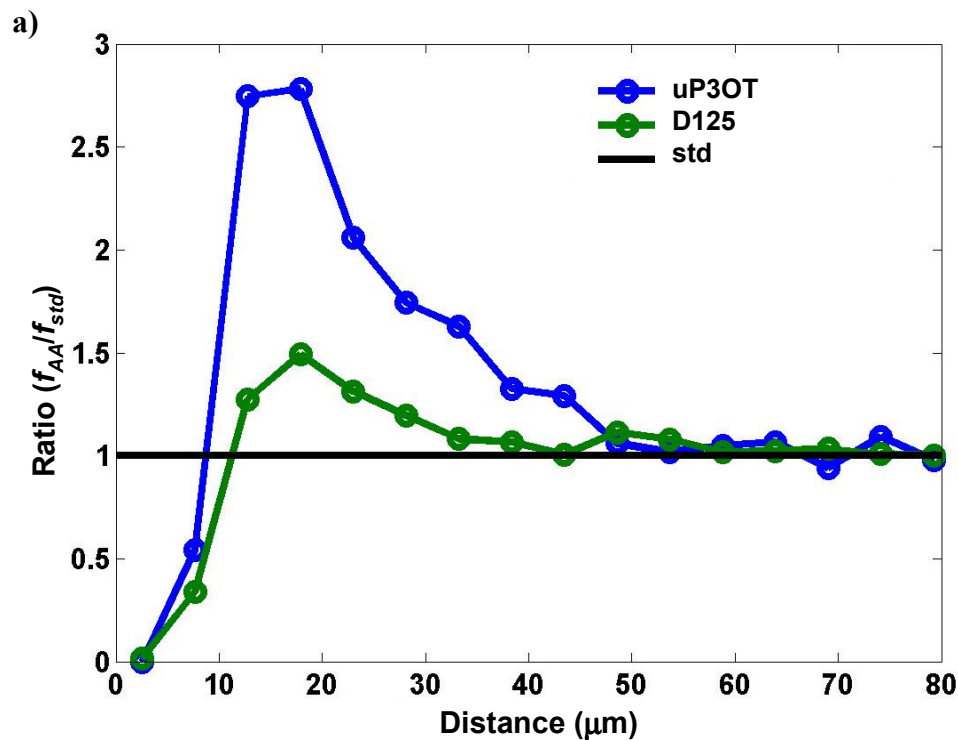


Figure 4.12. Normalized distributions: a) \tilde{f}_{AA} , b) \tilde{f}_{PP} , and c) f_{PR}/f_{RR} for cells cultured for a period of 24 hours on uP3OT and D125.

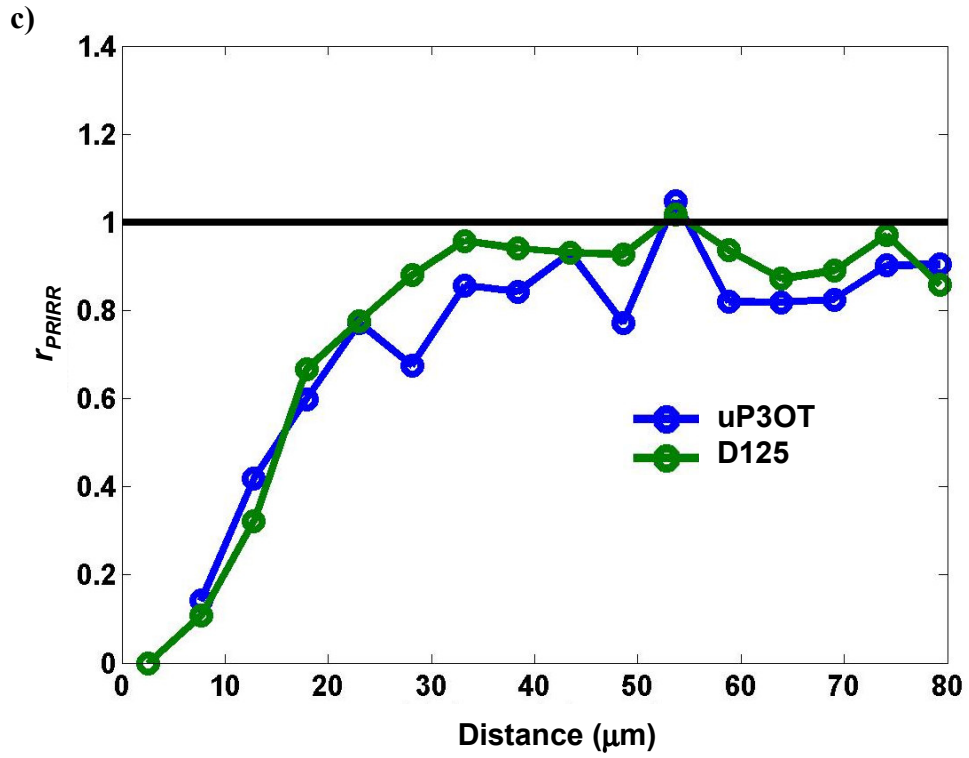
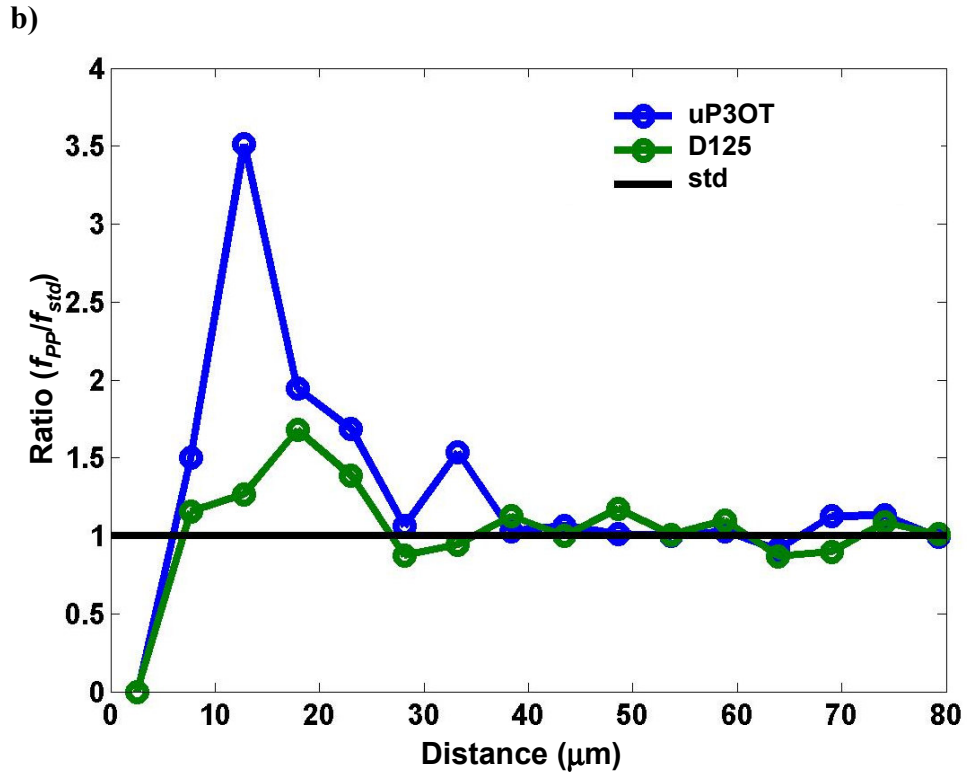


Figure 4.12. Continued.

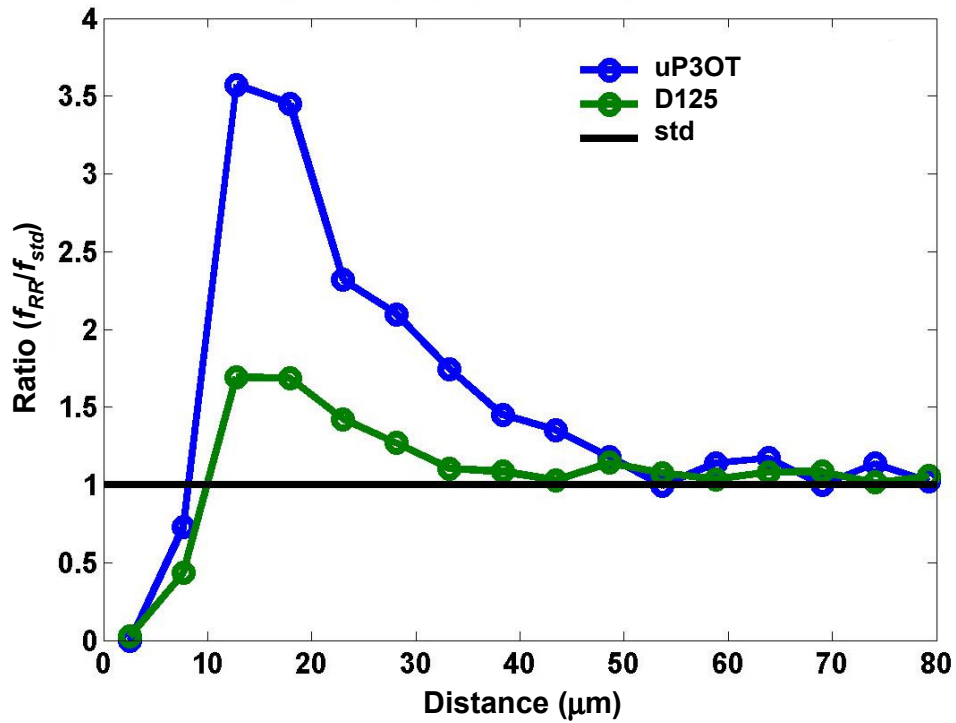


Figure 4.13. Normalized distribution, \tilde{f}_{RR} , for cells cultured for a period of 24 hours on uP3OT and D125.

The \tilde{f}_{AA} , \tilde{f}_{PP} , r_{PRIRR} , and \tilde{f}_{RR} profiles at 48 and 72 hours of culture are shown in Figures A.4 and A.5, respectively. The \tilde{f}_{AA} deviations of uP3OT and D125 at 48 hours are always less than 1 when the distance between cell nuclei becomes less than $\sim 30 \mu\text{m}$. At 48 hours, there is slightly higher likelihood of finding AA pairs at distances below $\sim 30 \mu\text{m}$ on uP3OT vs. D125, but the likelihood of finding PP pairs is about the same for uP3OT and D125 at all distances.

The \tilde{f}_{AA} and \tilde{f}_{PP} deviations of uP3OT at 72 hours are always greater than 1 when the distance between cell nuclei becomes less than $\sim 50 \mu\text{m}$. A similar behavior was observed for uP3OT at 24 hours. The \tilde{f}_{AA} and \tilde{f}_{PP} curves for D125 at 72 hours are close to 1 except at very short distances ($< 18 \mu\text{m}$ for \tilde{f}_{AA} and $< 9 \mu\text{m}$ for \tilde{f}_{PP}). Also the

frequency of AA and PP pairs at distances shorter than $\sim 50 \mu\text{m}$ is always higher for uP3OT compared to D125 at 72 hours.

From the r_{PRIRR} profiles one can observe contact inhibition of proliferation for both uP3OT and D125 at 48 and 72 hours but no definite conclusion can be made on whether the PO on uP3OT are always higher or lower compared to D125 at any given distance combination.

Overall, \tilde{f}_{AA} and \tilde{f}_{PP} profiles were similar at 24 and 72 hours (i.e., $f_{AA(uP3OT)} > f_{AA(D125)}$ and $f_{PP(uP3OT)} > f_{PP(D125)}$) and $f_{AA} \approx f_{PP}$ at 48 hours. We observed that f_{AA} , obtained for uP3OT and D125 from the local analysis ($f_{AA(24h)} > f_{AA(72h)} > f_{AA(48h)}$ at $\sim 18 \mu\text{m}$) correlated with the proliferation values obtained from the global analysis ($Prol_{(24h)} > Prol_{(72h)} > Prol_{(48h)}$). The effect of contact inhibition on proliferation is similar on uP3OT and D125 at 24, 48, and 72 hours of culture.

4.5 Conclusions

In summary, we demonstrated that doping P3OT with FeCl_3 has a strong effect on MC3T3-E1 cell attachment and proliferation. In particular doping increases cell density and area, decreases circularity, and decreases proliferation after 24 and 72 hours of culture. We used a local approach to study cell contact effects on proliferation that were otherwise masked by the global approach. The local analysis gave insight to the cell's sensitivity to the presence of other cells in the local environment, and how this sensitivity changes depending on substrate doping. Cell-to-cell sensitivity, in turn, influences proliferation suppression. Our results indicate that cell proliferation behavior can be tuned by doping P3OT and suggests that the different proliferation behaviors arise from changes in cell-cell contact sensitivity on doped versus undoped surfaces.

CHAPTER 5

EFFECT OF P3OT THICKNESS AND FILM PREPARATION CONDITIONS ON OSTEOBLAST ATTACHMENT AND PROLIFERATION

5.1 Abstract

Previous work showed that poly(3-octylthiophene) (P3OT), a semi-conductor in its undoped state, can sustain attachment and proliferation of MC3T3-E1 osteoblasts and that FeCl₃-doped P3OT can be used to regulate osteoblast functions. P3OT electronic properties are known to vary with thickness, solvent used for film preparation, and thermal annealing. In this work we used discrete and combinatorial methods to make a preliminary assessment of the effect of P3OT thickness and film preparation conditions on osteoblast attachment and proliferation. For rapid screening, we developed P3OT thickness gradient libraries over a high range (130 – 200 nm) and discrete thickness films over a low range (20, 30, and 50 nm). We also investigated the effect of thermal annealing (annealed at 80°C vs. unannealed) and solvent used for film preparation (CHCl₃ vs. THF). We demonstrate that cell attachment over the low range and cell attachment and proliferation over the high range were not affected by P3OT thickness. We also demonstrate that annealing had *opposite* effect on cell density, area, and circularity on films prepared from CHCl₃ when compared to films prepared from THF.

5.2 Introduction

Conducting polymers (CPs) are having increased attention for use in biomedical applications such as biosensors,[83-85] molecular actuators,[60] and cell support substrates.[22, 23, 49] One key advantage of CPs over other materials is their ability to conduct electricity upon doping. Besides tuning conductivity, most research has focused on biological and physical modification of CPs for further optimization when targeting a specific application. For example, for biosensors it is important to tune the surface energy, conductivity, and reactive functionalities to successfully incorporate biomolecules to improve detection of binding events. For tissue engineering, CP properties such as roughness, hydrophobicity, three-dimensional geometry, and degradability are critical. Although it is known that surface properties are critical to promote attachment and growth of certain cells the desirable properties to elicit specific cell functions are still not clear.

CPs such as polypyrrole and polythiophene are able, via electrical stimulation, to modulate the behavior of certain electrically responsive cells (e.g., nerve, muscle, bone, and cardiac cells).[100, 101] Substituted polythiophenes have shown increased interest for biomedical applications because of their versatility and unique surface properties.[102, 103] We recently showed that poly(3-octylthiophene) (P3OT) is a suitable substrate to sustain attachment and proliferation of MC3T3-E1 osteoblasts and that FeCl₃-doped P3OT can be used to alter osteoblast functions.[86] P3OT properties are known to vary with thickness,[28, 34] solvent used for film preparation,[35, 36] and thermal annealing.[37, 38] For example, Taka et al.[35] showed that solvent type affects the macromolecular structure and organization of P3OT films cast from solution. They

observed higher crystallinity in films made from THF compared to films made from CHCl_3 . Chattopadhyay et al.[28, 34] recently showed that thickness strongly affects the surface energy of P3OT. In their studies the adhesion force, measured by AFM, experienced a minimum at a P3OT thickness of 170 nm (Figure 5.1). They concluded that the van der Waals (VDW) interactions of P3OT with the AFM tip are a complex function of thickness, including a change in the slope sign of force versus thickness.

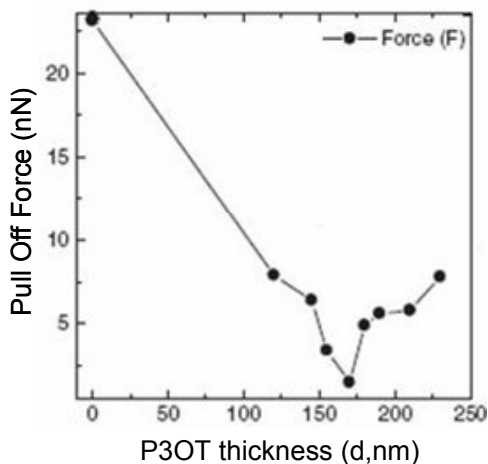


Figure 5.1. Adhesive pull of force profile of P3OT thickness gradient film.[28]

In addition, Singh et al.[37] observed changes in surface morphology of P3OT films by soft thermal annealing. They showed that thermal annealing induces an ordered corrugated rod-type morphology in P3OT films (Figure 5.2).

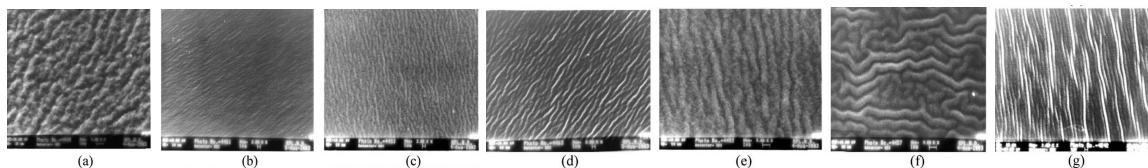


Figure 5.2. SEM micrographs of pristine P3OT films annealed at 373 K for different interval of time (a) unannealed—303 K (b) 1 h, (c) 5 h, (d) 12 h, (e) 24 h, (f) 48 h, and (g) 72 h.[37]

The potential to easily modify the physical, electrical and chemical properties of P3OT presents an advantage for discovering properties to elicit desirable functions in

cells and thus allowing for optimal design and development of biomaterials. In this work we used combinatorial and discrete methods to make an initial assessment of the effects of P3OT thickness, thermal annealing, and solvent used for film preparation, on the attachment and proliferation of MC3T3-E1 osteoblasts.

We studied the response of cell attachment and proliferation by fluorescent labeling of F-actin fibers and 5-Bromo-2'-deoxyuridine (BrdU) incorporation, respectively.

5.3 Materials and Methods

5.3.1 Preparation of P3OT films

P3OT (>98.5% head-to-tail regioregular, Aldrich) thickness gradient films were prepared from 2 wt% chloroform solution on 32 mm x 32 mm silicon chips (Silicon Inc.) and discrete films were prepared from 1 wt% chloroform (CHCl₃) solution or 2 wt% tetrahydrofuran (THF) solution on 24 mm x 24 mm silicon chips (Silicon Inc.) that were previously cleaned in a Piranha solution (70% sulfuric acid – 30% hydrogen peroxide) followed by 48% hydrofluoric acid (HF) etching. HF etching was required to render the surface hydrophobic and prevent film delamination during the cell culture period. Thickness gradient and discrete thickness films were prepared using a knife-edge coating apparatus[67-69] and kept under vacuum at room temperature for several days to remove residual solvent. Thermal annealing of P3OT discrete thickness films was done under vacuum at 80° for 15 hours.

5.3.2 Characterization of P3OT films

Film thickness was measured using a high-throughput UV-Vis-NIR reflectance interferometer (Stellar Net EPP 2000). The UV-Vis spectra for all films were obtained using a Cary 5000 Spectrophotometer (Varian Inc.). Surface topography characterization was performed by tapping mode atomic force microscopy (AFM) with an MFP-3D AFM system (Asylum Research). Root-mean-square (RMS) roughness for a 5 x 5 μm scan size was calculated using the instrument's software. Water contact angle was measured with a VCA 2500 XE contact angle system (AST Products, Inc.).

5.3.3 Cell culture

MC3T3-E1 osteoblast-like cells (Riken Cell Bank, Japan) were cultured in alpha modification of Eagle's minimum essential medium (α -MEM) (Mediatech, Inc.) supplemented with 10% fetal bovine serum (FBS) (ATCC) and 1% penicillin-streptomycin (Mediatech, Inc.) at 37°C in a fully humidified atmosphere at 5% CO_2 . Prior to seeding, cells were washed with Dulbecco's Phosphate Buffered Saline (DPBS) without Ca^{2+} and Mg^{2+} (Mediatech, Inc.) and trypsinized with 0.05% Trypsin/0.53mM EDTA in HBSS (Mediatech, Inc.). P3OT thickness gradient films were placed in 60 mm petri dishes (VWR) and discrete thickness films were placed in Costar six-well microplates (Corning, Inc.). Films were sterilized by immersion in a 70% ethanol solution for 30 min followed by 3 washes of DPBS with Ca^{2+} and Mg^{2+} (5 min each). Cells, at passage 6, were seeded at a density of 5000 cells/cm².

5.3.4 Cell attachment and spreading

Cell attachment and spreading were observed by fluorescent labeling of F-actin fibers with Fluorescein phalloidin (Invitrogen) 4 hours after seeding. Cells were fixed in 3.6% paraformaldehyde (w/v) for 10 min and then permeabilized with 0.1% Triton X-100 in 1% BSA/PBS for 5 min. F-actin fibers were stained with Fluorescein phalloidin (Invitrogen) in 1% BSA/PBS at a proportion of 1:20 for 30 min at room temperature. Cells were washed with PBS and cell nuclei were counterstained with Hoechst (Invitrogen) at a proportion of 1:10,000 in PBS for 15 min at room temperature.

5.3.5 Cell proliferation

Cell proliferation was assayed at 24 and 48 hours using 5-Bromo-2'-deoxyuridine (BrdU) (Sigma), a thymidine analog that incorporates into newly replicated DNA. BrdU (10 μ M) was added to the cell culture media 1 hour prior to cell fixation. Cells were fixed with 70% ethanol for 30 min and then treated with 0.07N NaOH for 2 minutes followed by immersion in PBS (pH 8.5). Cells were then incubated for 30 min in a humidified chamber with monoclonal anti-BrdU (Becton Dickinson) mixed with 0.5% Tween 20/PBS at proportion of 20:50. Following washing with PBS, cells were incubated in Alexa Fluor 488 conjugated goat anti-mouse IgG antibody (Invitrogen) at a proportion of 1:200 in PBS. After washing with PBS cell nuclei were counterstained with Hoechst (Invitrogen) at a proportion of 1:10,000 in PBS for 15 min.

5.3.6 Image acquisition and analysis

Cell attachment, spreading, and proliferation were assayed by fluorescence microscopy with an Olympus BX51 upright microscope equipped with a translation stage. Thickness gradient samples were imaged in a (8 x 10) grid and discrete samples

were imaged in a (13 x 4) grid, both at a magnification of 10X. Two fluorescent images were captured at each grid position: (1) a green channel image for Fluorescein phalloidin (attachment) or Alexa Fluor 488 conjugated antibody (proliferation); and (2) a blue channel image of Hoechst-stained cell nuclei. For the attachment experiments, green images were used to determine cell area and circularity and blue images were used to determine cell number. Values of cell area and circularity represent ~2000 cells analyzed for each surface. Cells were scored for proliferation as the ratio of cells positive for BrdU incorporation (green images) relative to cell nuclei (blue images). Image processing was carried out with ImageJ and statistical analysis was carried out with Minitab software. Cell density, area, and circularity medians were compared using the Mann-Whitney nonparametric test because variances were not equal and values were not normally distributed; $p < 0.05$ was considered significant. Differences in proliferation on the thickness gradient films were tested by ANOVA with Tukey's multiple comparison test ($p < 0.05$). All results are expressed as medians or means \pm 95% confidence intervals.

5.4 Results and Discussion

For simplicity, annealed P3OT will be referred to as aP3OT, unannealed P3OT as uaP3OT, P3OT films prepared from CHCl_3 as P3OT/ CHCl_3 and P3OT films prepared from THF as P3OT/THF, throughout the rest of this chapter

5.4.1 Surface characterization

Figure 5.3 shows a representative thickness map for P3OT thickness gradient films over the high range. Films thicknesses ranged from approximately 130 nm to 200

nm and had a polynomial dependence on position, y (mm), on the wafer. Representative plots for constant thickness films (20, 30, and 50 nm) are shown in Figure 5.4.

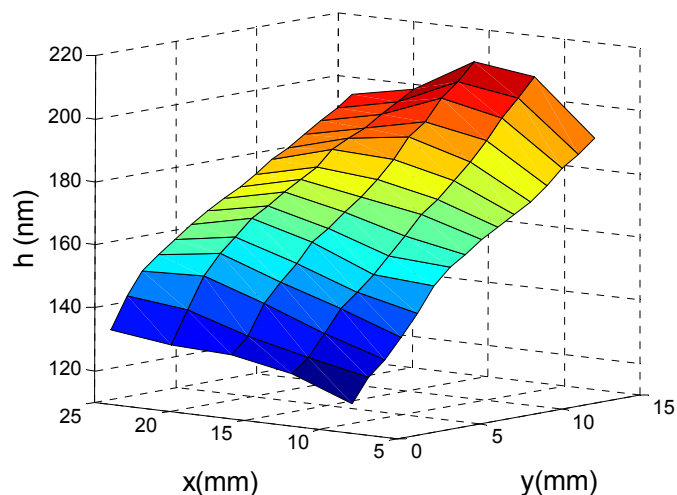


Figure 5.3. Representative three-dimensional thickness map of the thickness gradient P3OT films.

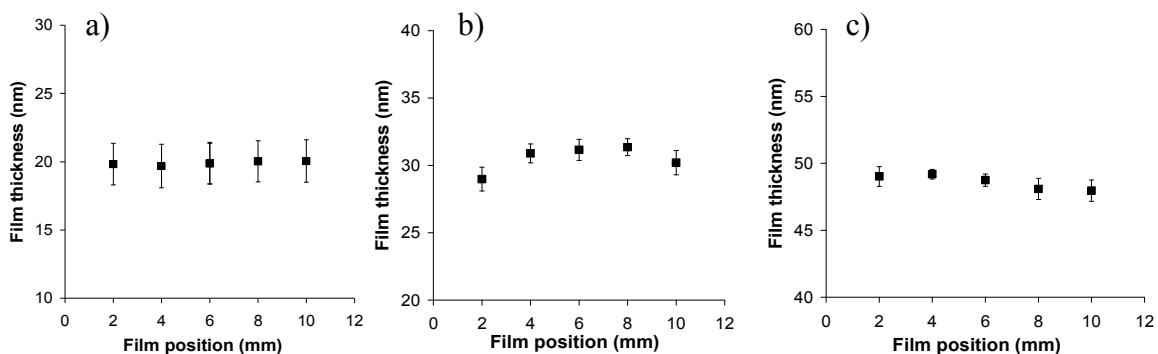


Figure 5.4. Representative plots of constant thickness films: a) 20 nm, b) 30 nm, and c) 50 nm. Values are presented as mean \pm SEM.

The water contact angle of thickness gradient films (Figure 5.5) initially decreases with thickness and plateaus at thicknesses greater than 180 nm ($\sim 97^\circ$). Water contact angles were $106.4^\circ \pm 0.3^\circ$, $105.1^\circ \pm 0.9^\circ$, $106.4^\circ \pm 0.5^\circ$, and $107.0^\circ \pm 0.7^\circ$ for uaP3OT/ CHCl_3 , aP3OT/ CHCl_3 , uaP3OT/THF, and aP3OT/THF, respectively.

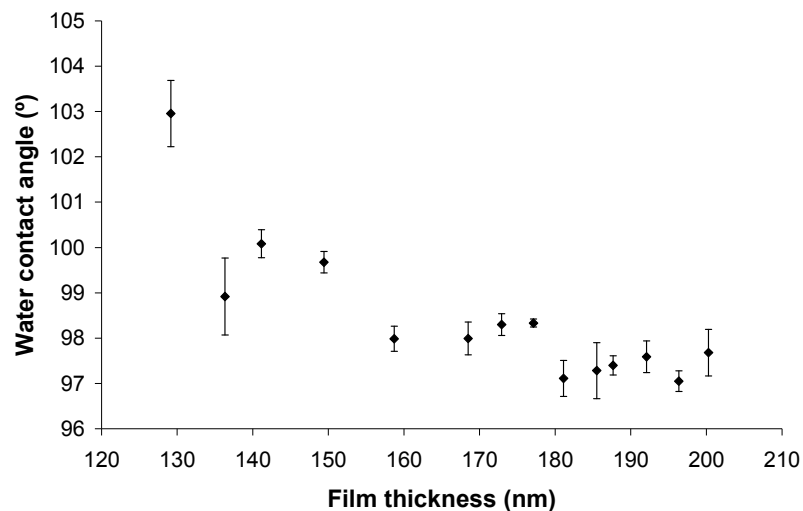


Figure 5.5. Water contact angle for thickness gradient films.

Figure 5.6 shows the UV-Vis absorption spectra for aP3OT and uaP3OT films prepared from CHCl_3 and THF. Maximum absorption peaks were observed at 524 nm (uaP3OT) and 523 nm (aP3OT) for films made from CHCl_3 and 526 nm (uaP3OT) and 524 nm (aP3OT) for films made from THF. Although there were minor shifts toward higher energies for aP3OT/ CHCl_3 and aP3OT/THF, the trend observed was similar to what others have shown for annealed samples of P3ATs.[104, 105]

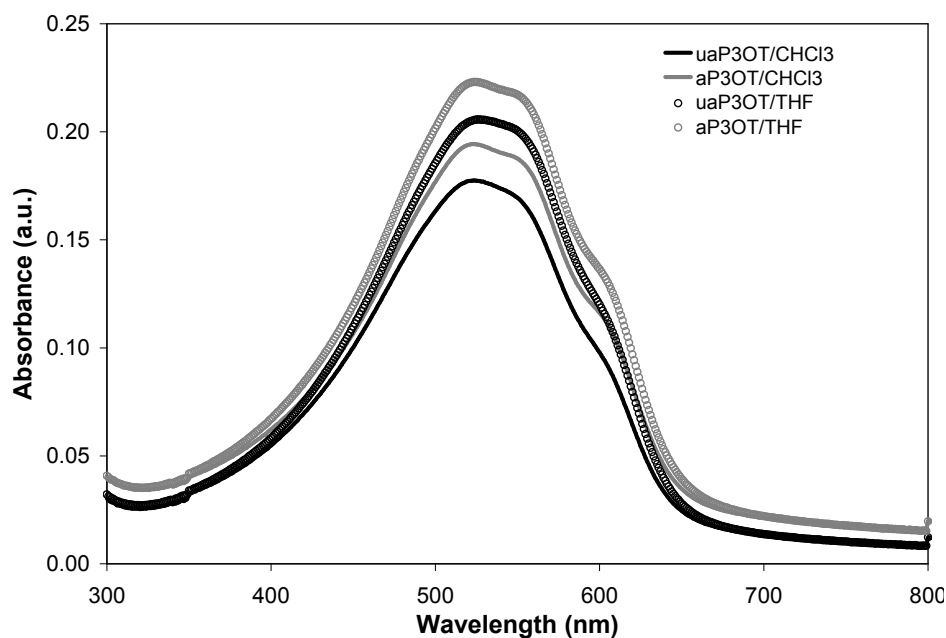


Figure 5.6. UV-Vis absorption spectra for aP3OT and uaP3OT films made from CHCl_3 and THF.

Figure 5.7 shows AFM topography images of unannealed and annealed P3OT films prepared from CHCl_3 and THF. The RMS values determined by the instrument's software were 2.19 nm, 2.70 nm, 3.07 nm, and 3.33 nm for uaP3OT/ CHCl_3 , aP3OT/ CHCl_3 , uaP3OT/THF, and aP3OT/THF films, respectively. In general, film roughness slightly increased with annealing while the number of features decreased with annealing. Unannealed P3OT/ CHCl_3 samples (Figure 5.7a) showed a combination of islands and pits of various heights and depths that dewetted after annealing (Figure 5.7b) to form pits of uniform depth (~ 20 nm). Unannealed P3OT/THF samples (Figure 5.7c) showed an increased number of islands of ~ 10 nm in height. Annealing P3OT/THF films (Figure 5.7d) resulted in a decrease in the number of islands along with a two-fold increase in island height (~ 20 nm).

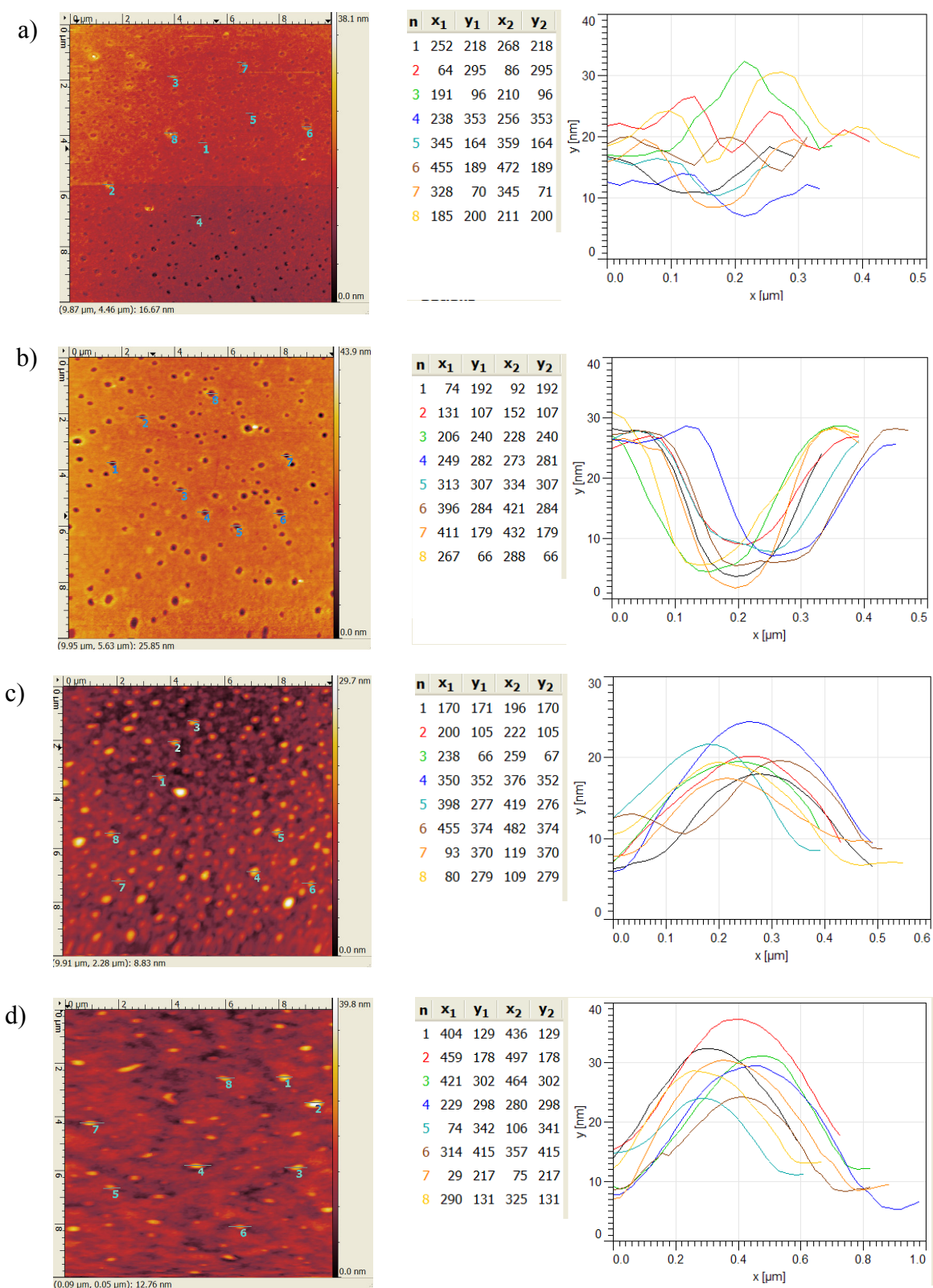


Figure 5.7. AFM topography images of (a) uaP3OT/CHCl₃, (b) aP3OT/CHCl₃, (c) uaP3OT/THF, and (d) aP3OT/THF.

5.4.2 Cell attachment – high thickness range

Cell attachment density 4 hours after seeding is shown in Figure 5.8. Cell density, area, and circularity was binned into 7 thickness ranges (130 – 140 nm, 140 – 150 nm, 150 – 160 nm, 160 – 170 nm, 170 – 180 nm, 180 – 190 nm, and 190 – 200 nm). There was no statistical difference between cell density values when comparing different thickness bins and no trend was observed for cell density as a function of film thickness.

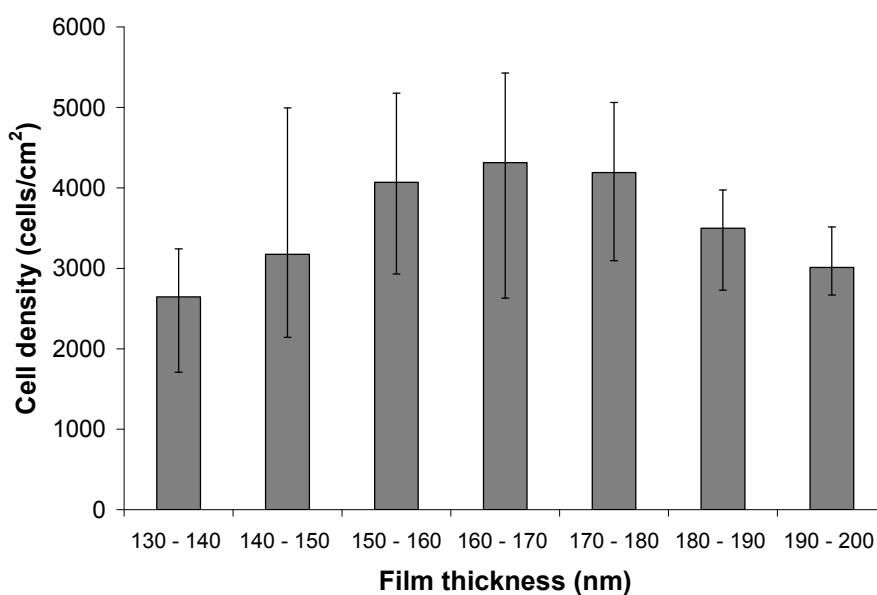


Figure 5.8. MC3T3-E1 cell attachment density on thickness gradient films. Values are presented as median \pm 95% confidence intervals.

Cell area and circularity 4 hours after seeding is shown in Figure 5.9. There were no statistical differences between cell area or circularity values for the different thickness bins and no trend was observed as a function of film thickness. These results suggest that slight changes in surface energy obtained by variations in film thickness are not enough to affect MC3T3-E1 cell attachment.

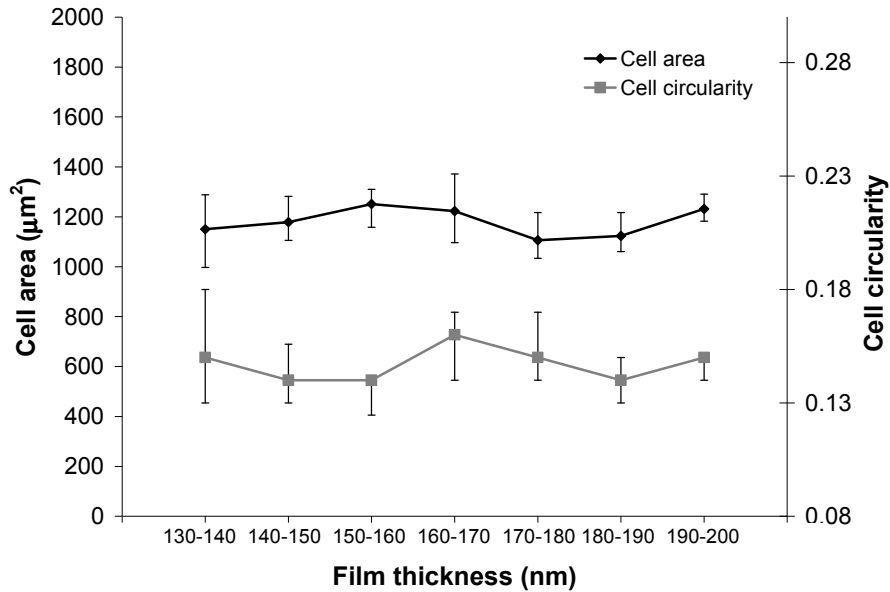


Figure 5.9. Area and circularity of MC3T3-E1 cells after 4 hours of culture on thickness gradient films. Values are presented as median \pm 95% confidence intervals.

5.4.3 Cell proliferation – high thickness range

Figure 5.10 shows the proliferation ratio of MC3T3-E1 cells after 24, 48, and 72 hours of culture on thickness gradient P3OT films. Cell proliferation was binned into 7 thickness ranges (130 – 140 nm, 140 – 150 nm, 150 – 160 nm, 160 – 170 nm, 170 – 180 nm, 180 – 190 nm, and 190 – 200 nm). Proliferation ratio differences were tested by ANOVA with Tukey’s multiple comparison test ($p < 0.05$). After 24 hours of culture there were no statistically significant differences in the proliferation ratio on the different thickness ranges, except between 150 – 160 nm and 170 – 180 nm. There were no statistically significant differences in the proliferation ratio after 48 hours and after 72 hours only 140 – 150 nm and 190 – 200 nm were significantly different.

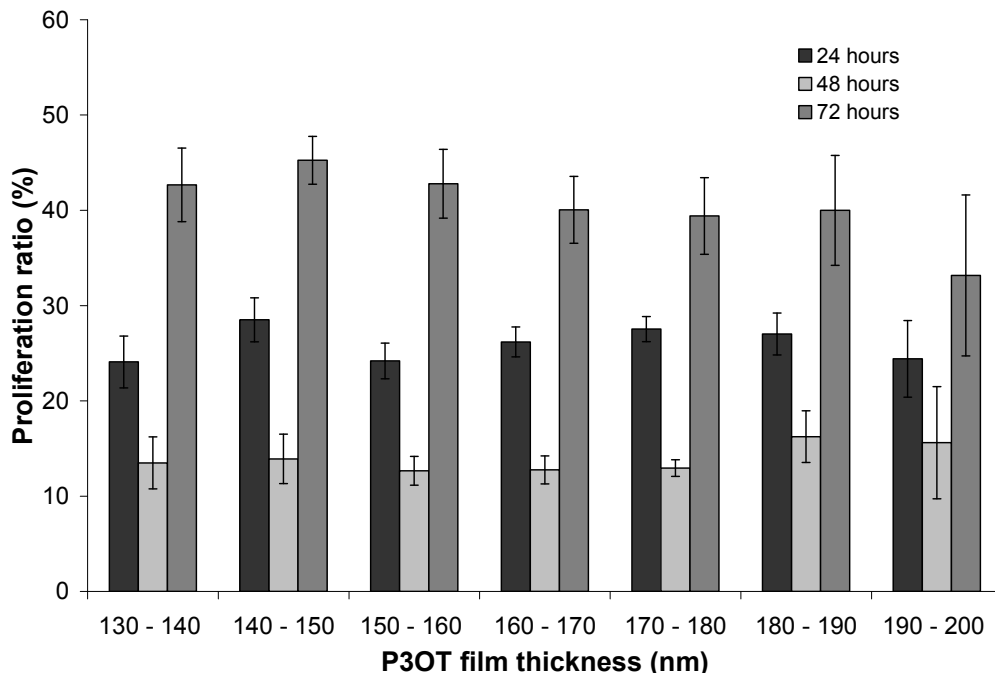


Figure 5.10. Proliferation ratio as a function of P3OT thickness of cells cultured for a period of 24, 48, and 72 hours. Values are presented as mean \pm 95% confidence intervals.

When comparing proliferation ratios at different time points (i.e., 24, 48, and 72 hours) for each thickness range bin one can observe that $Prol_{(24h)} > Prol_{(72h)} > Prol_{(48h)}$, which is the same trend observed previously for P3OT constant thickness films (30 nm). These findings suggest that MC3T3-E1 proliferation is affected by the P3OT chemistry and not by the slight differences in surface energy/wettability observed for thickness gradient P3OT films.

5.4.4 Cell attachment – film thickness and preparation conditions

We investigated the effect of thickness (20, 30, and 50 nm) on the attachment of osteoblasts cultured on P3OT/CHCl₃ and P3OT/THF. Cell attachment density values are shown in Figure 5.11. Cell density on P3OT/CHCl₃ was significantly higher for 30 nm (~3000 cell/cm²) and 50 nm (~2700 cells/cm²) when compared to 20 nm (~2000

cells/cm²) ($p < 0.05$); there was no significant difference between the 30 nm and 50 nm films. Cell density on P3OT/THF was only significantly different between 30 nm (~2100 cells/cm²) and 50 nm (~1900 cells/cm²). Overall, cell density was higher for higher thickness P3OT/CHCl₃ films but no trend was observed on P3OT/THF. When evaluating the effect of solvent on cell density we observed that there was no significant difference on the 20 nm films but cell density was significantly higher on 30 nm and 50 nm P3OT/CHCl₃ films compared to P3OT/THF films.

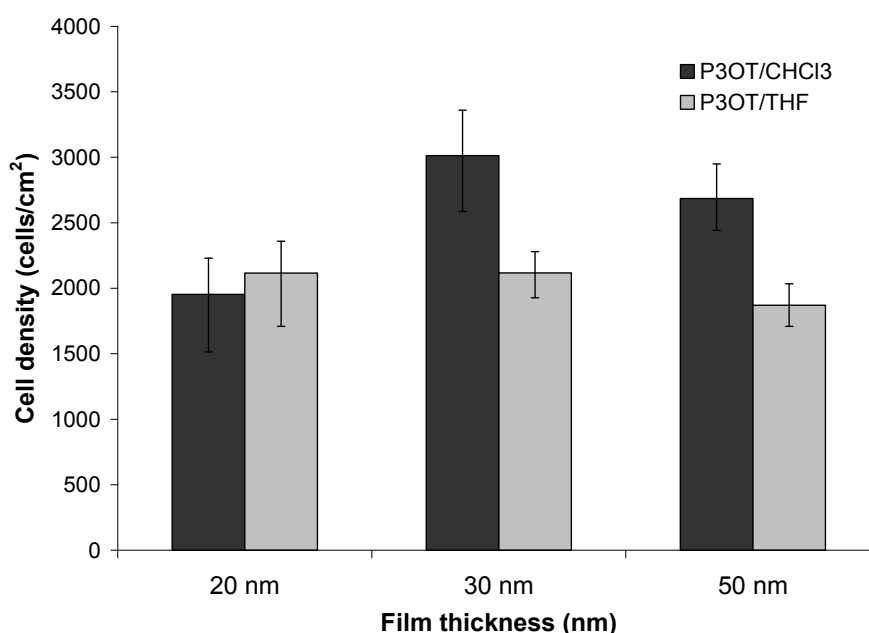


Figure 5.11. MC3T3-E1 cell attachment density on P3OT films (20, 30, and 50 nm) made from CHCl₃ and THF 4 hours after seeding. Values are presented as median \pm 95% confidence intervals.

Figure 5.12 shows cell area of cells cultured on P3OT films (20, 30, and 50 nm) made from CHCl₃ and THF. Cell area values on P3OT/CHCl₃ were significantly different when comparing all thicknesses: 20 nm (~1200 μ m²), 30 nm (~980 μ m²), and 50 nm (~1070 μ m²). Cell area on P3OT/THF was only significantly different between 20 nm (~1080 μ m²) and 30 nm (~1150 μ m²). When evaluating the effect of solvent in cell

area we observed an opposite trend to the one observed for cell density on P3OT 30 nm and 50 nm films. In other words, cell density was higher on P3OT/CHCl₃ when compared to P3OT/THF and cell area was higher on P3OT/THF when compared to P3OT/CHCl₃ for 30 nm and 50 nm films.

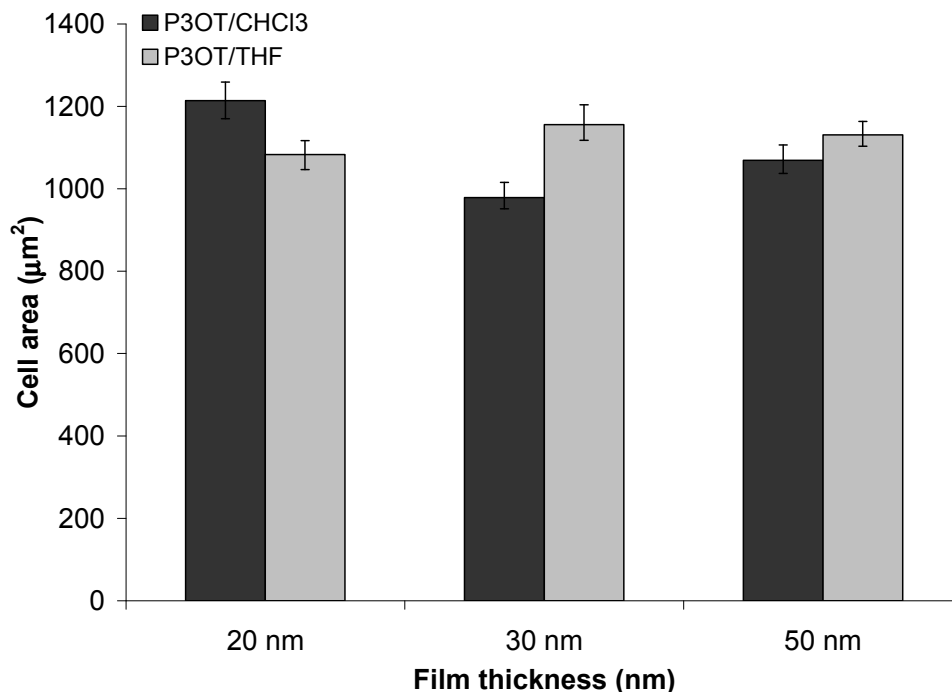


Figure 5.12. Area of MC3T3-E1 cells after 4 hours of culture on P3OT films (20, 30, and 50 nm) made from CHCl₃ and THF. Values are presented as median ± 95% confidence intervals.

Figure 5.13 shows circularity of cells cultured on P3OT films (20, 30, and 50 nm) made from CHCl₃ and THF. Cell circularity was only significantly higher on 30 nm P3OT/CHCl₃ films (0.14) when compared to all the samples. All other circularity values were not significantly different. This observation is not surprising as it has been proposed that MC3T3-E1 cell morphology (aspect ratio) varies with surface chemistry,[75] which was not varied in this case.

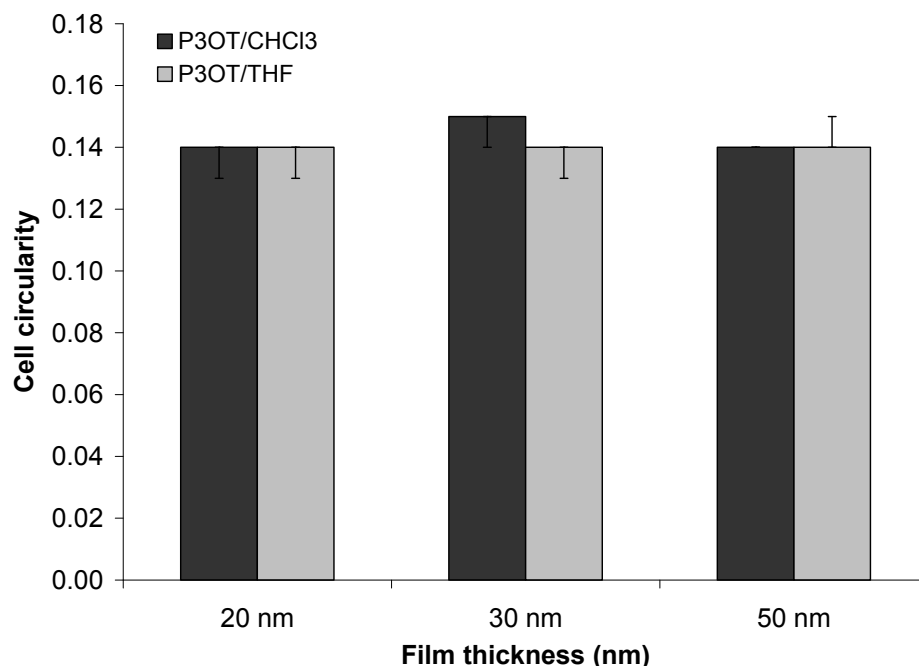


Figure 5.13. Circularity of MC3T3-E1 cells after 4 hours of culture on P3OT films (20, 30, and 50 nm) made from CHCl₃ and THF. Values are presented as median \pm 95% confidence intervals.

We also investigated the effect of film preparation conditions (i.e., annealed vs. unannealed and CHCl₃ vs. THF) on the attachment of osteoblasts. Cell attachment density 4 hours after seeding is shown in Figure 5.14. The number of adherent cells was significantly greater ($p < 0.05$) on uaP3OT/CHCl₃ (~ 3000 cells/cm²) compared to aP3OT/CHCl₃ (~ 2300 cells/cm²). The opposite was observed for P3OT/THF films in which cell density was ~ 3000 cells/cm² and ~ 2100 cells/cm² on aP3OT and uaP3OT, respectively.

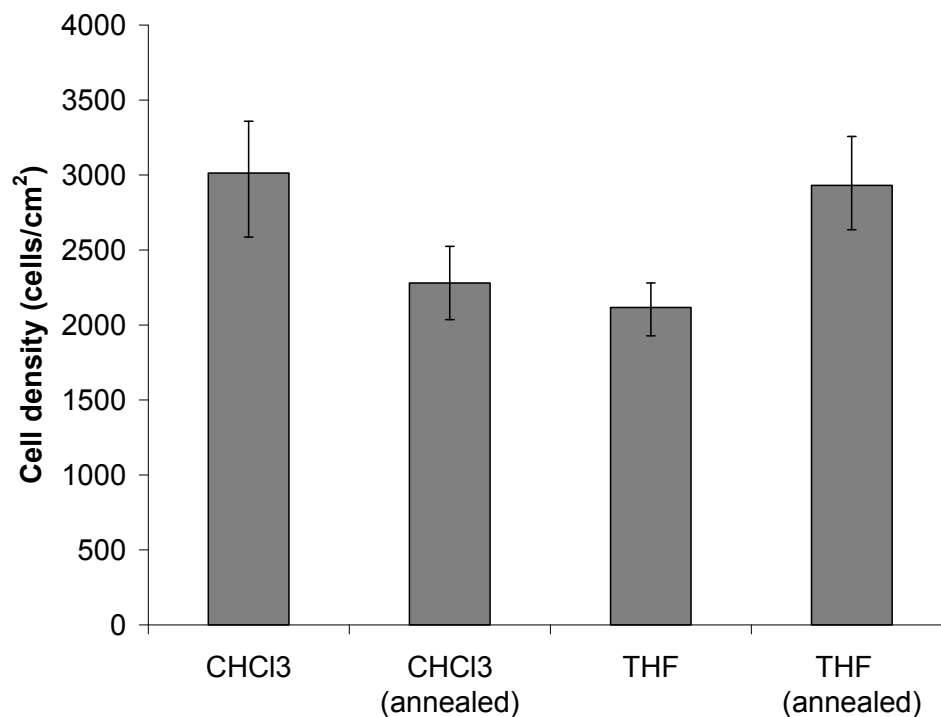


Figure 5.14. MC3T3-E1 cell attachment density on aP3OT and uaP3OT films made from CHCl₃ and THF 4 hours after seeding. Values are presented as median \pm 95% confidence intervals.

Figure 5.15 shows the cell area and circularity of cells cultured on annealed and unannealed P3OT films made from CHCl₃ and THF. Cell area was significantly greater on annealed ($\sim 1070 \mu\text{m}^2$) compared to unannealed ($\sim 980 \mu\text{m}^2$) films made from CHCl₃. The opposite was observed for cell cultured on films made from THF ($\sim 930 \mu\text{m}^2$ and $\sim 1150 \mu\text{m}^2$ for unannealed and annealed, respectively). When comparing cell area for different solvents it was significantly higher on uaP3OT/THF compared to uaP3OT/CHCl₃ and significantly lower on aP3OT/THF when compared to aP3OT/CHCl₃. Cell circularity was only significantly higher for cell cultured on aP3OT/THF.

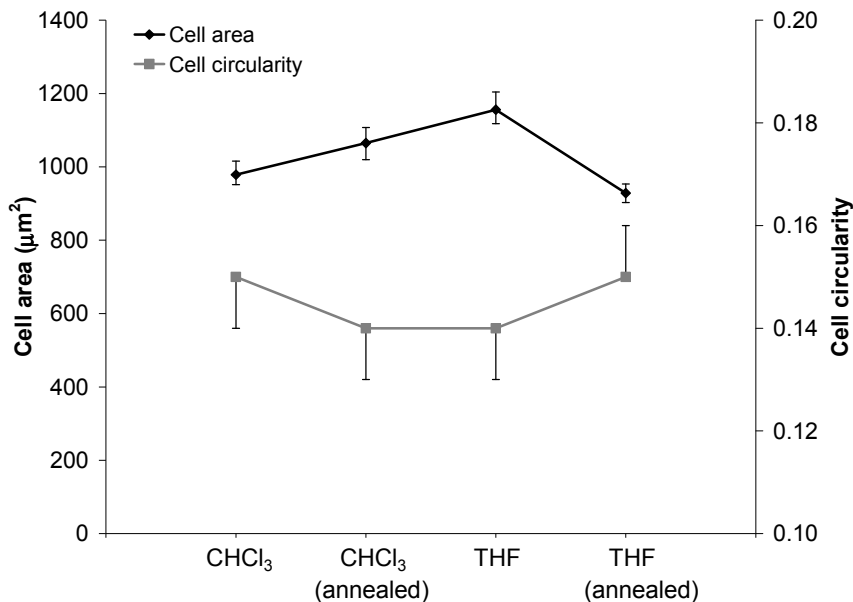


Figure 5.15. Area and circularity of MC3T3-E1 cells after 4 hours of culture on aP3OT and uaP3OT films made from CHCl₃ and THF. Values are presented as median ± 95% confidence intervals.

Nanoscale features (e.g., islands and pits) are known to affect cell functions such as attachment and spreading.[106-108] Therefore, the differences observed in cell density, area and circularity of P3OT films made from CHCl₃ and THF could be explained by the differences in surface morphology that arise from casting films using different solvents and by thermal annealing.

5.5 Conclusions

We developed P3OT thickness gradient libraries over a high range (130 – 200 nm) and discrete thickness films over a low range (20, 30, and 50 nm). We also investigated the effect of thermal annealing (annealed at 80°C vs. unannealed) and solvent used for film preparation (CHCl₃ vs. THF). In summary, we demonstrate that P3OT film preparation conditions through their effects on surface morphology can be

used to alter MC3T3-E1 attachment. We demonstrate that cell attachment over the low range and cell attachment and proliferation over the high range were not affected by P3OT thickness. We also demonstrate that annealing had opposite effect on cell density, area, and circularity on films prepared from CHCl_3 when compared to films prepared from THF.

CHAPTER 6

CONCLUSIONS AND FUTURE DIRECTIONS

6.1 Conclusions

The objective of this project was to assess the suitability of P3OT to sustain MC3T3-E1 attachment and growth. Our central hypothesis was that P3OT film properties (i.e., thickness, film preparation conditions, and level of doping) are able to regulate osteoblast functions (i.e., attachment and proliferation). We formulated this hypothesis based on preliminary studies on P3OT and the fact that other substituted polythiophenes have been tuned to regulate and elicit desired functions in cells that are known to respond to electrical stimulation. Using discrete and high-throughput methods we demonstrate that P3OT is a suitable surface to sustain MC3T3-E1 attachment and proliferation with no cytotoxicity observed relative to TCPS. We also demonstrate that doping P3OT with FeCl_3 has a strong effect on MC3T3-E1 cell attachment and proliferation and that film preparation conditions can be used to regulate attachment and proliferation in osteoblasts. This work is significant because it contributes to the growing area of conducting polymers in biomedical applications and establishes P3OT, for the first time, as a potential cell substrate that sustains MC3T3-E1 attachment and promotes high levels of cell proliferation.

6.2 Future directions

The research presented here could be expanded further to enhance our understanding P3OT-cell interactions. It is important to note that the methods described

in this section could be applied to other cell types that are known to respond to electrical stimulation (e.g., nerve, muscle, bone, and cardiac cells).

6.2.1 Protein expression and mineralization

The immature MC3T3-E1 cell line used in this work is known to exhibit a developmental sequence analogous to osteoblasts in bone tissue, namely proliferation of undifferentiated osteoblast precursors followed by expression of differentiated osteoblast phenotype, and subsequent mineralization of extracellular matrix (ECM) when mature.[52] In this work we studied the initial events (i.e., attachment and proliferation) that occur when MC3T3-E1 cells are cultured on P3OT thin films. Further studies should address the ability of MC3T3-E1 cells to express the genes associated with bone cell differentiation when cultured on P3OT. It is known that extracellular matrix maturation and mineralization follow proliferation in osteoblast cells.[109] Therefore, the expression of bone matrix proteins (e.g., alkaline phosphatase, osteocalcin, and osteopontin) as well as mineralization of MC3T3-E1 cells should be further studied.

6.2.2 Regulating P3OT-cell interactions by adsorbed proteins

Cell adhesion to synthetic materials is crucial to many biomedical applications.[110, 111] It is believed that cell adhesion is mediated by a layer of adsorbed proteins, such as vitronectin, fibrinogen, and fibronectin.[112] Moreover, pre-adsorbed serum proteins are known to play an important role in modifying surface characteristics which in turn modulate cell attachment and growth.[74, 76, 77] For example, De Giglio et al. showed that osteoblast adhesion was enhanced up to 230% on RGDS peptide-modified PPy surfaces. In this work we showed that pre-soaking P3OT with serum containing media enhanced proliferation of MC3T3-E1 cells. This work

should be extended further to investigate the effect of specific adsorbed proteins (e.g., RGDS peptide, fibronectin, and vitronectin) on osteoblast attachment and proliferation.

6.2.3 Combinatorial methods to generate doping gradients

In this work we showed that doping P3OT with FeCl_3 has a strong effect on MC3T3-E1 cell attachment and proliferation. It would be of interest to study the effect of multiple doping concentrations on cell functions. Generating doping concentration gradients could provide a rapid way of studying the level of doping effect on cell functions. Vertical dipping methods, similar to the ones developed for layer-by-layer deposition,[113] could be customized to generate doping gradients. A gradient in dipping time could be used to create a gradient in the level of doping across a polymer film. Combinatorial and high-throughput methods[114] could then be used to analyze cell response to P3OT doping gradients.

6.2.4 Combination of electrical and topographical characteristics

In this work we demonstrated that P3OT is a suitable substrate to sustain attachment and proliferation of osteoblasts and that its properties can be tailored to modulate cell functions. Surface topography is also known to play an important role in modulating osteoblast functions such as adhesion[115] and proliferation.[116] The simultaneous use of conductivity and surface patterns to stimulate cells is a novel idea that has recently been investigated.[117] Therefore, it would be of interest to expand this research to study the combined effect of conductivity and patterning on MC3T3-E1 cells using P3OT as the conducting substrate.

Surface patterning can be achieved by a variety of soft lithographic techniques such as microcontact printing, replica molding, and solvent-assisted microcontact

molding as well as other techniques including dip-pen nanolithography, photolithography, and dewetting.[118] Most of these techniques require clean-room facilities and some are expensive. Dewetting is an inexpensive technique and does not require a clean room. Dewetting of thin polymer films is caused by a destabilization process that yields a rupture of an initially homogeneous film.[119, 120]

Chatthopadhyay et al.[28, 34] developed and characterized dewetting patterns on polystyrene (PS)/P3OT bilayers (Figure 6.1). In these studies the authors showed that characterizing film dewetting utilizing orthogonal thickness gradient libraries of P3OT and PS is an efficient way of capturing the VDW stability regimes in the PS/P3OT system.

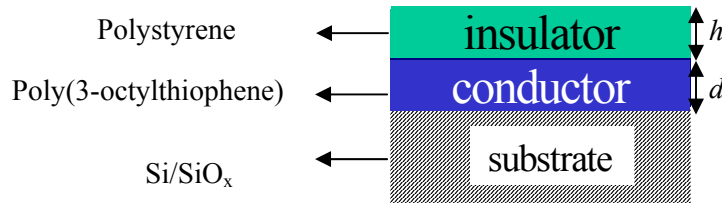


Figure 6.1. Schematic of the conductor/insulator bilayer system.

Figure 6.2 shows the different dewetting patterns that can be obtained from various PS thicknesses (21 nm, 23 nm, and 25 nm) coated on top of a 170 nm P3OT film. By dewetting PS/P3OT bilayers of PS thicknesses ranging from 20 – 30 nm and P3OT thickness of 170 nm for 10 minutes at 100 °C, hole diameters < 50 μm can be achieved. Previous studies have shown enhanced protein expression and F-actin production of osteoblasts in poly(D,L-lactide)/poly(ε-caprolactone) temperature-composition libraries having microstructures with diameters within this range (20 – 40 μm).[91, 114, 121] Therefore, dewetted PS/P3OT bilayers may present an economic and plausible way of studying the combined effects of conductivity and patterning on MC3T3-E1 functions.

In this work we characterized the attachment and proliferation of osteoblasts on P3OT but one important question that may arise if the PS/P3OT system is used is whether or not cells are capable of attaching and proliferating on PS thin films. We investigated the proliferation of MC3T3-E1 cells cultured on PS for 24, 48, and 72 hours (Figure 6.3) and demonstrated that PS is also a suitable substrate that sustains high levels of proliferation.

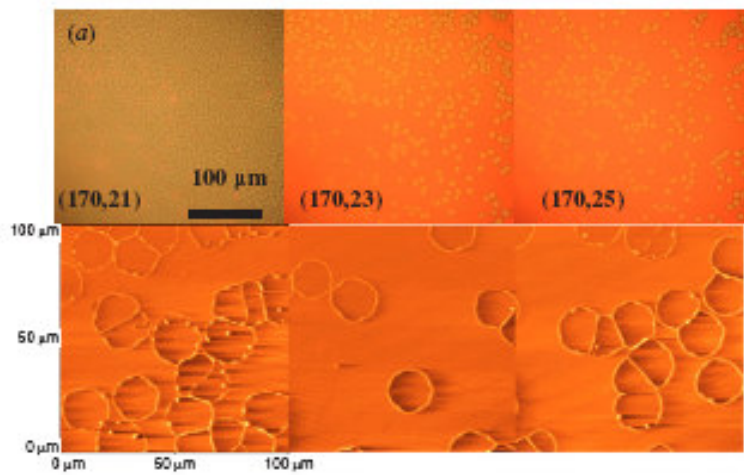


Figure 6.2. Optical micrograph and corresponding AFM topograph of dewetting pattern for various PS thicknesses in 10 min at 100°C on P3OT coated silicon substrate of 170 nm P3OT thickness.[28]

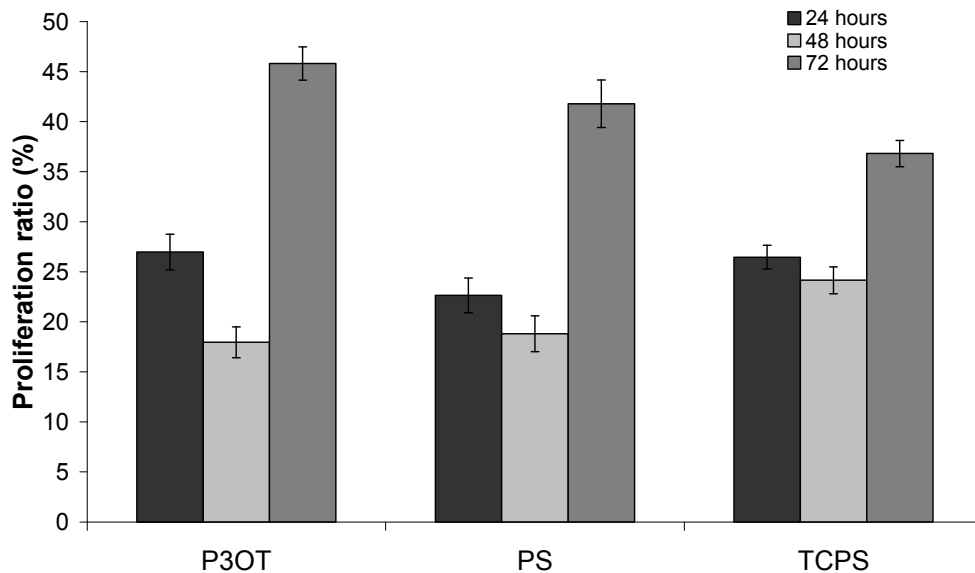


Figure 6.3. Proliferation ratio of MC3T3-E1 cells after 24, 48, and 72 hours of culture on P3OT, PS, and TCPS. Values are presented as mean \pm 95% confidence intervals.

6.2.5 Electrical stimulation

A number of studies have shown that electrical stimulation using conducting polymers can modulate cellular response. For example, Wong et al.[56] studied the effect of doped polypyrrole (PPy) on the attachment and spreading of endothelial cells. They showed that oxidized PPy resulted in cell spreading, whereas reduction of PPy to its neutral state led to cell rounding. Other studies have shown that cell growth and function can be enhanced at the interface of PPy undergoing electrical stimulation.[122]

Electrical stimulation of bone has been shown to enhance bone cell functions *in vivo* [65] and *in vitro*. [101, 123, 124] The mechanism by which cell functions are regulated by electrical stimulation is a matter of great interest. It is well known that on both sides of the cell membrane there are free ions such as K^+ , Ca^{2+} , Na^+ , and Cl^- , which play an important role in signal transduction processes and are responsible for the difference in voltage, or electric potential, that exists across the plasma membrane.[53] Previous studies have suggested that osteoblast response to electric fields is accompanied by an increase in cytosolic calcium concentration and might involve the calcium/calmodulin pathway.[101, 125] *In vitro* studies have been performed using the main forms of electrical stimulation: direct electrical current,[126] capacitive coupling,[101] and inductive coupling.[127] For example, Wang et al.[126] showed increased proliferation and calcification of cultured osteoblast cells when direct current was applied. The electrochemical reactions involved during constant direct current stimulation of bone cells *in vitro* have also been studied.[128] In this study the authors showed that a current density of $100 \mu A/cm^2$ was effective in opening the calcium passage and produced limited electrochemical reactions.[128, 129]

These findings provide a framework that could be used to study the effect of electrical stimulation on the attachment and proliferation of MC3T3-E1 cells cultured on undoped and doped P3OT films. Electrical stimulation has also been shown to affect the amount of protein adsorbed on conducting surfaces.[130] Therefore, the use of electrical stimulation could be expanded further to study its effect on protein adsorption to P3OT and thus cell shape and growth.

APPENDIX A

Additional Figures

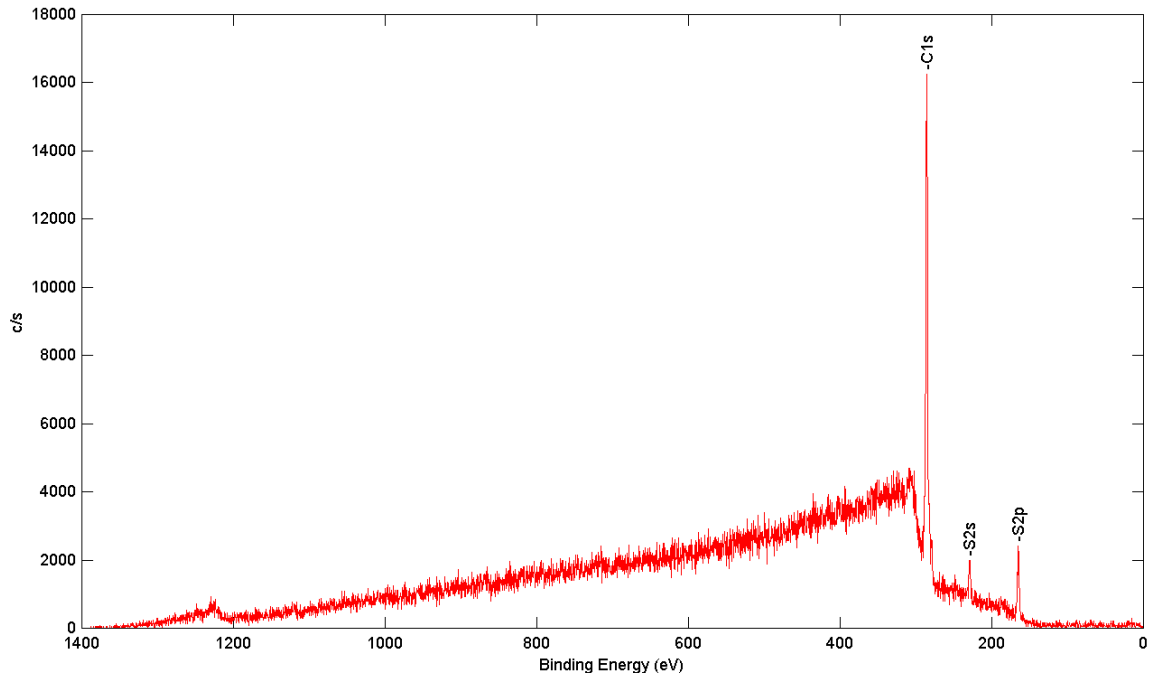


Figure A.1. XPS spectra of P3OT thin films (30 nm).

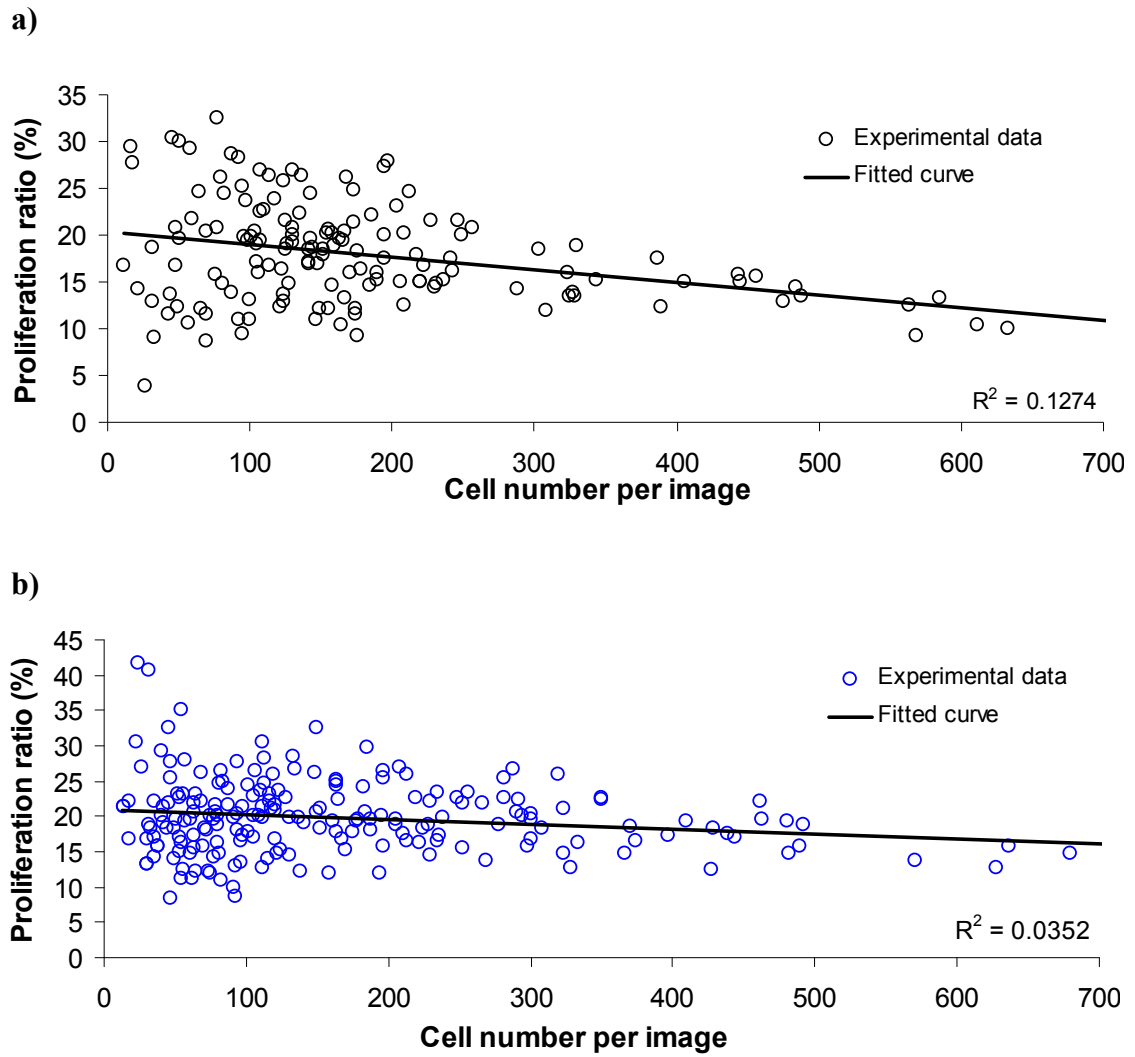


Figure A.2. Effect of cell density on cell proliferation for MC3T3-E1 cultured on (a) uP3OT and (b) D125 for a period of 48 hours.

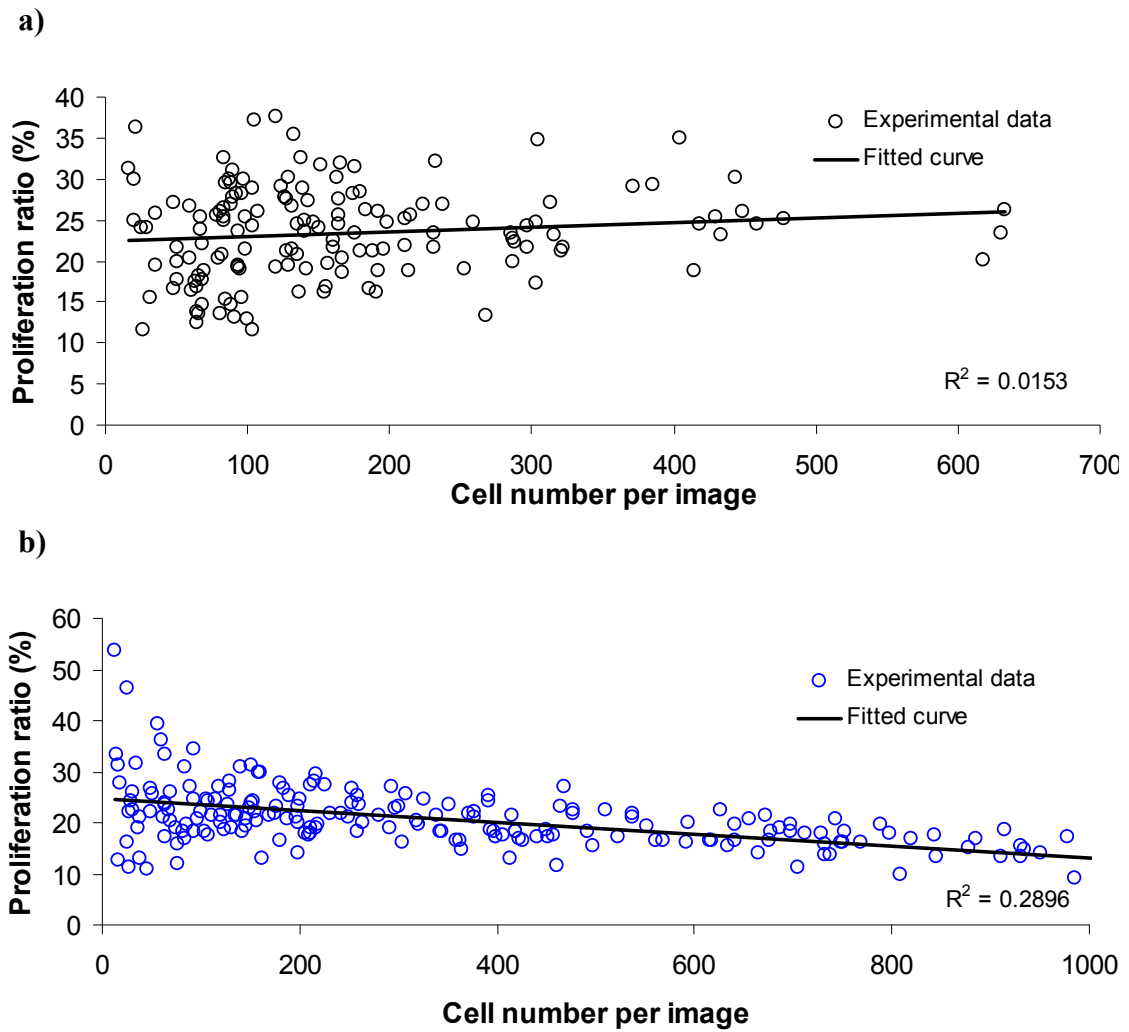


Figure A.3. Effect of cell density on cell proliferation for MC3T3-E1 cultured on (a) uP30T and (b) D125 for a period of 72 hours.

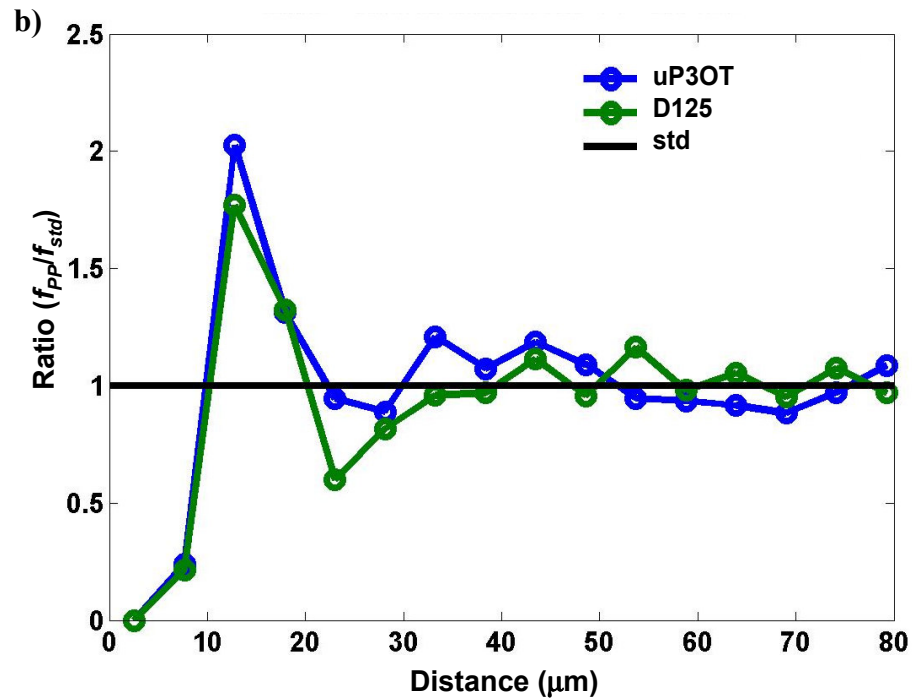
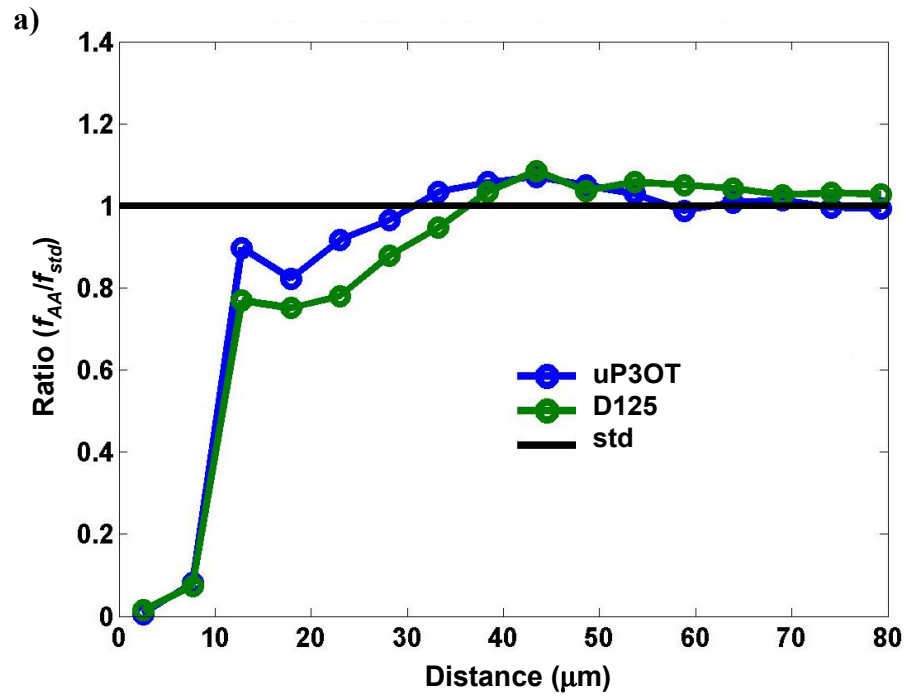


Figure A.4. Normalized distributions: a) \tilde{f}_{AA} , b) \tilde{f}_{PP} , c) f_{PR}/f_{RR} , and d) \tilde{f}_{RR} for cells cultured for a period of 48 hours on uP3OT and D125.

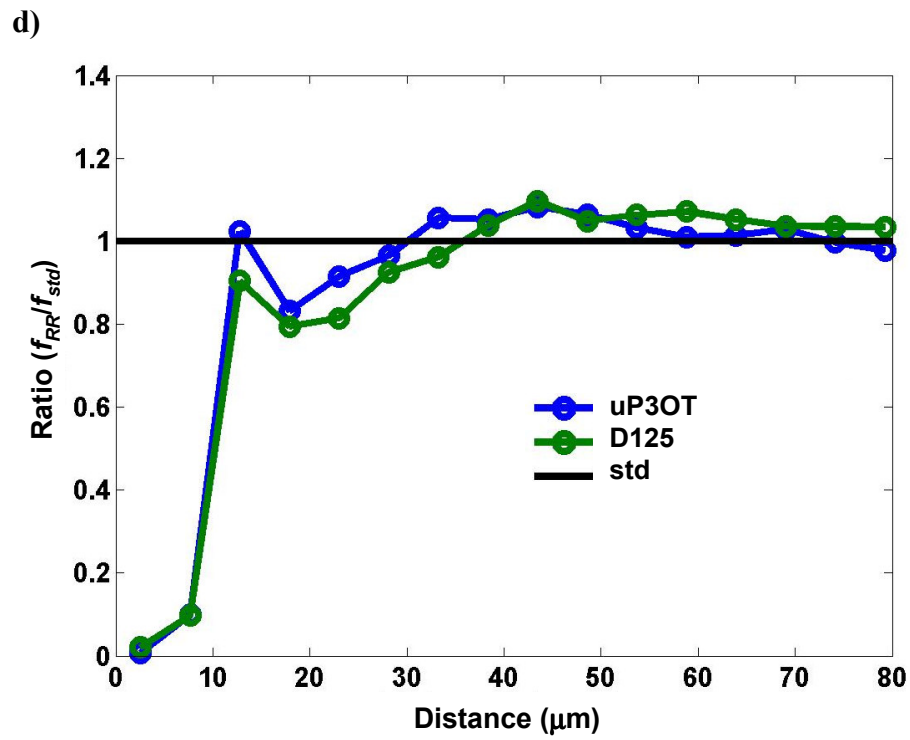
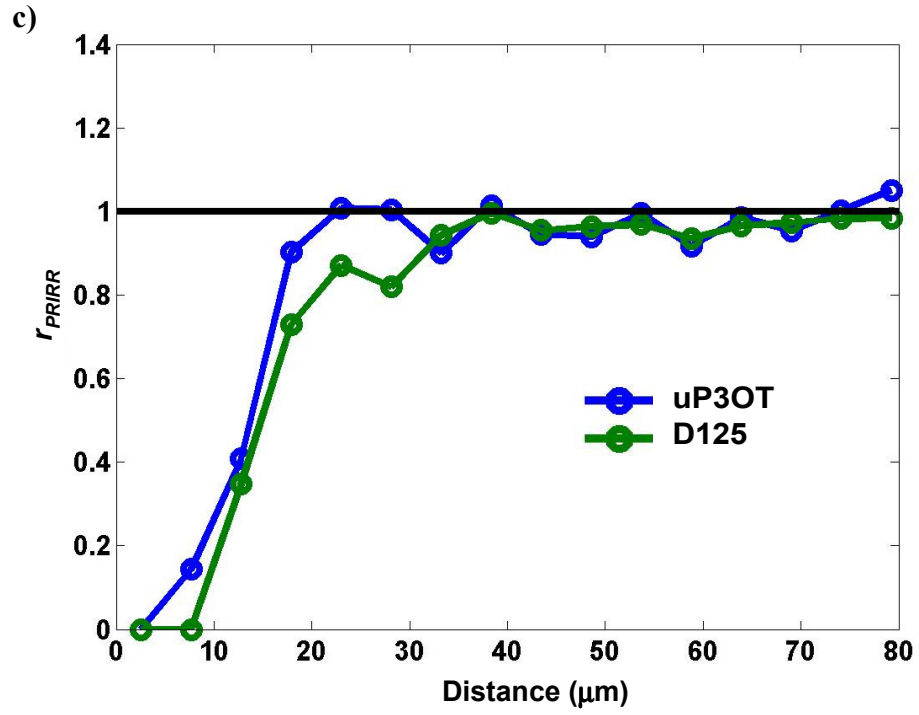


Figure A.4. Continued.

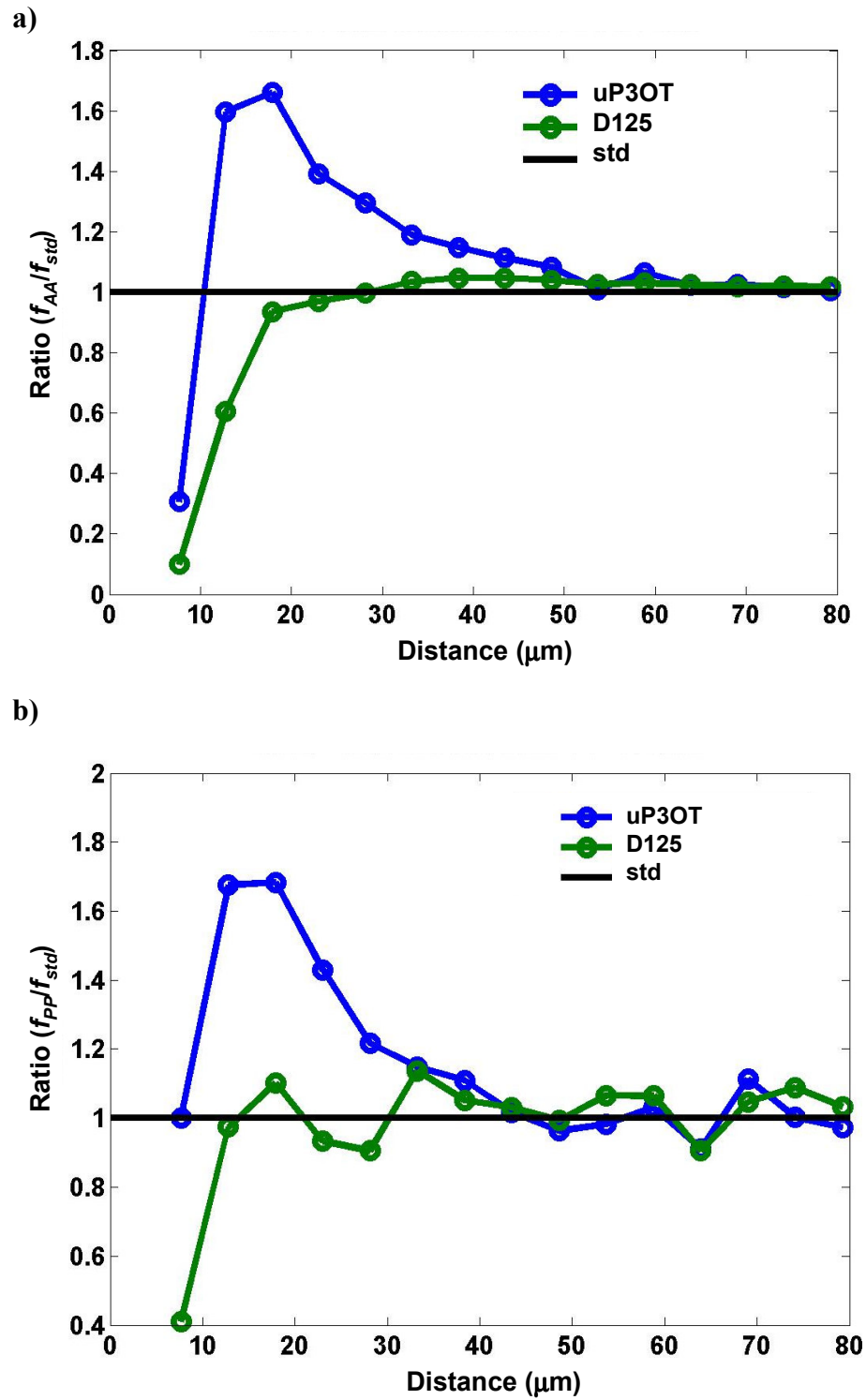


Figure A.5. Normalized distributions: a) \tilde{f}_{AA} , b) \tilde{f}_{PP} , c) f_{PR}/f_{RR} , and d) \tilde{f}_{RR} for cells cultured for a period of 72 hours on uP3OT and D125.

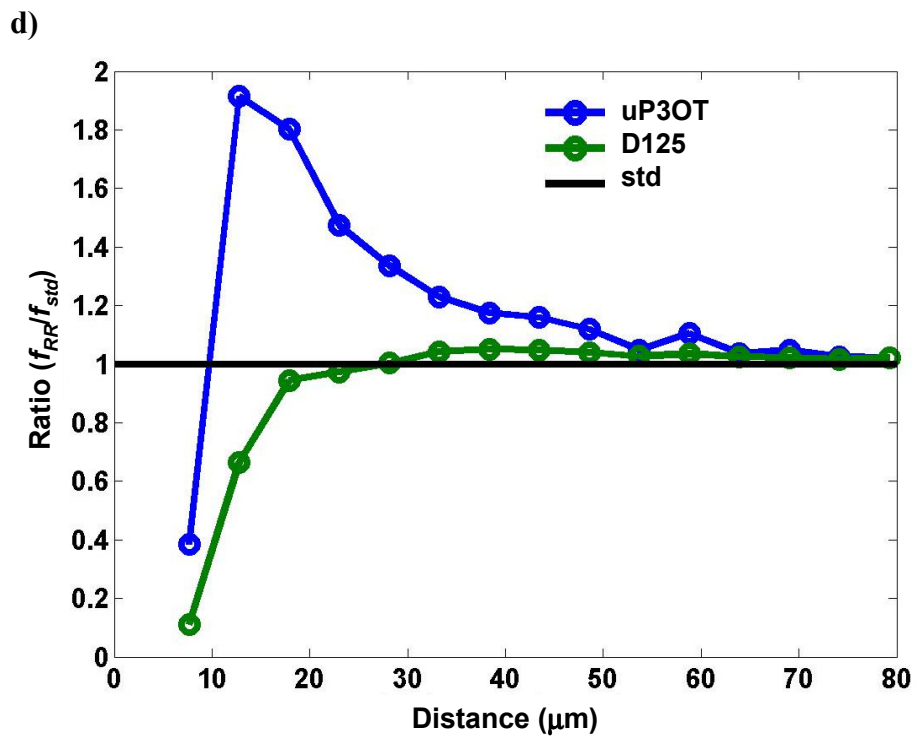
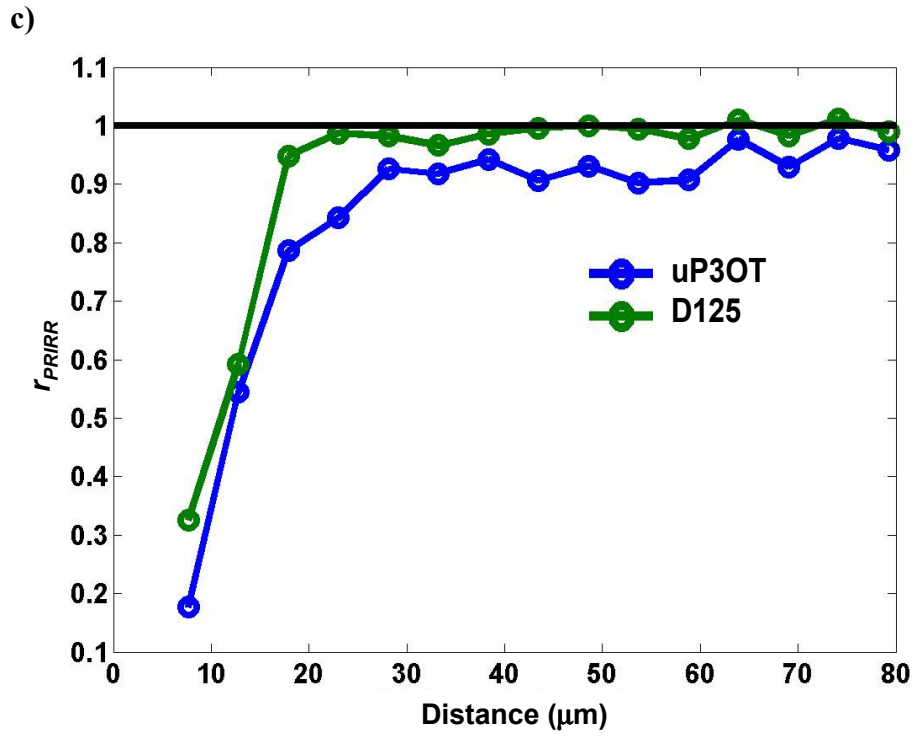


Figure A.5. Continued.

REFERENCES

1. McNeill, R., et al., *ELECTRONIC CONDUCTION IN POLYMERS .I. CHEMICAL STRUCTURE OF POLYPYRROLE*. Australian Journal of Chemistry, 1963. **16**(6): p. 1056-&.
2. Shirakawa, H., et al., *Synthesis Of Electrically Conducting Organic Polymers - Halogen Derivatives Of Polyacetylene, (Ch)X*. Journal Of The Chemical Society-Chemical Communications, 1977(16): p. 578-580.
3. Shirakawa, H., *Nobel Lecture: The discovery of polyacetylene film - the dawning of an era of conducting polymers*. Reviews Of Modern Physics, 2001. **73**(3): p. 713-718.
4. Guimard, N.K., N. Gomez, and C.E. Schmidt, *Conducting polymers in biomedical engineering*. Progress in Polymer Science, 2007. **32**(8-9): p. 876-921.
5. Skotheim, T.A., R.L. Elsenbaumer, and J.R. Reynolds, *Handbook of conducting polymers*. 2nd ed. 1998, New York: M. Dekker. xiii, 1097 p.
6. Heeger, A.J., *Semiconducting and metallic polymers: the fourth generation of polymeric materials*. Synthetic Metals, 2001. **125**(1): p. 23-42.
7. Gurunathan, K., et al., *Electrochemically synthesised conducting polymeric materials for applications towards technology in electronics, optoelectronics and energy storage devices*. Materials Chemistry and Physics, 1999. **61**(3): p. 173-191.
8. Collier, J.H., et al., *Synthesis and characterization of polypyrrole-hyaluronic acid composite biomaterials for tissue engineering applications*. Journal of Biomedical Materials Research, 2000. **50**(4): p. 574-584.
9. Wang, X.D., et al., *Evaluation of biocompatibility of polypyrrole in vitro and in vivo*. Journal of Biomedical Materials Research Part A, 2004. **68A**(3): p. 411-422.
10. George, P.M., et al., *Fabrication and biocompatibility of polypyrrole implants suitable for neural prosthetics*. Biomaterials, 2005. **26**(17): p. 3511-3519.
11. Cui, X.Y. and D.C. Martin, *Electrochemical deposition and characterization of poly(3,4-ethylenedioxythiophene) on neural microelectrode arrays*. Sensors and Actuators B-Chemical, 2003. **89**(1-2): p. 92-102.
12. Foulds, N.C. and C.R. Lowe, *ENZYME ENTRAPMENT IN ELECTRICALLY CONDUCTING POLYMERS - IMMOBILIZATION OF GLUCOSE-OXIDASE IN POLYPYRROLE AND ITS APPLICATION IN AMPEROMETRIC GLUCOSE*

- SENSORS*. Journal of the Chemical Society-Faraday Transactions I, 1986. **82**: p. 1259-1264.
13. Kang, S.K., et al., *Synthesis of polythiophene derivatives and their application for electrochemical DNA sensor*. Polymer Journal, 2004. **36**(12): p. 937-942.
 14. Otero, T.F. and M.T. Cortes, *A sensing muscle*. Sensors and Actuators B-Chemical, 2003. **96**(1-2): p. 152-156.
 15. Tahhan, M., et al., *Carbon nanotube and polyaniline composite actuators*. Smart Materials & Structures, 2003. **12**(4): p. 626-632.
 16. Abidian, M.R., D.H. Kim, and D.C. Martin, *Conducting-polymer nanotubes for controlled drug release*. Advanced Materials, 2006. **18**(4): p. 405-+.
 17. Li, Y.L., K.G. Neoh, and E.T. Kang, *Controlled release of heparin from polypyrrole-poly(vinyl alcohol) assembly by electrical stimulation*. Journal of Biomedical Materials Research Part A, 2005. **73A**(2): p. 171-181.
 18. Otero, T.F., et al., *ELECTROCHEMOMECHANICAL PROPERTIES FROM A BILAYER - POLYPYRROLE NONCONDUCTING AND FLEXIBLE MATERIAL ARTIFICIAL MUSCLE*. Journal of Electroanalytical Chemistry, 1992. **341**(1-2): p. 369-375.
 19. Chan, H.S.O. and S.C. Ng, *Synthesis, characterization and applications of thiophene-based functional polymers*. Progress in Polymer Science, 1998. **23**(7): p. 1167-1231.
 20. Widge, A.S., et al., *Self-assembled monolayers of polythiophene conductive polymers improve biocompatibility and electrical impedance of neural electrodes*. Biosensors & Bioelectronics, 2007. **22**(8): p. 1723-1732.
 21. Bera-Aberem, M., H.A. Ho, and M. Leclerc, *Functional polythiophenes as optical chemo- and biosensors*. Tetrahedron, 2004. **60**(49): p. 11169-11173.
 22. del Valle, L.J., et al., *Cellular adhesion and proliferation on poly(3,4-ethylenedioxythiophene): Benefits in the electroactivity of the conducting polymer*. European Polymer Journal, 2007. **43**(6): p. 2342-2349.
 23. Waugaman, M., et al., *Synthesis, characterization and biocompatibility studies of oligosiloxane modified polythiophenes*. European Polymer Journal, 2003. **39**(7): p. 1405-1412.
 24. Elsenbaumer, R.L., K.Y. Jen, and R. Oboodi, *Processible And Environmentally Stable Conducting Polymers*. Synthetic Metals, 1986. **15**(2-3): p. 169-174.

25. Jen, K.Y., G.G. Miller, and R.L. Elsenbaumer, *Highly Conducting, Soluble, And Environmentally-Stable Poly(3-Alkylthiophenes)*. Journal Of The Chemical Society-Chemical Communications, 1986(17): p. 1346-1347.
26. Aasmundtveit, K.E., et al., *Structural studies of polyalkylthiophenes with alternating sidechain positioning*. Synthetic Metals, 2000. **113**(1): p. 7.
27. Braun, D., et al., *Electroluminescence And Electrical Transport In Poly(3-Octylthiophene) Diodes*. Journal Of Applied Physics, 1992. **72**(2): p. 564-568.
28. Chattopadhyay, S. and J.C. Meredith, *Combinatorial screening of organic electronic materials: thin film stability*. Measurement Science & Technology, 2005. **16**(1): p. 128-136.
29. Nicho, M.E., et al., *Synthesis of derivatives of polythiophene and their application in an electrochromic device*. Solar Energy Materials and Solar Cells, 2004. **82**(1-2): p. 105-118.
30. Winokur, M.J., et al., *Structural Evolution In Iodine-Doped Poly(3-Alkylthiophenes)*. Macromolecules, 1991. **24**(13): p. 3812-3815.
31. Lane, P.A., X. Wei, and Z.V. Vardeny, *Spin and spectral signatures of polaron pairs in pi-conjugated polymers*. Physical Review B, 1997. **56**(8): p. 4626-4637.
32. Singh, R., et al., *Mechanism of charge transport in poly(3-octylthiophene)*. Journal of Applied Physics, 2006. **100**(1).
33. Kumar, J., et al., *Effect of FeCl₃ on the stability of pi-conjugation of electronic polymer*. Corrosion Science, 2008. **50**(2): p. 301-308.
34. Chattopadhyay, S. and J.C. Meredith, *Instability and Dewetting of Conducting-Insulating Polymer Thin-Film Bilayers*. Macromolecular Rapid Communications, 2004. **25**(1): p. 275.
35. Taka, T., et al., *CHARACTERIZATION OF UNDOPED POLY(3-OCTYL THIOPHENE)*. Synthetic Metals, 1993. **55**(1): p. 414-419.
36. Zhokhavets, U., et al., *Anisotropic optical properties of thin poly(3-octylthiophene)-films as a function of preparation conditions*. Synthetic Metals, 2004. **143**(1): p. 113-117.
37. Singh, R., et al., *Effect of thermal annealing on surface morphology and physical properties of poly(3-octylthiophene) films*. Polymer, 2005. **46**(21): p. 9126-9132.
38. Kumar, J., et al., *The combined effect of intercalated oxidant and thermal annealing on surface morphology and photo-physical properties of poly(3-octylthiophene) films*. Materials Chemistry and Physics, 2007. **101**(2-3): p. 336-343.

39. Kumar, J., et al., *dc electrical conduction and morphology of poly(3-octylthiophene) films*. Journal of Physics D-Applied Physics, 2006. **39**(1): p. 196-202.
40. Prosa, T.J., et al., *X-Ray-Diffraction Studies Of Iodine-Doped Poly(3-Alkylthiophenes)*. Synthetic Metals, 1993. **55**(1): p. 370-377.
41. Qiao, X.Y., X.H. Wang, and Z.S. Mo, *The FeCl₃-doped poly(3-alkylthiophenes) in solid state*. Synthetic Metals, 2001. **122**(2): p. 449-454.
42. Singh, R.K., et al., *Structure-conductivity correlation in ferric chloride-doped poly(3-hexylthiophene)*. New Journal of Physics, 2006. **8**.
43. Ficker, J., et al., *Stability of polythiophene-based transistors and circuits*. Journal of Applied Physics, 2003. **94**(4): p. 2638-2641.
44. de Oliveira, M.A., W.B. de Almeida, and H.F. dos Santos, *Structure and electronic properties of alkylthiophenes coupled by Head-to-Tail and Head-to-Head regioselectivity*. Journal of the Brazilian Chemical Society, 2004. **15**(6): p. 832-838.
45. Aasmundtveit, K.E., et al., *Structural anisotropy of poly(alkylthiophene) films*. Macromolecules, 2000. **33**(8): p. 3120-3127.
46. Kline, R.J., M.D. McGehee, and M.F. Toney, *Highly oriented crystals at the buried interface in polythiophene thin-film transistors*. Nature Materials, 2006. **5**(3): p. 222-228.
47. Fukada, E. and I. Yasuda, *On The Piezoelectric Effect Of Bone*. Journal Of The Physical Society Of Japan, 1957. **12**(10): p. 1158-1162.
48. Shastri, V.P., et al., *Application of conductive polymers in bone regeneration*. Materials Research Society Symposium - Proceedings, 1999. **550**: p. 215.
49. Castano, H., et al., *Polypyrrole thin films formed by admicellar polymerization support the osteogenic differentiation of mesenchymal stem cells*. Macromolecular Bioscience, 2004. **4**(8): p. 785-794.
50. Supronowicz, P.R., et al., *Novel current-conducting composite substrates for exposing osteoblasts to alternating current stimulation*. Journal Of Biomedical Materials Research, 2002. **59**(3): p. 499-506.
51. Boyan, B.D., et al., *Mechanisms involved in osteoblast response to implant surface morphology*. Annual Review Of Materials Research, 2001. **31**: p. 357-371.

52. Quarles, L.D., et al., *Distinct Proliferative And Differentiated Stages Of Murine Mc3t3-E1 Cells In Culture - An Invitro Model Of Osteoblast Development*. Journal Of Bone And Mineral Research, 1992. **7**(6): p. 683-692.
53. Lodish, H.F., *Molecular cell biology*. 5th ed. 2003, New York: W.H. Freeman and Company. xxxiii, 973 , [79] p.
54. Gratzner, H.G., *Monoclonal-Antibody To 5-Bromodeoxyuridine And 5-Iododeoxyuridine - A New Reagent For Detection Of Dna-Replication*. Science, 1982. **218**(4571): p. 474-475.
55. Dickinson, B., *Monoclonal Antibody Source Book*. 1995.
56. Wong, J.Y., R. Langer, and D.E. Ingber, *ELECTRICALLY CONDUCTING POLYMERS CAN NONINVASIVELY CONTROL THE SHAPE AND GROWTH OF MAMMALIAN-CELLS*. Proceedings of the National Academy of Sciences of the United States of America, 1994. **91**(8): p. 3201-3204.
57. Stauffer, W.R. and X.T. Cui, *Polypyrrole doped with 2 peptide sequences from laminin*. Biomaterials, 2006. **27**(11): p. 2405-2413.
58. Kros, A., N. Sommerdijk, and R.J.M. Nolte, *Poly(pyrrole) versus poly(3,4-ethylenedioxythiophene): implications for biosensor applications*. Sensors and Actuators B-Chemical, 2005. **106**(1): p. 289-295.
59. Nien, P.C., T.S. Tung, and K.C. Ho, *Amperometric glucose biosensor based on entrapment of glucose oxidase in a poly(3,4-ethylenedioxythiophene) film*. Electroanalysis, 2006. **18**(13-14): p. 1408-1415.
60. Marsella, M.J. and R.J. Reid, *Toward molecular muscles: Design and synthesis of an electrically conducting poly[cyclooctatetrathiophene]*. Macromolecules, 1999. **32**(18): p. 5982-5984.
61. Ullmann, K.R., et al., *Osteoblast responses to electrical stimulation*. American Society of Mechanical Engineers, Bioengineering Division (Publication) BED, 1999. **42**: p. 189.
62. Bassett, C.A., R.J. Pawluk, and R.O. Becker, *Effects Of Electric Currents On Bone In Vivo*. Nature, 1964. **204**(495): p. 652-&.
63. Bassett, C.A.L., R.J. Pawluk, and A.A. Pilla, *Augmentation Of Bone Repair By Inductively Coupled Electromagnetic-Fields*. Science, 1974. **184**(4136): p. 575-577.
64. Friedenb.Zb, et al., *Bone Reaction To Varying Amounts Of Direct Current*. Surgery Gynecology And Obstetrics With International Abstracts Of Surgery, 1970. **131**(5): p. 894-&.

65. Yonemori, K., et al., *Early effects of electrical stimulation on osteogenesis*. Bone, 1996. **19**(2): p. 173-180.
66. Brighton, C.T., et al., *Invitro Bone Cell Response To A Capacitively Coupled Electrical-Field - The Role Of Field-Strength, Pulse Pattern, And Duty Cycle*. Clinical Orthopaedics And Related Research, 1992(285): p. 255-262.
67. Meredith, J.C., et al., *Combinatorial materials science for polymer thin-film dewetting*. Macromolecules, 2000. **33**(26): p. 9747-9756.
68. Karim, A., et al., *Combinatorial mapping of polymer blends phase behavior, in Experimental design for combinatorial and high throughput materials development*, J.N. Cawse, Editor. 2003, John Wiley & Sons, Inc.: Hoboken. p. 73-88.
69. Stafford, C.M., et al., *Generating thickness gradients of thin polymer films via flow coating*. Review of Scientific Instruments, 2006. **77**(2).
70. Chen, T.A., X.M. Wu, and R.D. Rieke, *Regiocontrolled Synthesis Of Poly(3-Alkylthiophenes) Mediated By Rieke Zinc - Their Characterization And Solid-State Properties*. Journal Of The American Chemical Society, 1995. **117**(1): p. 233-244.
71. Folkman, J. and A. Moscona, *ROLE OF CELL-SHAPE IN GROWTH-CONTROL*. Nature, 1978. **273**(5661): p. 345-349.
72. Chen, C.S., et al., *Micropatterned surfaces for control of cell shape, position, and function*. Biotechnology Progress, 1998. **14**(3): p. 356-363.
73. Ruardy, T.G., et al., *ADHESION AND SPREADING OF HUMAN SKIN FIBROBLASTS ON PHYSICOCHEMICALLY CHARACTERIZED GRADIENT SURFACES*. Journal of Biomedical Materials Research, 1995. **29**(11): p. 1415-1423.
74. Schakenraad, J.M., et al., *THE INFLUENCE OF SUBSTRATUM SURFACE FREE-ENERGY ON GROWTH AND SPREADING OF HUMAN-FIBROBLASTS IN THE PRESENCE AND ABSENCE OF SERUM-PROTEINS*. Journal of Biomedical Materials Research, 1986. **20**(6): p. 773-784.
75. Webb, K., V. Hlady, and P.A. Tresco, *Relationships among cell attachment, spreading, cytoskeletal organization, and migration rate for anchorage-dependent cells on model surfaces*. Journal of Biomedical Materials Research, 2000. **49**(3): p. 362-368.
76. Balcells, M. and E.R. Edelman, *Effect of pre-adsorbed proteins on attachment, proliferation, and function of endothelial cells*. Journal of Cellular Physiology, 2002. **191**(2): p. 155-161.

77. Sousa, S.R., et al., *Osteoblast adhesion and morphology on TiO₂ depends on the competitive preadsorption of albumin and fibronectin*. Journal of Biomedical Materials Research Part A, 2008. **84A**(2): p. 281-290.
78. Liu, J.S., et al., *Polythiophene containing thermally removable solubilizing groups enhances the interface and the performance of polymer-titania hybrid solar cells*. Journal of the American Chemical Society, 2004. **126**(31): p. 9486-9487.
79. Shaheen, S.E., et al., *2.5% efficient organic plastic solar cells*. Applied Physics Letters, 2001. **78**(6): p. 841-843.
80. Poplavskyy, D., J. Nelson, and D.D.C. Bradley, *Ohmic hole injection in poly(9,9-dioctylfluorene) polymer light-emitting diodes*. Applied Physics Letters, 2003. **83**(4): p. 707-709.
81. Dodabalapur, A., et al., *Organic smart pixels*. Applied Physics Letters, 1998. **73**(2): p. 142-144.
82. Ong, B.S., et al., *High-performance semiconducting polythiophenes for organic thin-film transistors*. Journal of the American Chemical Society, 2004. **126**(11): p. 3378-3379.
83. Brahim, S., et al., *Chemical and biological sensors based on electrochemical detection using conducting electroactive polymers*. Microchimica Acta, 2003. **143**(2-3): p. 123-137.
84. Malhotra, B.D., A. Chaubey, and S.P. Singh, *Prospects of conducting polymers in biosensors*. Analytica Chimica Acta, 2006. **578**(1): p. 59-74.
85. Entezami, A.A. and B. Massoumi, *Artificial muscles, biosensors and drug delivery systems based on conducting polymers: A review*. Iranian Polymer Journal, 2006. **15**(1): p. 13-30.
86. Rincón, C. and J.C. Meredith, *Osteoblast Adhesion and Proliferation on Poly(3-octylthiophene) Thin Films*. Journal of Biomedical Materials Research A, 2008. **submitted**.
87. Yamamoto, A., R. Honma, and M. Sumita, *Cytotoxicity evaluation of 43 metal salts using murine fibroblasts and osteoblastic cells*. Journal of Biomedical Materials Research, 1998. **39**(2): p. 331-340.
88. Yamamoto, A., et al., *Generic tendency of metal salt cytotoxicity for six cell lines*. Journal of Biomedical Materials Research, 1999. **47**(3): p. 396-403.
89. Loponen, M.T., et al., *DOPING AND DEDOPING PROCESSES IN POLY(3-ALKYLTHIOPHENES)*. Synthetic Metals, 1991. **41**(1-2): p. 479-484.

90. Su, J., *PhD Dissertation, Georgia Institute of Technology*. 2008.
91. Su, J. and J.C. Meredith, *Local Histogram Analysis: Detecting Cell-Microstructure Interactions on Combinatorial Biomaterial Libraries*. Combinatorial Chemistry & High-Throughput Screening, 2008. **in press**.
92. Meyer, F. and S. Beucher, *Morphological segmentation*. J Vis Commun Image Represent 1990. **1**(1): p. 21-46.
93. Robinson, L., et al., *Electrochemical wettability switches gate aqueous liquids in microfluidic systems*. Lab on a Chip, 2006. **6**(10): p. 1277-1278.
94. Robinson, L., et al., *Electrochemical control of surface wettability of poly(3-alkylthiophenes)*. Surface Science, 2006. **600**(11): p. L148-L152.
95. Kaniowski, T., et al., *Optical studies of regioregular poly(3-octylthiophene)s under pressure*. Synthetic Metals, 1998. **94**(1): p. 111-114.
96. Nicho, M.E., et al., *Physicochemical and morphological properties of spin-coated poly(3-alkylthiophene) thin films*. Solar Energy Materials and Solar Cells, 2008. **in press**.
97. Lopez-Mata, C., et al., *Optical and morphological properties of chemically synthesized poly(3-octylthiophene) thin films*. Thin Solid Films, 2005. **490**(2): p. 189-195.
98. Singh, R., et al., *Low frequency ac conduction and dielectric relaxation in pristine poly(3-octylthiophene) films*. New Journal of Physics, 2007. **9**.
99. Marx, K.A., et al., *Quartz crystal microbalance study of endothelial cell number dependent differences in initial adhesion and steady-state behavior: Evidence for cell-cell cooperativity in initial adhesion and spreading*. Biotechnology Progress, 2003. **19**(3): p. 987-999.
100. Aebischer, P., et al., *Piezoelectric guidance channels enhance regeneration in the mouse sciatic nerve after axotomy*. Brain Research, 1987. **436**(1): p. 165-168.
101. Ozawa, H., et al., *Electric-Fields Stimulate Dna-Synthesis Of Mouse Osteoblast-Like Cells (Mc3t3-E1) By A Mechanism Involving Calcium-Ions*. Journal Of Cellular Physiology, 1989. **138**(3): p. 477-483.
102. Wallace, G.G., et al., *Conductive Electroactive Polymers: Intelligent Materials Systems*. 2nd ed. 2003, Boca Raton: CRC Press.
103. Hatada, K., T. Kitayama, and O. Vogl, *Macromolecular Design of Polymeric Materials*. 1997: CRC Press.

104. Inganas, O., et al., *THERMOCHROMIC AND SOLVATOCHROMIC EFFECTS IN POLY(3-HEXYLTHIOPHENE)*. Synthetic Metals, 1988. **22**(4): p. 395-406.
105. Li, G., et al., *High-efficiency solution processable polymer photovoltaic cells by self-organization of polymer blends*. Nature Materials, 2005. **4**(11): p. 864-868.
106. Biggs, M.J.P., et al., *The effects of nanoscale pits on primary human osteoblast adhesion formation and cellular spreading*. Journal of Materials Science-Materials in Medicine, 2007. **18**(2): p. 399-404.
107. Curtis, A.S.G., et al., *Cells react to nanoscale order and symmetry in their surroundings*. Ieee Transactions on Nanobioscience, 2004. **3**(1): p. 61-65.
108. Kripparamanan, R., et al., *Nanotopography: Cellular responses to nanostructured materials*. Journal of Nanoscience and Nanotechnology, 2006. **6**(7): p. 1905-1919.
109. Owen, T.A., et al., *Progressive development of the rat osteoblast phenotype in vitro: Reciprocal relationships in expression of genes associated with osteoblast proliferation and differentiation during formation of the bone extracellular matrix*. Journal of Cellular Physiology, 1990. **143**(3): p. 420-430.
110. Hench, L.L. and J.M. Polak, *Third-generation biomedical materials*. Science, 2002. **295**(5557): p. 1014-+.
111. Langer, R. and J.P. Vacanti, *TISSUE ENGINEERING*. Science, 1993. **260**(5110): p. 920-926.
112. Wilson, C.J., et al., *Mediation of biomaterial-cell interactions by adsorbed proteins: A review*. Tissue Engineering, 2005. **11**(1-2): p. 1-18.
113. Decher, G., *Fuzzy nanoassemblies: Toward layered polymeric multicomposites*. Science, 1997. **277**(5330): p. 1232-1237.
114. Meredith, J.C., et al., *Combinatorial characterization of cell interactions with polymer surfaces*. Journal Of Biomedical Materials Research Part A, 2003. **66A**(3): p. 483-490.
115. He, W., et al., *Micro/nanomachining of polymer surface for promoting Osteoblast cell adhesion*. Biomedical Microdevices, 2003. **5**(2): p. 101-108.
116. Washburn, N.R., et al., *High-throughput investigation of osteoblast response to polymer crystallinity: influence of nanometer-scale roughness on proliferation*. Biomaterials, 2004. **25**(7-8): p. 1215-1224.
117. Gomez, N., et al., *Micropatterned polypyrrole: A combination of electrical and topographical characteristics for the stimulation of cells*. Advanced Functional Materials, 2007. **17**(10): p. 1645-1653.

118. Xia, Y.N., D. Qin, and Y.D. Yin, *Surface patterning and its application in wetting/dewetting studies*. Current Opinion In Colloid & Interface Science, 2001. **6**(1): p. 54-64.
119. Muller-Buschbaum, P., *Dewetting and pattern formation in thin polymer films as investigated in real and reciprocal space*. Journal of Physics Condensed Matter, 2003. **15**(36): p. 1549-1582.
120. Sehgal, A., et al., *Pattern-directed dewetting of ultrathin polymer films*. Langmuir, 2002. **18**(18): p. 7041.
121. Zapata, P., et al., *Quantitative high-throughput screening of osteoblast attachment, spreading, and proliferation on demixed polymer blend micropatterns*. Biomacromolecules, 2007. **8**(6): p. 1907-1917.
122. Schmidt, C.E., et al., *Stimulation of neurite outgrowth using an electrically conducting polymer*. Proceedings Of The National Academy Of Sciences Of The United States Of America, 1997. **94**(17): p. 8948-8953.
123. Wiesmann, H.P., et al., *Electrical stimulation influences mineral formation of osteoblast-like cells in vitro*. Biochimica Et Biophysica Acta-Molecular Cell Research, 2001. **1538**(1): p. 28-37.
124. Chang, W.H.S., et al., *Effect of pulse-burst electromagnetic field stimulation on osteoblast cell activities*. Bioelectromagnetics, 2004. **25**(6): p. 457-465.
125. Zhuang, H.M., et al., *Electrical stimulation induces the level of TGF-beta 1 mRNA in osteoblastic cells by a mechanism involving calcium/calmodulin pathway*. Biochemical And Biophysical Research Communications, 1997. **237**(2): p. 225-229.
126. Wang, Q., et al., *Osteogenesis of electrically stimulated bone cells mediated in part by calcium ions*. Clinical Orthopaedics And Related Research, 1998(348): p. 259-268.
127. Heermeier, K., et al., *Effects of extremely low frequency electromagnetic field (EMF) on collagen type I mRNA expression and extracellular matrix synthesis of human osteoblastic cells*. Bioelectromagnetics, 1998. **19**(4): p. 222-231.
128. Wang, Q., et al., *Electrochemical Reactions During Constant Dc Current Stimulation - An In-Vitro Experiment With Cultured Rat Calvarial Cells*. Electro- And Magnetobiology, 1995. **14**(1): p. 31-40.
129. Wang, Q., et al., *DNA synthesis and Ca²⁺ metabolism of isolated rat osteoblast-like cells under direct current stimulation*. Electro- And Magnetobiology, 1997. **16**(2): p. 87-93.

130. Kotwal, A. and C.E. Schmidt, *Electrical stimulation alters protein adsorption and nerve cell interactions with electrically conducting biomaterials*. *Biomaterials*, 2001. **22**(10): p. 1055-1064.

VITA

CHARLENE RINCON-ROSENBAUM

Charlene Rincón-Rosenbaum was born in San Juan, Puerto Rico. Charlene graduated in 1998 from *La Academia San José* and then in 2003 obtained a B.S. in Chemical Engineering (*Magna Cum Laude*) from the University of Puerto Rico-Mayagüez. Before joining GA Tech, Charlene participated in internship programs at the Massachusetts Institute of Technology, Kimberly-Clark, and the Georgia Tech Research Institute. At GA Tech, Charlene has been the recipient of multiple fellowships including the prestigious National Institutes of Health Predoctoral Research Fellowship and the Goizueta Fellowship. Charlene has also been the recipient of multiple accolades including the 2007 Best Teaching Assistant Award given by her peers for her contributions to undergraduate instruction. At the laboratory of Prof. J. Carson Meredith, Charlene researched polymer surface-cell interactions. Her research has been presented in multiple national and international conferences and she has coauthored various publications submitted to peer-reviewed journals. In 2006 Charlene interned at Amgen, Inc. where she joined efforts to implement and optimize their protein purification processes. When Charlene is not working she enjoys jogging, dancing, reading, and scuba diving. To those close to her, Charlene is known for being organized, witty but most of all sympathetic. Charlene will be joining the Process Development Department at Amgen, Inc. in Juncos, Puerto Rico.